OPTIMIZATION OF THE COMPONENTS OF A WICKING FIBER-BASED CANINE LYMPHOMA DIAGNOSTIC FOR ENHANCING CELL TYPE SEPARATION

by

COURTNEY LONG

(Under the Direction of Karen JL Burg)

ABSTRACT

According to the American Animal Hospital Association, canines are 2-5 times more likely to develop lymphoma than humans; however, only 4% of canines are diagnosed during a routine appointment[1,2]. This work focused on modifying a novel fiber-based diagnostic to enhance heterogenous cell sample separation for rapid, routine lymphoma diagnosis. Through fiber size, configuration, biomaterial, and surface modifications, this work focused on optimizing the passive wicking properties of the fiber bundle. A dopamine-treated polylactide (PL) fiber bundle and twisted nylon fiber bundle had the most favorable wicking properties. This work also focused on identifying a biomaterial cap on the fiber bundle to promote cell wicking and capture. Alginate, three-dimensional printed PL and paper-based materials were tested. A freeze-dried sodium alginate hydrogel material was identified as the most promising biomaterial cap. Further fiber bundle and cap biomaterial optimization for increased cell recovery and cell visibility will lead to a clinically relevant prototype.

INDEX WORDS: Cancer; Cell movement; Capillary action; In vitro diagnostic.

OPTIMIZATION OF THE COMPONENTS OF A WICKING FIBER-BASED CANINE LYMPHOMA DIAGNOSTIC FOR ENHANCING CELL TYPE SEPARATION

by

COURTNEY LONG

BS, University of Georgia, 2022

A Thesis Submitted to the Graduate Faculty of The University of Georgia in Partial Fulfillment of the Requirements for the Degree

MASTER OF SCIENCE

ATHENS, GEORGIA

2023

OPTIMIZATION OF THE COMPONENTS OF A WICKING FIBER-BASED CANINE LYMPHOMA DIAGNOSTIC FOR ENHANCING CELL TYPE SEPARATION

by

COURTNEY LONG

Major Professor:	Karen JL Burg
Committee:	Timothy Burg
	Cheryl Gomillion

Electronic Version Approved:

Ron Walcott
Vice Provost for Graduate Education and Dean of the Graduate School
The University of Georgia
May 2023

ACKNOWLEDGEMENTS

I would like to sincerely thank the following individuals and organizations that supported this work:

To the Harbor Lights Endowment and the National Science Foundation for providing the funding for this work.

To Dr. Karen Burg and Dr. Timothy Burg for their mentorship and advice throughout this work.

To Harbor Lights researchers Kelsey Collins and Joshua Kim for assisting in many of the research experiments throughout this work and for inspiring many developments.

To Dr. Weitong Chen for his mentorship and guidance throughout the work and for sharing his expertise on chemical surface treatments.

TABLE OF CONTENTS

LIST OF TABLES

Page

LIST OF FIGURES

Page

PREFACE

Diagnosis of canine lymphoma needs real time diagnostic capability. Currently, routine wellness visits only accommodate preliminary testing for disease and only if something extraordinary, like a lump, is first noted during examination. Definitive diagnostics for canine lymphoma involve extended time and specialty appointments to accommodate post appointment analysis with high-end instrumentation and additional expense. Because of the additional time and expenses associated with receiving a definitive canine lymphoma diagnosis, there is a need for a rapid, low cost diagnostic device that will provide ample information for the veterinarian to confidently diagnose lymphoma during the routine wellness visit.

Capillary action is a passive wicking mechanism used to move fluids without external force. Fiber-based wicking systems are commonly used in the textile industry to passively transport fluid to the outside of the textile for an advanced cooling effect. Due to the limitations of current cancer diagnostics in veterinary medicine, the purpose of this work is to employ the same fiber-based wicking systems for passive wicking of a heterogenous cell sample for cell type separation and subsequent rapid cancer diagnosis. Previous work identified that a fiber-based passive transport system could separate cell types over the length of the fiber[98,99]. This work aims to optimize the materials used for the fiber bundle and the cap biomaterial to enhance cell type separation for cancer diagnostic applications.

This work is divided into four chapters: the project background, fiber bundle optimization, cap biomaterial optimization, and cell type separation. Chapter 1 will begin with a brief introduction of the motivation for the project and a literature review on current research

into rapid cancer diagnostics. Chapter 2 will focus on the optimization of the fiber bundles for enhanced cell separation. Aim 1 of Chapter 2 studies was to increase the hydrophilicity of the fiber bundle material to increase wicking speed and the amount of fluid sample processed. The Aim 2 of Chapter 2 studies was to decrease the size of the capillary channel radii to increase wicking speed and the amount of fluid sample processed. Experiments with surface treatment modifications were presented at the 2022 and 2023 University of Georgia (UGA) Center for Undergraduate Research Opportunities (CURO) Symposium[143,144]. Results from water contact angle analysis, dopamine surface treatments effect on wicking properties, and decreasing capillary channel radii through a twisted fiber bundle configuration were all presented at the 2023 Annual Meeting and Exposition of the Society for Biomaterials (SFB) in San Diego, California[145]. Chapter 3 will focus on the optimization of the cap biomaterial for clear cell visibility on the cap biomaterial and enhanced cell capture within the cap biomaterial. Aim 1 of Chapter 3 studies was to clearly count cells within the cap biomaterial and to increase the number of cells captured within the cap biomaterial. Experiments with different cap material types were presented at the 2022 Annual Meeting and Exposition of the SFB in Baltimore, Maryland[146]. Experiments with the 3D printed polylactide mesh cap were also presented at the 2022 UGA CURO Symposium[143]. Lastly, Chapter 4 will focus on cell type separation over the length of the fiber bundle. Chapter 4 studies identified the fiber bundle that separated the most cancerous cells from a heterogenous cell population and the cap biomaterial that captured the most cells within the cap biomaterial. The overall flow of experiments is shown in Figure 1.

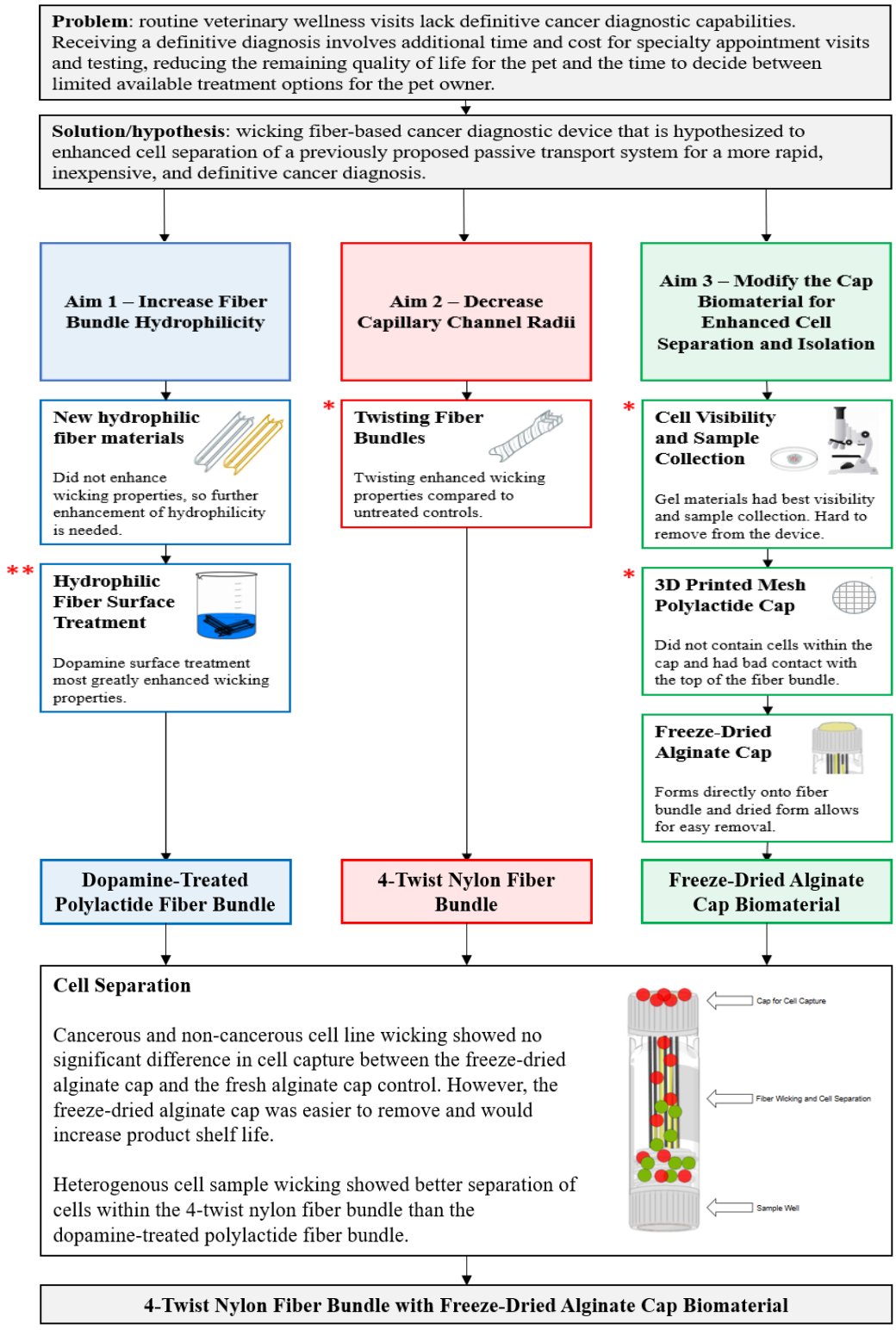

Figure 1. Flow of the experimental process for this work. A red asterisk indicates a presentation of the experiment as stated in the text.

CHAPTER ONE

BACKGROUND

Introduction

In human and veterinary medicine, an early cancer diagnosis is critical to minimizing the negative health effects associated with cancer. However, it has been shown that only 4% of canines with cancer received a diagnosis at a routine veterinary wellness appointment where there were no advanced signs or symptoms[1]. There are no routine cancer diagnostics at veterinary wellness appointments; hence it is only when a lump is identified or serious signs and symptoms emerge that diagnostic testing is employed. The pet and pet owner then must wait as the pet undergoes testing over several specialty appointment visits, wasting valuable time and resources as detailed in Figure 2. At this point, the cancer has already progressed to tumor formation, limiting the treatment options and remaining quality of life for the animal. For this reason, there is a serious need for an inexpensive, rapid cancer diagnostic device for veterinary medicine applications to reduce the emotional and financial stress of the pet and pet owner, while also maximizing the remaining quality of life for the animal by providing a cancer diagnostic device that can detect cancer in the early stages prior to tumor formation.

Current diagnostics in veterinary medicine include physical examination of the lump and other tissues, bloodwork, fine needle aspirates (FNA), biopsies, X-rays, ultrasounds, computed tomography scans, magnetic resonance imaging scans, cytology, and histopathology reports. Each of these steps provide insight into the possibility of cancer and the location of the lump, but typically a sample must be sent to a specialty lab for definitive results after performing many of

these tests[2]. In an effort to detect cancer in its early stages prior to tumor formation, research is being conducted, investigating the use of liquid biopsy samples for rapid cancer detection using biomarker or physical cancer cell separation techniques. However, there remain limitations to this research that must be addressed, which leads to the need for this work. This work will focus on modifying components of a previously proposed cell separation device to enhance cell separation for a wicking-fiber based cancer diagnostic device.

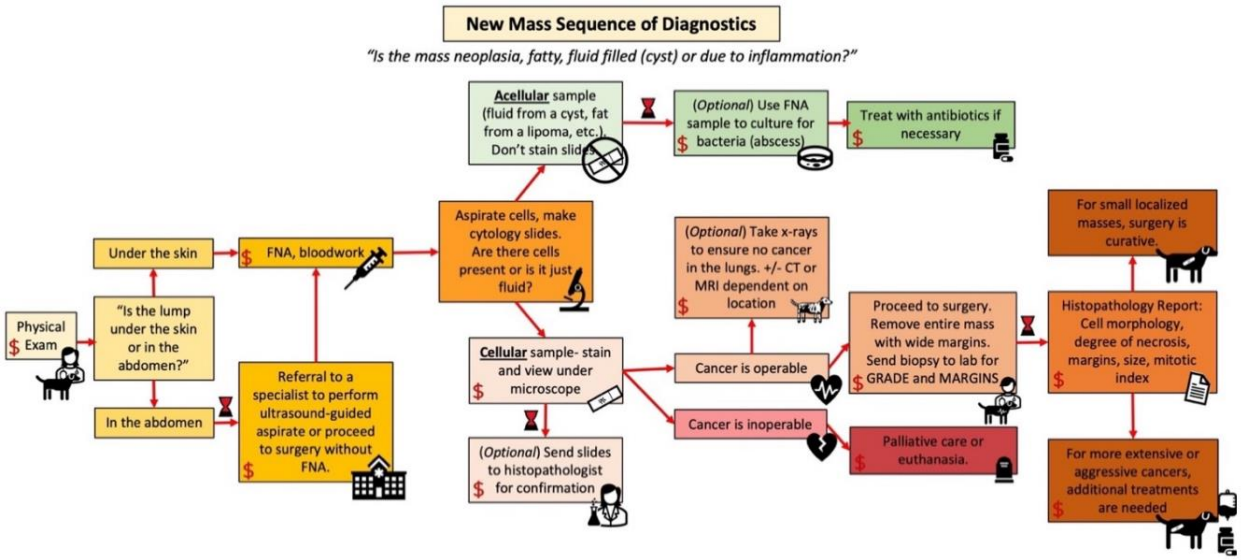

Figure 2. A schematic showing the steps between the initial routine veterinary appointment to diagnosing a lump. Red hour glasses indicate a waiting period for the physician and the client between the indicated and the next step. Red dollar signs indicate an additional cost for diagnosis. Courtesy of Kelsey Collins (2022).

Literature Review

Current Development in Rapid Cancer Diagnostic Devices

Current research on developing a rapid cancer diagnostic device in the literature aims to exploit genotypic and phenotypic differences in cancerous cells and non-cancerous cells in order to detect cancer in the body with two key detection methods: cell-free DNA (cfDNA) and circulating tumor cell (CTC) detection. The cfDNA and CTC samples can be collected via liquid biopsy or primary tumor sample. A liquid biopsy can be generally defined as a sample of

biological fluids such as blood, urine, or cerebral spinal fluid that is analyzed for analytes of interest[3]. A primary tumor sample is typically taken through a FNA which is a sampling technique that involves sticking a hollow needle into a lump or mass to extract a small cell sample that can be stained and examined under a microscope. These methods aim to develop a diagnostic testing method that process a sample already common in routine or specialty follow-up appointments for easy integration. A rapid diagnostic device that can process these types of samples would ideally eliminate the need for expert analysis of the sample to allow for earlier detection of cancer and reduce the time between noticing symptoms and a definitive diagnosis. However, general limitations for these proposed methods include difficulty recognizing tumor heterogenicity, detecting localized or low metastatic cancers, not having a high enough target molecule concentration, or having too low of a detection rate to yield definitive, consistent results[1,3,4]. Limitations of each specific cancer detection method will be discussed in the following sections.

Cell-free DNA Detection

Cell-free DNA (cfDNA) detection is a common method in the literature being developed for cancer detection and diagnosis. cfDNA fragments are degraded during apoptosis or necrosis in minutes to hours for human and animal species, readily releasing cfDNA into the blood stream for detection[3,4]. For this reason, cfDNA detection uses a liquid blood biopsy sample to process and identify cfDNA. Detection of cfDNA looks for specific genomic alterations that are cancer cell specific to aid in cancer diagnosis[5]. It has been confirmed that different cancer types will have different genomic alterations in human and canine populations and that cfDNA for multiple cancer types are present in canine populations[6-10]. This will allow for detection of specific cancer types with the cfDNA detection method. Studies have shown that the accuracy of the cfDNA

detection method for the purposes of cancer diagnosis need improvement, accurately detecting cfDNA in only half of the preclinical and clinical cancer diagnosis patients[1]. However, the cfDNA detection method had improved results when detecting higher metastatic potential, giving positive results for cfDNA presence in 83.8% of cancer patients[1]. While the cfDNA detection method improved cancer detection in preclinical patients and patients with high metastatic potential, there are several limitations still to be addressed with this method. cfDNA detection does a poor job at detecting localized cancers, smaller tumors, and specific tumor types because they do not readily shed cfDNA into the bloodstream[1,3]. It is recommended that cfDNA detection methods still be used in conjunction with confirmatory cancer evaluations like cytology or histology for certain cancer types, as the cfDNA detection method is still not accurate enough for a definitive diagnosis[1,4]. This method still has several positive attributes that will keep the cfDNA detection method a strong contender in cancer diagnostic research moving forward like the non-invasive nature of a liquid biopsy that has the potential to provide the same information as an invasive biopsy[4]. The cfDNA detection method can also characterize heterogeneity within the genome if cfDNA sheds from many locations on the tumor, which many current cancer diagnostic methods lack[3].

Circulating Tumor Cell Detection

Circulating tumor cells (CTCs) are tumor cells that are shed from the primary tumor in the body and enters the peripheral bloodstream to help the cancer metastasize[11]. They are another target of recent cancer detection research because CTCs have biomarkers that can be distinguished as cancerous and classified by the stage of the disease[12]. CTC detection is advantageous because the whole cancer cell gives more detailed information on the cancer and its metastatic potential compared to cfDNA fragments or exosomes[11]. CTC samples are obtained through a liquid biopsy

of the bloodstream, which would save time and resources for pet owners when looking for a cancer diagnosis. There are two categories of CTC detection, each with promising and limiting attributes that affect their use as a widely available method for cancer detection: affinity-based CTC detection and non-affinity-based CTC detection. Generally, CTC detection devices are limited by extremely low concentrations of CTCs in the bloodstream at approximately 1-10 CTCs/mL of blood[13]. However, CTC detection has been approved as a good predictive method for the state of the tumor, since the number of CTCs present in the bloodstream typically correlates to the metastatic potential and disease progression of the cancer[13-18].

Affinity-Based CTC Detection Methods

Affinity based CTC detection methods rely on the interaction between components of a device and the CTCs. More specifically, CTC detection methods popular in the literature include immunochemical interactions with magnetic beads and surface marker overexpression[13,19-31]. Magnetic bead isolation is promising due to its ability to target cancerous-related antibodies in CTCs that are not expressed in other molecules in the bloodstream and will bind those antibodies to the beads[32-34]. Several devices using the magnetic bead CTC isolation method on the market are the AdnaTest, CTC-iChip, and Isoflux[13,25]. Surface marker expression has also shown to be a promising CTC detection and isolation method because the targeted biomarkers have been shown to be chronically overexpressed in cancer cells versus healthy cells that are present in a liquid biopsy blood sample[12]. Common surface biomarkers tested for CTC detection include EpCAM, VAR2CSA malaria protein, CD44 exon6, aptamer, and peptides[26-31].

The key limitation to all affinity-based approaches discussed is the inability to consistently detect cancer cells within a sample. Major limitations of the common CTC isolation method targeting EpCAM include: it misses partial stem-cell like CTC phenotypes and EpCAM

becomes extremely downregulated as CTCs undergo the necessary changes for metastasis[35,36]. The VAR2CSA malaria protein, CD44 exon6, and aptamer identification methods improve upon the traditional EpCAM identification by identifying CTC phenotypes shown to be missed or that do not express the EpCAM marker, however, all the biomarker identification methods fall short of recognizing the heterogenic nature of tumors[27-30,37]. One US Food and Drug Administration approved device using the biomarker-based CTC isolation method on the market is CellSearch that targets the EpCAM protein[13]. Many studies have shown that the purity produced from the CellSearch device is not satisfactory[38,39]. The CellSearch device was also shown to only detect cancer in half of the advanced cancer patients tested and could detect no difference in patients with early to late-stage cancer when compared to patients with benign disease[40,41]. Clearly, biomarkers are limited by the inconsistent overexpression of the target biomarker and the inconsistent lack of expression of the target biomarker in healthy patients. It has been proven that some targeted biomarkers are not present in the early stages of cancer and they can be unusually overexpressed in healthy patients as well for unrelated reasons[42]. Lastly, another major limitation of affinity-based CTC detection is CTCs cannot be identified unless the target biomarker or mutation is known before of testing[43].

The most recent and most promising work on affinity-based approaches has focused on a biomarker independent charge-mediated isolation technique that utilizes a surface-charged superparamagnetic nanoprobe to target and isolate CTCs[44-52]. It has been proven that a negative surface charge is a characteristic distinction between cancer cells and normal cells due to tumor cells undergoing anaerobic glycolysis as opposed to aerobic respiration[37,44,52]. The charge mediated CTC isolation is much more sensitive than biomarker isolation techniques due to the

strong electrostatic binding of the cancerous cells to the positively charged probes of the device[45-47].

Non-Affinity-Based CTC Detection Methods

Non-affinity-based CTC detection methods rely on exploiting physical differences in cancerous cells versus non-cancerous cells. Typical non-affinity-based approaches are centrifuging deflection, dielectrophoretic separation, and a combination of size-based and deformability-based filtration[53-65]. Each of these methods are promising for CTC isolation because they can identify and isolate both epithelial and mesenchymal CTC phenotypes, which is more representative of tumor heterogenicity unlike most affinity-based approaches[66]. There are several devices on the market that use non-affinity-based approaches for CTC isolation. The Ficoll and OncoQuick devices use density gradient centrifugation to isolate CTCs from non-cancerous cells[13,67]. The DEPArray device uses dielectrophoretic CTC separation techniques[68,69]. Lastly, the Parsortix system, ISET, ScreenCell, JETTATM, and CanPatrol devices target differences in cell size or cell deformability between cancerous and non-cancerous cells[13,70-76]. However, each of these non-affinity-based CTC isolation methods are limited by technology bias and reaching a balance of capture efficiency, purity, and cell viability[66].

The CTC isolation method that has been most heavily researched is cell deformability-based and size-based separation. Filters and microchips have both been used to facilitate cell deformability-based and cell size-based CTC separation[14,66,75,77-85]. These devices rely on the correlation between increased deformability of the cell and increased metastatic potential, allowing CTCs with higher metastatic potential to pass through the filter or further into the microchip as micropore sizes decrease[86,93]. The increased deformability of cancer cells is a phenotype associated with the overexpression of multiple genes that are involved in cancer

motility and metastasis, where the overexpressed genes in deformable cells also cause greater cell motility[77]. While differences in cell size can be a factor for separating cancerous and non-cancerous cell types, several groups concluded that the differences in cell deformability was the primary cause for separation in filters and in microchip devices[85,94,95]. It has also been noted that the cytoskeleton of the cell is much more flexible than the nuclei, meaning separation could be dependent on cytoskeleton deformability of the cell and nuclei size versus the cell size[66].

Microchip devices contain artificial micro barriers that mechanically separate deformable cells from stiff cells using hydrodynamic force[77]. Micro barrier sizes are strongly correlated with CTC size for isolation, with approximately 2 um variability for those cells that have high deformation characteristics[85]. Some microchips have been shown to separate CTCs from a whole blood sample with over 90% cell recovery and over 80% purity[83,84]. While the cell recovery and purity of CTCs in microchip devices are promising, limitations still arise from clogging of the microchips and heterogenicity of CTC phenotypes in relation to deformability[85,95-97]. Using a whole blood sample from a liquid biopsy can also be challenging since leukocytes and erythrocytes are highly deformable and would pass through the chip with high metastatic CTCs[83].

Proposed Wicking Fiber Cancer Diagnostic Device

The plan for this work builds upon a previously described novel passive transport system to improve cell separation and isolation. The original fibers used in the passive transport device was used to improve wicking properties in textile applications, but was then shown to effectively separate cancerous cell populations from non-cancerous cell populations and high metastatic cancer cells from lower metastatic cancer cells[98,99]. The separation mechanism is believed to be due to a variety of physical cell properties: cell size, deformability, surface friction, and cell

adhesion molecule expression as previously discussed in the literature review[98,99]. It is also noted that the wicking characteristics and cell-fiber interactions play a role in how the cell types separate as well[98,99]. This approach to cancer cell separation and isolation is promising due to its simplistic and inexpensive nature compared to other cancer cell isolation techniques on the market. Its ability to separate cancer cells based on their metastatic potential over the length of the fiber bundle, characterizing the heterogenicity in the tumor is also advantageous[99]. The novel passive transport system was created to be used with a liquid biopsy or primary tumor sample, making translation into a clinical diagnostic device promising[99]. With fiber bundle modifications and device cap biomaterial modifications to enhance capillary action, this work modifies the passive transport device to rapidly diagnose cancer in a cheaper, simpler way by enhancing cell separation.

Fiber Bundle Modifications

Fiber Material and Surface Modification

The mechanism that drives wicking within the wicking fiber bundle is capillary action. Capillary action occurs when the adhesive forces between the liquid molecule and the surface are stronger than the cohesive forces between liquid molecules. However, the cohesive forces between liquid molecules are also responsible for the surface tension of the liquid that pulls neighboring liquid molecules up the channel surface against gravity. It has been shown that a hydrophilic surface enhances adhesive forces between the surface and the liquid molecules[100]. For this reason, the hydrophilicity of the fiber bundle should be enhanced to increase capillary action of the sample.

The previous work on the passive wicking transport fiber bundle used a polylactide (PL) material[98,99]. PL is a polymer commonly used for healthcare products, packaging, and automotive applications[101]. PL is biocompatible and has good thermal processability,

contributing to its popularity for extrusion purposes[101]. However, PL is considered a hydrophobic polyester with a water contact angle of approximately 85° in the literature[102] Since PL's water contact angle is almost hydrophobic at 90°, new fiber materials and chemical surface treatments will be investigated to increase the hydrophilicity of the previously proposed passive wicking transport fiber bundle.

Two new materials were investigated for use in the wicking fiber bundle: nylon 6,6 and polyethylene terephthalate glycol (PETG). Nylon 6,6 is a high strength yet flexible polymer that is used in a variety of applications such as cords, fish nets, clothes, parachutes, and elastic products[103,104]. Nylon is known for its ability to absorb water with a water contact angle of approximately 70° in the literature, making nylon more hydrophilic than that of PL[103,105]. Nylon is also a popular polymer used in sample swabs where product development companies state that nylon flocked swabs enhance the capillary action and quick uptake of the sample being collected, making nylon a promising material for the wicking fiber bundle application[106,107]. Polyethylene terephthalate glycol (PETG) is a copolymer that possesses the properties of polyethylene terephthalate and glycol. PETG is a common polymer used in extrusion due to its good thermal stability and high strength[108-110]. The water contact angle of PETG in the literature is approximately 81°, slightly below the definition of a hydrophobic material[105]. Many resources also list PETG as having poor moisture resistance which can lead to the material being brittle[108-110]. The water contact angle and poor moisture resistance could suggest that PETG is a promising material for the wicking fiber bundle application.

Chemical surface treatments of the fiber bundles are also used as another way of increasing the hydrophilicity of the polymers in the literature. Lysol, ethanol, sodium hydroxide, and dopamine have all been investigated as chemical treatments to increase the hydrophilicity of

a hydrophobic polymer surface[111-124]. The components that make up Lysol are not well documented, but the main component of disinfectants is typically benzalkonium chloride. Benzalkonium chloride is a cationic surfactant that can induce polymer degradation for increased hydrophilicity[111]. Alcohols and acids like ethanol and sodium hydroxide have been shown to cause partial hydrolysis of polymer surfaces, increasing hydrophilicity[112-118]. Lastly, dopamine solutions have been shown to increase the hydrophilicity of polymer materials through covalent bond and hydrogen bond interactions[119-124].

Fiber Bundle Orientation Modification

Another factor that can influence capillary action is the capillary pressure within the fiber bundle. Capillary pressure can be represented by the Laplace equation in Equation 1, where P_c is capillary pressure, γ is liquid surface tension, θ is the contact angle, and R_c is the capillary radii[125]. From this equation, the hydrophilicity of the fiber bundle is represented by the contact angle and has influence over the capillary action within the fiber bundle as previously discussed. However, the capillary radii size also plays a key role in determining capillary action. Throughout the literature, capillary radius is recognized as a good predictor of capillary action potential, where a decreased capillary radii will lead to increased capillary pressure and increased capillary action[125-127]. For this reason, modifications to the fiber bundle should be made to decrease the size of the capillary channels within the fiber bundle to enhance sample wicking.

$$P_c = \frac{2\gamma\cos(\theta)}{R_c} \qquad \text{Equation 1}$$

Cap Biomaterial Modifications

In addition to fiber bundle modifications having a positive effect on wicking properties of the fiber bundle, modifications of the cap biomaterial also have the potential to have a positive effect

on wicking properties. Plants use a mechanism called transpiration throughout literature to drive the passive uptake of water and nutrients from the ground up through the leaves of the plant[128-131]. Transpiration is a process by which water is evaporated from the leaves of the plant, causing a shift in equilibrium and an increase in capillary action to pull more water from the ground into the plant. A similar concept can be applied to the passive transport system for cell separation by modifying the preexisting alginate biomaterial cap that has already proven to enhance cell separation within the fiber bundle[98]. Hydrogels have been shown to mimic this transpiration process in a hydrated and dehydrated state, with the dehydrated state further driving the uptake of water to restore equilibrium[132-135]. Dehydrated alginate hydrogels have also been shown to maintain their original shape when rehydrated, which could contribute to longer shelf-life and simplistic removal of the biomaterial cap for the prototype[136].

CHAPTER TWO

FIBER BUNDLE CHARACTERIZATION

Introduction

The National Cancer Institute estimates that 6 million dogs will be diagnosed with some form of cancer each year, with 50% of dogs over the age of 10 developing cancer[137,138]. Cancer in canine populations can be particularly fatal due to the time-consuming nature of cancer diagnosis. Current diagnostic methods are too time-consuming, expensive, and yield subjective results. These factors drive the need for a rapid diagnostic device that can process a liquid sample and be performed during a routine appointment time. Previous work used a wicking fiber-based passive transport system to effectively separate cancerous and non-cancerous cell types from a heterogenous cell sample[98,99]. However, cell samples were allowed to wick for 0.5 hour and 24-hour time points, showing significant difference in the number of cells wicked in 0.5 hours versus 24 hours[98]. While a 24-hour diagnostic test would still be an improvement for cancer diagnosis in veterinary medicine, the goal is to introduce a rapid diagnostic test that can be performed within an appointment time without sacrificing effective cell type separation.

In this chapter, we have investigated the wicking fiber diagnostic prototype to increase capillary action. As indicators of enhanced capillary action, we will be looking at increasing wicking speed, sample mass pulled into the fiber bundle system, and sample dispersion at the top of the fiber bundle using a highlighter fluid sample. To achieve these specific aims, part of this chapter focused on altering the fiber bundle design using different sized fibers or fiber configurations within the fiber bundle. The second part of this chapter focuses on altering the

hydrophilicity of the fiber bundles through different material compositions and chemical surface treatments.

First, fiber configurations within the fiber bundle were tested for sample dispersion at the top of the fiber bundle using a highlighter fluid sample to identify the fiber bundle configuration with the ability to wick the most sample to the top of the fiber bundle. It is believed that increasing the number of fibers within the fiber bundle will increase the sample dispersion due to an increase in contact points between fibers within the fiber bundle. Next, the ability of large E70 fiber bundles versus small E30 fiber bundles were tested for wicking speed, sample wicked into the fiber bundle system, and sample dispersion at the top of the fiber bundle to identify the proper fiber size to meet the specific aims. This study was performed with a highlighter fluid sample. It is believed that the larger fiber bundle size will wick more sample into the system, but that the smaller fiber bundle size may have a faster wicking speed.

Following the selection of fiber bundle characteristics, the hydrophilicity of the fiber bundle material was tested using water contact angle analysis. Polyethylene terephthalate glycol and nylon material filament were investigated to increase the hydrophilicity of the fiber bundle compared to the previously used polylactide fiber bundle material[98,99]. To further increase the hydrophilicity of the fiber bundle and consequently enhance wicking abilities, Lysol and ethanol combination, 2M sodium hydroxide, and dopamine chemical surface treatments were used to treat the fiber bundle material and were tested using water contact angle analysis.

The later section of the chapter revisits the use of fiber bundle configuration to replace the need for time-consuming chemical surface treatment to enhance wicking capabilities. A twisted fiber bundle configuration is investigated to enhance wicking capabilities by decreasing

the size of capillary channels and increasing the number of contact points between fibers within the fiber bundle[125].

A summary of the fiber size, configuration, material, chemical surface treatment, sample type used, and analysis used to analyze wicking capabilities is listed in Table 1.

Table 1. Summary of the type of fiber bundle configurations tested, the chemical surface treatments used, sample type used to test wicking capabilities, and the analysis methods used.

Wicking fiber configuration	Treatment	Sample type	Analysis
E70 Polylactide	None	Highlighter fluid	Wicking time, sample mass wicked, and stereoscope sample dispersion
	Lysol and ethanol	Highlighter fluid	Wicking time and stereoscope sample dispersion
	2M sodium hydroxide	Highlighter fluid	Wicking time, stereoscope sample dispersion, and degradation analysis
	Dopamine	Highlighter fluid	Wicking time, stereoscope sample dispersion, and degradation analysis
E70 twisted polylactide	None	Highlighter fluid	Wicking time, sample mass wicked, and stereoscope sample dispersion
E30 Polylactide	Lysol and ethanol	Highlighter fluid	Wicking time, sample mass wicked, and stereoscope sample dispersion
E30 twisted polylactide	None	Highlighter fluid	Wicking time, sample mass wicked, and stereoscope sample dispersion
E70 nylon	None	Highlighter fluid	Wicking time and stereoscope sample dispersion
	Dopamine	Highlighter fluid	Wicking time and stereoscope sample dispersion
E70 twisted nylon	None	Highlighter fluid	Wicking time and stereoscope sample dispersion
E70 polyethylene terephthalate glycol	None	Highlighter fluid	Wicking time and stereoscope sample dispersion
	Dopamine	Highlighter fluid	Wicking time and stereoscope sample dispersion

Selecting the Fiber Bundle Configuration

Materials and Methods

Fiber Preparation

Polylactide filament was extruded through a Monoprice Maker Ultimate 3D Printer at 210°C. Fibers had irregular cross-sectional dimensions of 3.33mm x 2.02mm and were defined as E70 sized fibers. Wicking fibers were laser cut into three individual fiber segments 35 mm in length. To enhance wicking properties, fiber segments were soaked in 10% Lysol for 15 minutes and left to air-dry for 15 minutes. Then, fiber segments were soaked in 70% ethanol for 15 minutes and left to air-dry for 15 more minutes.

Wicking Experiment Set-Up

To select the fiber bundle configuration with the most favorable wicking properties, two fiber bundle configurations were prepared to be tested. Configuration A was prepared with three 35 mm fiber segments as shown in Figure 3A. Configuration B was prepared with two 35 mm fiber segments oriented as shown in Figure 3B. Fiber bundles were then secured with a zip tie located in the center of the fiber bundle. Highlighter fluid sample was prepared by soaking one Sharpie Highlighter marker stick in 500 mL of deionized water for 24 hours. 1 mL of highlighter fluid sample was placed in a single well of a 12-well plate for wicking. Configuration A and configuration B fiber bundles were placed into separate wells simultaneously and allowed to wick sample for 5 minutes. After 5 minutes of wicking was completed, the top of each fiber bundle was imaged under the stereoscope. A blacklight flashlight was used to fluoresce the highlighter fluid sample at the top of the fiber bundle.

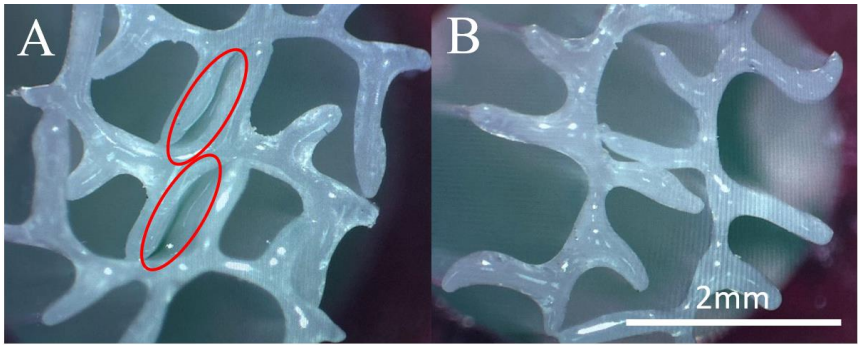

Figure 3. Stereoscope images of E70 polylactide fiber bundle configurations for wicking. (A) Three fiber per bundle configuration. (B) Two fiber per bundle configuration. A red circle indicates a dispersion area that sample has wicked to.

Analysis

The fiber bundle configuration with the most favorable wicking properties was defined as the bundle that wicked the most sample to the top of the fiber bundle. This was determined by visual sample dispersion percentage at the top of the fiber bundle. Sample dispersion percentage was calculated by counting the number of sample dispersion areas that were filled with highlighter fluid sample out of the 6 dispersion areas at the top of the E70 fiber bundle. The number of sample filled sample dispersion areas were then divided by 6 and multiplied by 100 to obtain the sample dispersion percentage. For this calculation, images were taken under the stereoscope of the top cross section of the fiber bundle while fluorescing the highlighter fluid sample with the blacklight flashlight. Sample dispersion areas were then counted from that image based upon how many dispersion areas had highlighter fluid fluorescing in them.

Results and Discussion

From the images collected after the wicking experiment concluded, the configuration A fiber bundle had a sample dispersion percentage of 33% and the configuration B fiber bundle had a sample dispersion percentage of 0% as seen in Figure 3. The configuration A fiber bundle had closer contact points within the fiber bundle than the configuration B fiber bundle. The

configuration A fiber bundle also had more consistent preparation compared to the configuration B fiber bundle. A general trend was observed that each additional fiber added to the fiber bundle would increase the contact points within the fiber bundles and the amount of fluid sample that could be wicked to the top of the wicking fiber bundle device. The modified cryovial prototype that secures the wicking fiber bundle was developed in parallel to selecting the fiber bundle configuration and can only secure up to three fibers per bundle. Due to the increased contact points in the configuration A fiber bundle and the size constraints of the developed modified cryovial prototype, the configuration A fiber bundle was selected to be used for the remainder of the wicking fiber bundle experiments.

Comparing E70 versus E30 Size Fibers

Materials and Methods

Fiber Preparation

Polylactide filament was extruded through a Monoprice Maker Ultimate 3D Printer at 210°C. Large fibers had irregular cross-sectional dimensions of 3.33mm x 2.02mm and were defined as E70 sized fibers as shown in Figure 4B. Small fibers had irregular cross-sectional dimensions of 2.97mm x 1.67mm and were defined as E30 sized fibers as shown in Figure 4A. Wicking fibers were laser cut into three individual fiber segments 35 mm in length. To enhance wicking properties, fiber segments were soaked in 10% Lysol for 15 minutes and left to air-dry for 15 minutes. Then, fiber segments were soaked in 70% ethanol for 15 minutes and left to air-dry for 15 more minutes.

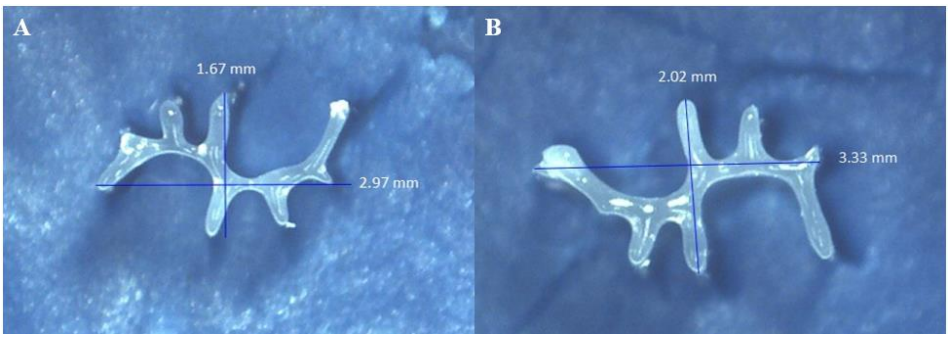

Figure 4. Stereoscope images of E30 and E70 sized fiber cross sections. (A) Dimensions of a E30 fiber cross section. (B) Dimensions of a E70 fiber cross section. Dimension lines have been labeled with the dimension measurements using ImageJ software.

Wicking Experiment Set-Up

To select the fiber size with the most favorable wicking properties, two fiber bundle types were prepared to be tested: one fiber bundle type made up of E70 fibers and one fiber bundle type made up of E30 fibers. All fiber bundles were prepared in configuration A as selected in the previous experiment. The modified cryovial prototype was used to secure the fiber bundle and run the wicking experiment. Highlighter fluid sample was prepared by soaking one Sharpie Highlighter marker stick in 500 mL of deionized water for 24 hours and stored in a 500 mL glass bottle. 1 mL of highlighter fluid sample was loaded in the sample well of the modified cryovial prototype for wicking. Wicking time began when the fiber bundles were placed in the prototype sample well and were allowed to wick for 10 minutes. After 10 minutes of wicking was completed, the top of each fiber bundle was imaged under the stereoscope. A blacklight flashlight was used to fluoresce the highlighter fluid sample at the top of the fiber bundle.

Analysis

The fiber bundle configuration with the most favorable wicking properties was defined as the bundle that wicked the most sample to the top of the fiber bundle and into the fiber bundle. This was determined by visual sample dispersion percentage at the top of the fiber bundle and the difference between the mass of sample in the sample well before and after wicking was

completed. Sample dispersion percentage was calculated by counting the number of sample dispersion areas that were filled with highlighter fluid sample out of the 6 dispersion areas at the top of the E70 fiber bundle. The number of sample filled sample dispersion areas were then divided by 6 and multiplied by 100 to obtain the sample dispersion percentage. For this calculation, images were taken under the stereoscope of the top cross section of the fiber bundle while fluorescing the highlighter fluid sample with the blacklight flashlight. Sample dispersion areas were then counted from that image based upon how many dispersion areas had highlighter fluid fluorescing in them. Statistical analysis of the quantifiable results was performed using t-test in the GraphPad Prism software.

Results and Discussion

On average, the E30 fiber bundles wicked the highlighter fluid sample more quickly to the top of the fiber bundle, however, the E70 fibers still wicked the highlighter fluid sample to the top of the fiber bundle in less than 5 minutes as shown in Figure 5A. The E70 fibers had slightly higher percent dispersion and consistently wicked more highlighter fluid sample into the fiber bundle system as shown in Figure 5B. The E70 fibers had slightly more sample dispersion seen at the top of the fiber bundles than that of the E30 fibers, with respective average sample dispersion percentages of 22% and 16% as shown in Figure 5C. Lastly, it was observed that printing the E70 fibers was more consistent, yielding a higher quality cross section. The E30 fiber size is promising because they quickly wick fluid sample to the top of the fiber bundle. However, the E70 fiber size was selected for wicking fiber bundle experiments moving forward because the extruded cross sections of the fibers were more consistent, average percent dispersion was better at the top of the fiber bundle, and the fluid sample was still wicked to the top of the fiber bundle in under 5 minutes. Variability was seen in both wicking time and sample mass wicked due to

the variability in extruded cross sections of the fiber bundles and inconsistencies when bundling the fibers together. Variability in fiber cross section or fiber configuration within the fiber bundle could lead to variability in wicking properties as seen in Figure 5.

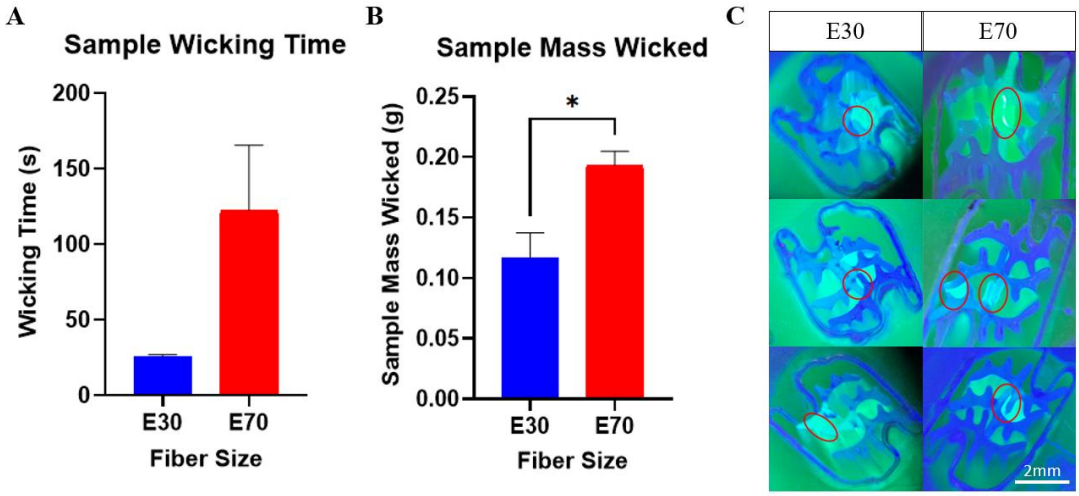

*Figure 5. Measured metrics of 10-minute wicking with E30 and E70 size fiber bundles. (A) Sample wicking speed of E30 and E70 fiber bundles. N=3 sample size. (B) Amount of sample wicked into the fiber bundle at the conclusion of 10-minute sample wicking is significantly different. N=3 sample size. (C) Stereoscope images of fiber bundle cross sections showing sample dispersion after 10-minute wicking. N=3 sample size. Red circles indicate a sample dispersion area filled with wicked sample. * indicates $p<0.05$.*

Increasing Hydrophilicity of Fiber Bundle with New Materials and Chemical Surface Treatments

Materials and Methods

Disc Preparation

Discs were made by cutting up polylactide, polyethylene terephthalate glycol, or nylon filament into approximately 30mm pieces and covering the bottom of a Teflon mold two inches in diameter. The mold was then placed in the carver press to melt the filament into a solid sheet, approximately 0.5 mm in thickness. Discs were then laser cut from the resulting sheet 10 mm in diameter for the purposes of testing water contact angle.

Chemical Surface Treatments

The Lysol and ethanol surface treatment begins with soaking the discs in a 10% Lysol solution for 15 minutes on a shaker plate. The discs are removed from the Lysol after 15 minutes, rinsed with DI water, and patted with gauze to dry. The same procedure is then followed in a 70% ethanol solution to complete surface treatment. For the sodium hydroxide surface treatment, discs are soaked in a beaker with a 2M sodium hydroxide solution for 40 minutes with a stir bar at 400 rpm. Discs were then rinsed with DI water and patted with gauze to dry after being removed from the sodium hydroxide solution. The dopamine surface treatment solution is made by combining a 10mM Tris-HCl buffer solution with dopamine powder. To prepare the Tris-HCl buffer solution, 7.84g of tris powder was added to 450 mL of DI water in a beaker. Four NaOH pellets were then dissolved in 30 mL of DI water and added dropwise into the 450 mL tris solution. The tris-HCl buffer was then diluted with DI water to a total volume of 500 mL. To make the dopamine solution, 0.4g of dopamine was added to 100 mL of tris-HCl buffer solution and dissolved. Direct airflow, 45°C heat, and a stir bar at 400 rpm were then added into the 100 mL dopamine solution to enhance the reaction. Discs were treated in the dopamine solution for 40 minutes. After treatment, discs were rinsed with DI water and patted dry with gauze.

Water Contact Angle Experiment Set-Up

For the water contact angle experiment, two polylactide discs were treated in each surface treatment to see the chemical surface treatment effect on polylactide hydrophilicity. A pedestal with a black backdrop was set up to take optimal water contact angle images for analysis. For each polylactide disc, the disc was placed in the middle of the pedestal for consistent images. 10 uL of water was pipetted onto the center of the polylactide disc. Images were taken with an iPhone 12 camera placed on the edge of the benchtop for each image taken for consistency. The

same process was repeated with untreated nylon, untreated polyethylene terephthalate glycol, dopamine-treated nylon, and dopamine-treated polyethylene terephthalate glycol discs.

Analysis

Images were analyzed using ImageJ software. Water contact angle was taken on the outside of either side of the water droplet. The measured water contact angle was subtracted from 180° to calculate the final water contact angle of each disc. The final water contact angles noted are from inside of the water droplet with respect to the horizontal plane. With this definition of water contact angle, the most hydrophilic disc will be defined as the disc with the lowest water contact angle. Statistical analysis of the quantifiable results was performed using one-way ANOVA tests in the GraphPad Prism software.

Results and Discussion

From the resulting water contact angles calculated in ImageJ, two water contact angles from either side of the water droplet on the discs were recorded. The nylon material was significantly more hydrophilic than both the polylactide and polyethylene terephthalate glycol fiber materials. The most consistent hydrophilic surface treatment was the dopamine treatment, followed by the 2M sodium hydroxide treatment, then the Lysol and ethanol treatment as shown in Figure 6A on the polylactide discs. Multiple material types were then tested with and without the dopamine treatments to compare water contact angles and hydrophilicity. As shown in Figure 6B, the dopamine-treated materials were all significantly more hydrophilic than their untreated counterpart. Treated polyethylene terephthalate glycol was the most hydrophilic, followed by treated nylon and treated polylactide, however, there was no significant difference between the water contact angles. Variability was seen in the average water contact angle of each of the surface treated material groups likely due to differences in fiber bundle degradation when

undergoing the surface treatments. Less variability was seen in the average water contact angle of the untreated material groups, however, this variability could be due to testing the water droplets on different points on the material disc that could have altered the average water contact angle. Because the degree of hydrophilicity of a flat disc compared to a fiber geometry could vary, each material with and without the dopamine chemical surface treatment will be tested for wicking properties to confirm the correlation between hydrophilicity and wicking properties in a fiber bundle.

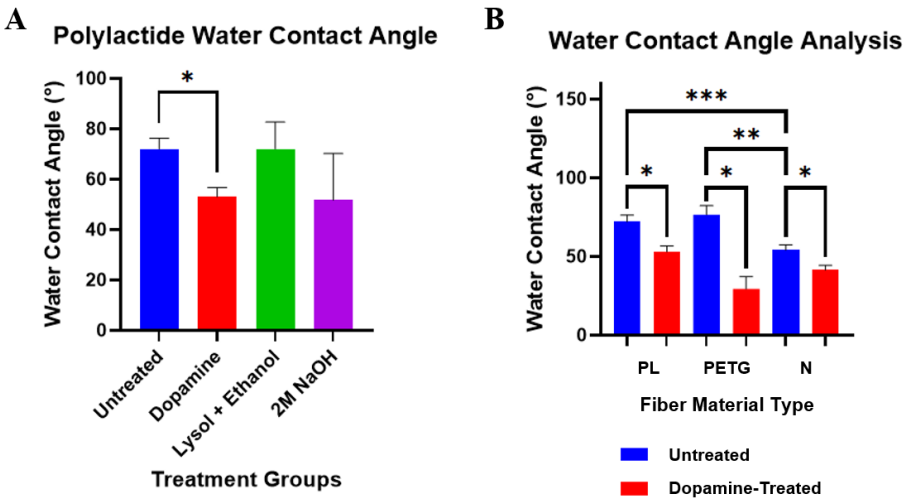

*Figure 6. Comparison of measured water contact angle between polymer materials and chemical surface treatments. (A) Water contact angle comparison between three chemical surface treatments and no chemical surface treatment on polylactide material. N=4 sample size. (B) Water contact angle comparison between untreated polymer materials and dopamine-treated polymer materials. The lowest water contact angle indicates the most hydrophilic material. N=4 sample size. * indicates $p<0.05$. ** indicates $p<0.01$. *** indicates $p<0.001$.*

Comparing Wicking Properties of New Materials

Materials and Methods

Fiber Preparation

Polylactide filament was extruded through a Monoprice Maker Ultimate 3D Printer at 210°C. Nylon filament was extruded through a Monoprice Maker Ultimate 3D Printer at 245°C.

Polyethylene terephthalate glycol filament was extruded through a Monoprice Maker Ultimate 3D Printer at 230°C. Fibers had irregular cross-sectional dimensions of 3.33mm x 2.02mm and were defined as E70 sized fibers. Wicking fibers were laser cut into three individual fiber segments 35 mm in length.

Wicking Experiment Set-Up

Three fiber bundles were prepared in the modified cryovial prototype per fiber material type. Highlighter fluid sample was prepared by soaking one Sharpie Highlighter marker stick in 500 mL of deionized water for 24 hours and stored in a glass bottle. 1 mL of highlighter fluid sample was loaded in the sample well of the modified cryovial prototype for wicking. Prior to wicking, the mass of the sample and the sample well were recorded. Wicking time began when the fiber bundles were placed in the prototype sample well and time was recorded when the first fluid sample visibly reached the top of the fiber bundle. Wicking was concluded after 10 minutes and the mass of the remaining sample and sample well were recorded. A blacklight flashlight was used to fluoresce the highlighter fluid sample at the top of the fiber bundle throughout the experiment.

Analysis

Two factors are considered when selecting the most efficient wicking fiber bundle: speed of wicking and sample dispersion at the top of the bundle. The fastest wicking bundle was defined as the fiber bundle with the lowest time it took for the fluid sample to reach the top of the fiber bundle once in contact with the fluid sample. Fiber bundles are then imaged under the stereoscope with the blacklight to fluoresce sample at the top of the fiber bundle. The fiber bundle with the most sample dispersion was defined as the fiber bundle with the highest percentage of sample dispersion. Sample dispersion percentage was calculated by counting the

number of sample dispersion areas that were filled with highlighter fluid sample out of the 6 dispersion areas at the top of the E70 fiber bundle. The number of sample filled sample dispersion areas were then divided by 6 and multiplied by 100 to obtain the sample dispersion percentage. For this calculation, images were taken under the stereoscope of the top cross section of the fiber bundle while fluorescing the highlighter fluid sample with the blacklight flashlight. Sample dispersion areas were then counted from that image based upon how many dispersion areas had highlighter fluid fluorescing in them. Statistical analysis of the quantifiable results was performed using one-way ANOVA tests in the GraphPad Prism software.

Results and Discussion

The nylon fiber bundles performed the best out of the polyethylene terephthalate glycol and polylactide fiber bundle groups as shown in Figure 7A. Polyethylene terephthalate glycol did not wick any sample to the top of the fiber bundle within the 10-minute time frame and the polylactide fiber bundles saw minimal sample wicked. However, improvements still need to be made in the amount of sample dispersion seen at the top of the nylon fiber bundles within the 10-minute time frame. The untreated nylon fiber bundle had the best average sample dispersion at 22%, followed by polylactide at 12% dispersion, and polyethylene terephthalate glycol at 0% dispersion as shown in Figure 7B. Overall, the wicking times show the general trend that the more hydrophilic the fiber material, the faster the fiber bundle wicks fluid sample. It was shown in the previous experiment that nylon, polylactide, then polyethylene terephthalate glycol was most to least hydrophilic materials. Even though each nylon fiber bundle wicked sample to the top of the fiber bundle, the chemical surface treatments will be used to increase the hydrophilicity of the fiber bundle and improve wicking properties in the following experiments. Variability was seen in wicking time and sample dispersion likely due to the inconsistencies in

fiber cross sections when extruded and the bundling of the fibers. Each of these factors have the potential to affect the surface area of contact between fibers within the fiber bundle that allow fluid sample to wick.

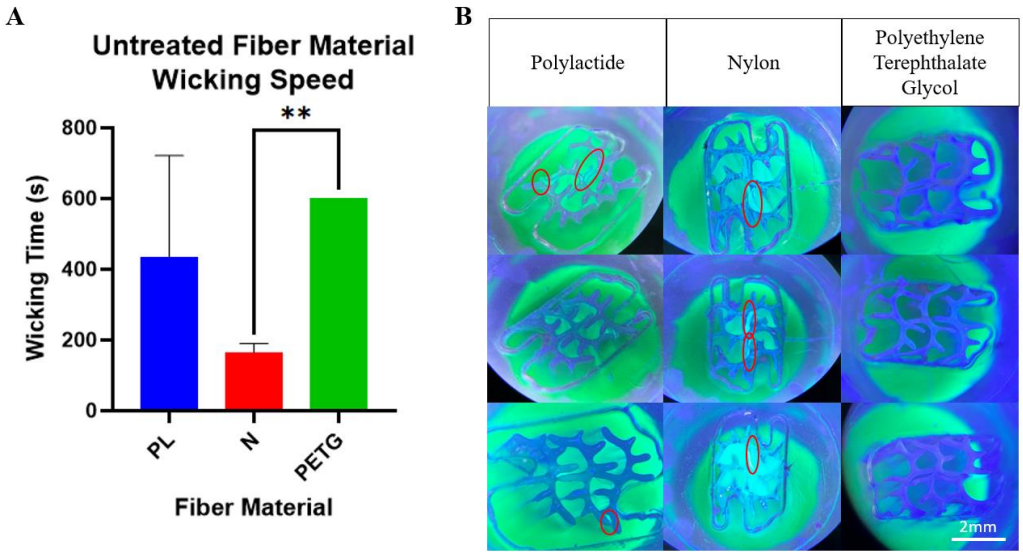

*Figure 7. Measured metrics from 10-minute wicking study comparing untreated fiber materials. (A) Compares sample wicking speed of untreated polylactide (PL), nylon (N), and polyethylene terephthalate glycol (PETG). N=3 sample size. (B) Stereoscope images of the top fiber bundle cross sections showing sample dispersion after 10-minute wicking. Red circles indicate a sample dispersion area filled with sample. N=3 sample size. ** indicates p<0.01.*

Effect of Chemical Surface Treatments on Fiber Wicking Properties

Materials and Methods

Fiber Preparation

Polylactide filament was extruded through a Monoprice Maker Ultimate 3D Printer at 210°C. Fibers had irregular cross-sectional dimensions of 3.33mm x 2.02mm and were defined as E70 sized fibers. Wicking fibers were laser cut into three individual fiber segments 35 mm in length.

Chemical Surface Treatments

The Lysol and ethanol fiber bundle surface treatment begins with soaking the polylactide fiber segments in a 10% Lysol solution for 15 minutes on a shaker plate. The fiber segments are

removed from the Lysol after 15 minutes, rinsed with DI water, and allowed to dry for 15 minutes on a shaker plate. The same procedure is then followed in a 70% ethanol solution to complete surface treatment. For the sodium hydroxide surface treatment, fiber segments are soaked in a beaker with a 2M sodium hydroxide solution for 40 minutes with a stir bar at 400 rpm. Polylactide fiber segments were then rinsed with DI water and allowed to dry for 15 minutes on a shaker plate after being removed from the sodium hydroxide solution. The dopamine surface treatment solution is made by combining a 10mM Tris-HCl buffer solution with dopamine powder. To prepare the Tris-HCl buffer solution, 7.84g of tris powder was added to 450 mL of DI water in a beaker. Four NaOH pellets were then dissolved in 30 mL of DI water and added dropwise into the 450 mL tris solution. The tris-HCl buffer was then diluted with DI water to a total volume of 500 mL. To make the dopamine solution, 0.4g of dopamine was added to 100 mL of tris-HCl buffer solution and dissolved. Direct airflow, 45°C heat, and a stir bar at 400 rpm were then added into the 100 mL dopamine solution to enhance the reaction. Fibers were treated in the dopamine solution for 40 minutes. After treatment, fibers were rinsed with DI water, placed in a petri dish with gauze, and allowed to dry for 15 minutes on a shaker plate.

Wicking Experiment Set-Up

Two fiber bundles were prepared in the modified cryovial prototype per surface treatment group. Highlighter fluid sample was prepared by soaking one Sharpie Highlighter marker stick in 500 mL of deionized water for 24 hours and stored in a 500 mL glass bottle. 1 mL of highlighter fluid sample was loaded in the sample well of the modified cryovial prototype for wicking. Wicking time began when the fiber bundles were placed in the prototype sample well and time was recorded when the first fluid sample visibly reached the top of the fiber bundle. Wicking was

concluded after 10 minutes. A blacklight flashlight was used to fluoresce the highlighter fluid sample at the top of the fiber bundle throughout the experiment.

Analysis

Degradation

Degradation analysis was performed by imaging treated fiber segments under the stereoscope. Images were captured through the stereoscope and degradation of the fibers were noted. Degradation was defined as areas of the fiber segment that seemed to have missing sections of the fiber bundle arms and grooves.

Wicking

Two factors are considered when selecting the most efficient wicking fiber bundle: speed of wicking and sample dispersion at the top of the bundle. The fastest wicking bundle was defined as the fiber bundle with the lowest time it took for the fluid sample to reach the top of the fiber bundle once in contact with the fluid sample. Fiber bundles are then imaged under the stereoscope with the blacklight to fluoresce sample at the top of the fiber bundle. The fiber bundle with the most sample dispersion was defined as the fiber bundle with the highest percentage of sample dispersion. Sample dispersion percentage was calculated by counting the number of sample dispersion areas that were filled with highlighter fluid sample out of the 6 dispersion areas at the top of the E70 fiber bundle. The number of filled sample dispersion areas were then divided by 6 and multiplied by 100 to obtain the sample dispersion percentage. For this calculation, images were taken under the stereoscope of the top cross section of the fiber bundle while fluorescing the highlighter fluid sample with the blacklight flashlight. Sample dispersion areas were then counted from that image based upon how many dispersion areas had

highlighter fluid fluorescing in them. Statistical analysis of the quantifiable results was performed using one-way ANOVA tests in the GraphPad Prism software.

Results and Discussion

Degradation

Degradation analysis of each chemical surface treatments effect on the polylactide fiber is shown in Figure 8. The Lysol and ethanol treated polylactide fibers showed no visible signs of degradation after treatment. The 2M sodium hydroxide treated polylactide fibers showed visible signs of degradation. Images captured large sections along the grooves of the fiber segment missing. In some fiber bundle, 2M sodium hydroxide treated polylactide fibers were missing a whole arm of the fiber segment after treatment concluded, which could inhibit wicking along the capillary channels. The dopamine-treated polylactide fibers showed few visible signs of degradation along the fiber segment, showing up as small ridges along the capillary channels. The small ridges within the capillary channels of the dopamine-treated polylactide fibers are not expected to inhibit wicking.

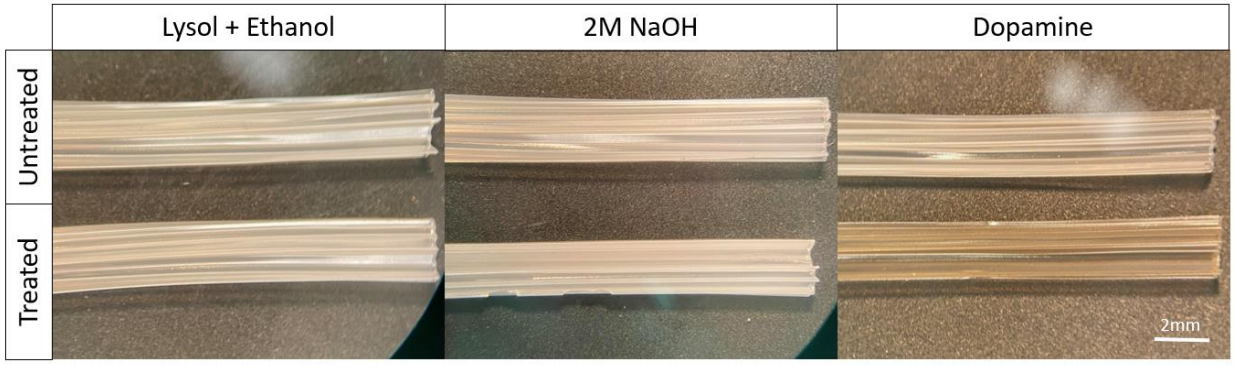

Figure 8. Stereoscope images of untreated polylactide (top) and chemically treated polylactide (bottom) for visual degradation analysis.

Wicking

The Lysol and ethanol treated fiber bundles had the fastest wicking times as shown in Figure 9A. The dopamine-treated fiber bundles had the second fastest wicking times, followed by the 2M sodium hydroxide treated fiber bundles with the third fastest wicking times. With respect to dispersion areas of sample at the top of the fiber bundles, the dopamine-treated fibers had the most fluid dispersion at the top, followed by the Lysol and ethanol treated fibers, then the 2M sodium hydroxide treated fibers as shown in Figure 9B. When considering the water contact angles found in previous experiments, the 2M sodium hydroxide-treated, dopamine-treated, Lysol and ethanol-treated, then untreated polylactide material was the most to least hydrophilic. We would expect to have a similar trend in wicking speed and dispersion areas, but that is not the case. It is likely that the 2M sodium hydroxide chemical surface treatment did not produce promising wicking properties because of the damaging degradation to the fiber bundles that inhibit wicking. Barring the sodium hydroxide-treated fiber bundles, the hydrophilicity results corresponded with the fluid sample dispersion area results, with the dopamine-treated fiber bundles having the highest average percent dispersion at 58%. The wicking speed results did not correspond with the hydrophilicity results, as the Lysol and ethanol-treated fiber bundles wicked the fastest out of each of the chemical surface treatment groups. However, due to the increased percent dispersion percentage at the top of the fiber bundle and each fiber bundle wicking sample to the top of the fiber bundle in under 30 seconds, the dopamine chemical surface treatment was identified as the most promising chemical surface treatment for enhancing wicking properties of the fiber bundle. Variability was seen in wicking time and sample dispersion likely due to the inconsistencies in fiber cross sections when extruded and the bundling of the fibers. Each of these factors have the potential to affect the surface area of contact between fibers within the

fiber bundle that allow fluid sample to wick. The dopamine chemical surface treatment will be experimented with on each of the fiber materials next.

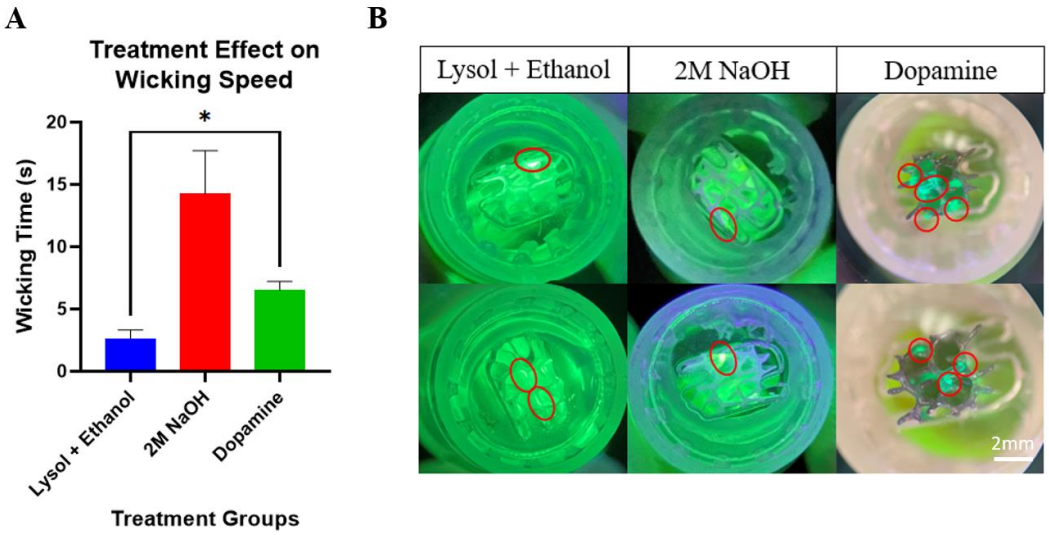

*Figure 9. Measured metrics from 10-minute wicking study of chemically treated polylactide fiber bundles. (A) Compares sample wicking speed of polylactide fiber bundles with different chemical surface treatments. N=2 sample size. (B) Stereoscope images of the top fiber bundle cross sections showing sample dispersion after 10-minute wicking. Red circles indicate a sample dispersion area filled with sample. N=2 sample size. * indicates $p<0.05$.*

Comparing Wicking Properties of Dopamine-Treated Polylactide, Nylon, and Polyethylene terephthalate glycol

Materials and Methods

Fiber Preparation

Polylactide filament was extruded through a Monoprice Maker Ultimate 3D Printer at 210°C. Nylon filament was extruded through a Monoprice Maker Ultimate 3D Printer at 245°C. Polyethylene terephthalate glycol filament was extruded through a Monoprice Maker Ultimate 3D Printer at 230°C. Fibers all had irregular cross-sectional dimensions of 3.33mm x 2.02mm and were defined as E70 sized fibers. Wicking fibers were laser cut into three individual fiber segments 35 mm in length

Chemical Surface Treatments

All fiber materials were treated in a dopamine solution for 40 minutes to increase the hydrophilicity of the fiber bundle materials. The dopamine surface treatment solution is made by combining a 10mM Tris-HCl buffer solution with dopamine powder. To prepare the Tris-HCl buffer solution, 7.84g of tris powder was added to 450 mL of DI water in a beaker. Four NaOH pellets were then dissolved in 30 mL of DI water and added dropwise into the 450 mL tris solution. The tris-HCl buffer was then diluted with DI water to a total volume of 500 mL. To make the dopamine solution, 0.4g of dopamine was added to 100 mL of tris-HCl buffer solution and dissolved. Direct airflow, a stir bar at 400 rpm, and 45°C heat from a hot plate were then added into the 100 mL dopamine solution to enhance the reaction. After treatment was complete, fibers were rinsed with DI water, placed in a petri dish with gauze, and allowed to dry for 15 minutes on a shaker plate.

Wicking Experiment Set-Up

Two fiber bundles were prepared in the modified cryovial prototype per fiber material type. Highlighter fluid sample was prepared by soaking one Sharpie Highlighter marker stick in 500 mL of deionized water for 24 hours and stored in a 500 mL glass bottle. 1 mL of highlighter fluid sample was loaded in the sample well of the modified cryovial prototype for wicking. Wicking time began when the fiber bundles were placed in the prototype sample well and time was recorded when the first fluid sample visibly reached the top of the fiber bundle. Wicking was concluded after 10 minutes. A blacklight flashlight was used to fluoresce the highlighter fluid sample at the top of the fiber bundle throughout the experiment.

Analysis

Two factors are considered when selecting the most efficient wicking fiber bundle: speed of wicking and sample dispersion at the top of the bundle. The fastest wicking bundle was defined as the fiber bundle with the lowest time it took for the fluid sample to reach the top of the fiber bundle once in contact with the fluid sample. Fiber bundles are then imaged under the stereoscope with the blacklight to fluoresce sample at the top of the fiber bundle. The fiber bundle with the most sample dispersion was defined as the fiber bundle with the highest percentage of sample dispersion. Sample dispersion percentage was calculated by counting the number of sample dispersion areas that were filled with highlighter fluid sample out of the 6 dispersion areas at the top of the E70 fiber bundle. The number of sample dispersion areas were then divided by 6 and multiplied by 100 to obtain the sample dispersion percentage. For this calculation, images were taken under the stereoscope of the top cross section of the fiber bundle while fluorescing the highlighter fluid sample with the blacklight flashlight. Sample dispersion areas were then counted from that image based upon how many dispersion areas had highlighter fluid fluorescing in them. Statistical analysis of the quantifiable results was performed using one-way ANOVA tests in the GraphPad Prism software.

Results and Discussion

The dopamine-treated polylactide bundle had the fastest wicking time and most sample dispersion at the top of the fiber bundle compared to the dopamine-treated nylon and polyethylene terephthalate glycol as shown in Figure 10. Sample dispersion areas at the top of the fiber bundle only slightly varied between fiber bundle material types, however, the dopamine-treated polylactide material had visibly more sample within the top section of the fiber bundle than either the dopamine-treated nylon or the dopamine-treated polyethylene

terephthalate glycol. The wicking time results from the untreated material wicking experiment and the dopamine-treated material wicking experiment were plotted against the average water contact angle for each material type in Figure 11, which roughly shows a linear trend between average water contact angle and wicking speed. The lack of correlation, however, leads to the conclusion that other factors also contribute to decreased wicking time other than fiber material hydrophilicity. A wicking time of 600 seconds indicates that sample fluid did not wick to the top of the fiber bundle, so there is an observed critical point around an average water contact angle of 72° where sample fluid no longer wicks to the top of the fiber bundle. Variability was seen in wicking time and sample dispersion likely due to the inconsistencies in fiber cross sections when extruded and the bundling of the fibers. Each of these factors have the potential to affect the surface area of contact between fibers within the fiber bundle that allow fluid sample to wick. These factors could have also affected the accuracy of the trend shown in Figure 11.

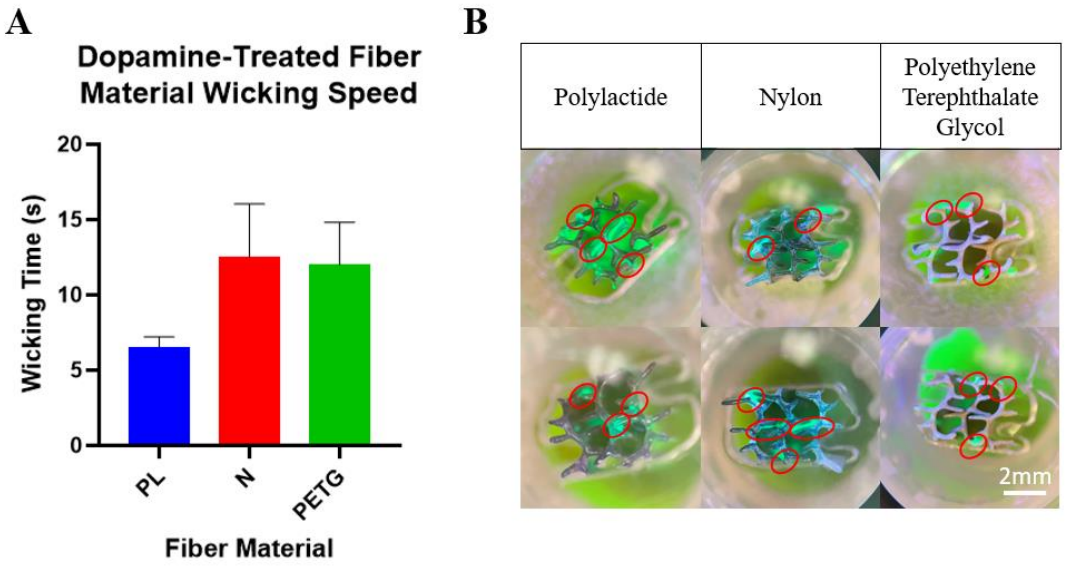

Figure 10. Measured metrics from 10-minute wicking study comparing dopamine-treated fiber materials. (A) Compares sample wicking speed of dopamine-treated polylactide (PL), nylon (N), and polyethylene terephthalate glycol (PETG). N=2 sample size. (B) Stereoscope images of the top fiber bundle cross sections showing sample dispersion after 10-minute wicking. Red circles indicate a sample dispersion area filled with sample. N=2 sample size.

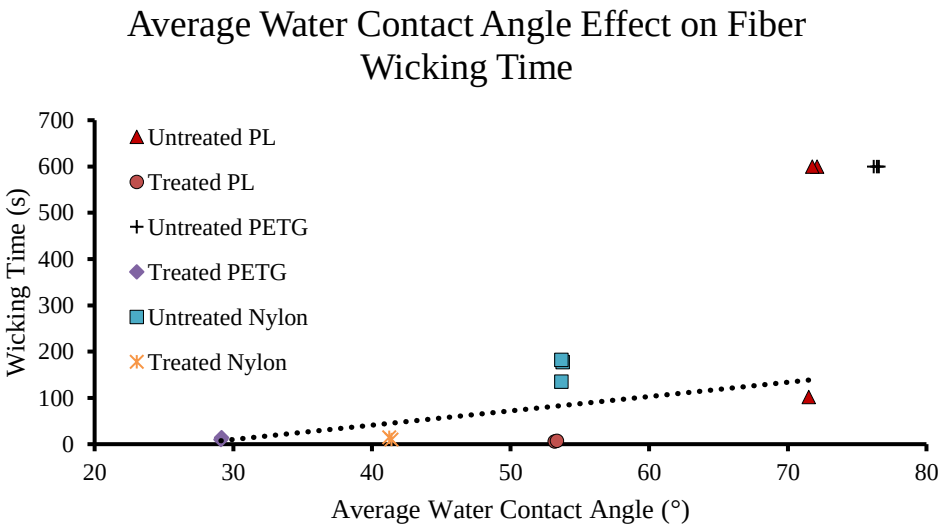

*Figure 11. Trend of material hydrophilicity's effect on fiber bundle wicking time. Wicking time versus average water contact angle is plotted for untreated polylactide (PL), polyethylene terephthalate glycol (PETG), and nylon materials as well as dopamine-treated polylactide (PL), polyethylene terephthalate glycol (PETG), and nylon. N=3 sample size. * indicates p<0.05. ** indicates p<0.01.*

Comparing Twist Tension in Twisted Fiber Bundle Configuration to Enhance Wicking Properties of Untreated Polylactide, Nylon, and Polyethylene terephthalate glycol

Materials and Methods

Fiber Bundle Preparation

Polylactide filament was extruded through a Monoprice Maker Ultimate 3D Printer at 210°C. Nylon filament was extruded through a Monoprice Maker Ultimate 3D Printer at 245°C. Polyethylene terephthalate glycol filament was extruded through a Monoprice Maker Ultimate 3D Printer at 230°C. Half of the fibers had irregular cross-sectional dimensions of 3.33mm x 2.02mm and were defined as E70 sized fibers. The other half of the fibers had irregular cross-sectional dimensions of 2.97mm x 1.67mm and were defined as E30 sized fibers. Wicking fibers were laser cut into three individual fiber segments 35 mm in length immediately following the printing process. Three 35 mm fiber segments were then bundled together and secured with one

prototype ring on one end of the fiber bundle. The other end of the fiber bundle was fastened tightly into the chuck of an electric power drill, then twisted as slow and consistent as possible to the desired twist tension. E70 polylactide fibers were twisted 0.75, 1, 1.5, and 2 rotations with the electric power drill. E30 polylactide fibers were twisted 1.5, 2, 2.5, and 3 rotations with the electric power drill. E70 nylon fibers were twisted 2, 3, and 4 rotations with the electric power drill. The twisted fiber bundle was then held in the twisted position for 60 seconds to solidify the twisted configuration.

Wicking Experiment Set-Up

Twisted Polylactide Wicking

One fiber bundle was prepared in the modified cryovial prototype per fiber bundle size and twist tension. Highlighter fluid sample was prepared by soaking one Sharpie Highlighter marker stick in 500 mL of deionized water for 24 hours and stored in a 500 mL glass bottle. 1 mL of highlighter fluid sample was loaded in the sample well of the modified cryovial prototype for wicking. Wicking time began when the fiber bundles were placed in the prototype sample well and time was recorded when the first fluid sample visibly reached the top of the fiber bundle. Wicking was concluded after 10 minutes. A blacklight flashlight was used to fluoresce the highlighter fluid sample at the top of the fiber bundle throughout the experiment.

Twisted Nylon Wicking

One fiber bundle was prepared in the modified cryovial prototype per fiber bundle twist tension. Only E70 fiber bundles were used in this experiment. One E70 2-twist polylactide fiber bundle was prepared as the control to compare materials. Highlighter fluid sample was prepared by soaking one Sharpie Highlighter marker stick in 500 mL of deionized water for 24 hours and stored in a 500 mL glass bottle. 1 mL of highlighter fluid sample was loaded in the sample well

of the modified cryovial prototype for wicking. Wicking time began when the fiber bundles were placed in the prototype sample well and time was recorded when the first fluid sample visibly reached the top of the fiber bundle. Wicking was concluded after 10 minutes. A blacklight flashlight was used to fluoresce the highlighter fluid sample at the top of the fiber bundle throughout the experiment.

Analysis

When considering which fiber bundle is the most efficient wicking fiber bundle, two factors are considered: speed of wicking and sample dispersion at the top of the bundle. The fastest wicking bundle was defined as the fiber bundle with the lowest time it took for the fluid sample to reach the top of the fiber bundle once in contact with the fluid sample. The fiber bundle with the most sample dispersion was defined as the fiber bundle with the highest percentage of sample dispersion. Sample dispersion percentage was calculated by counting the number of sample dispersion areas that were filled with highlighter fluid sample out of the 6 dispersion areas at the top of the E70 fiber bundle. The number of sample filled sample dispersion areas were then divided by 6 and multiplied by 100 to obtain the sample dispersion percentage. For this calculation, images were taken under the stereoscope of the top cross section of the fiber bundle while fluorescing the highlighter fluid sample with the blacklight flashlight. Sample dispersion areas were then counted from that image based upon how many dispersion areas had highlighter fluid fluorescing in them. For the twisted fiber bundles, dispersion areas were counted if the highlighter fluid sample had reached the top section of the fiber bundle the protrudes out from the modified cryovial prototype. Statistical analysis of the quantifiable results for the nylon twisting experiments was performed using one-way ANOVA tests in the GraphPad Prism software.

Results and Discussion

Polylactide Twisting

The 1.5 and 2-twist E70 and E30 polylactide fiber bundles wicked the fastest wicking speed and had the most sample dispersion, though minimal, of the twisted E70 and E30 polylactide fiber bundles respectively as seen in Figure 12. Comparing the E70 and E30 twisted polylactide fiber bundles, The E70 twisted polylactide fiber bundles wicked sample to the top of the fiber bundle faster and wicked more sample into the fiber bundle system than the E30 twisted polylactide fiber bundles as seen in Figure 12. This could be due to the E30 fiber bundles blocking inner capillary channels when twisted the same amount as the E70 twisted fiber bundles.

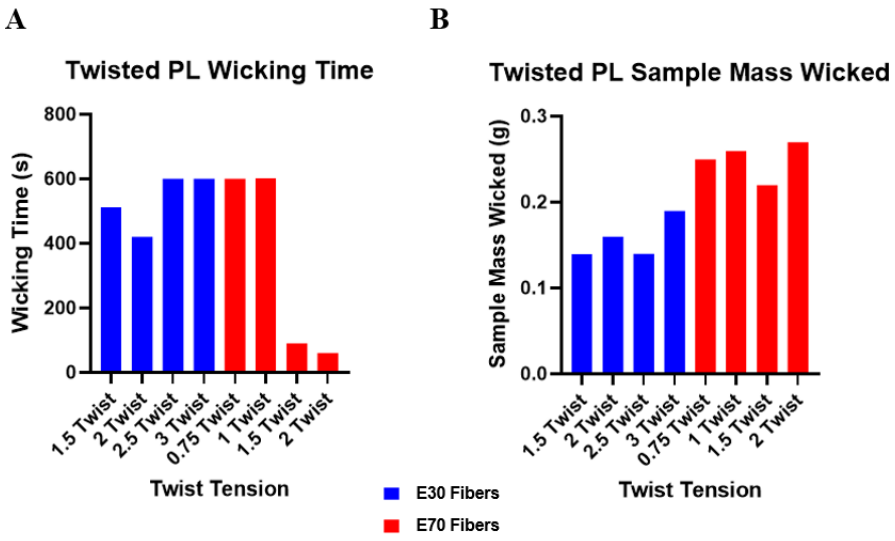

Figure 12. Measured metrics from 10-minute wicking study comparing twisted polylactide twist tension and fiber size. (A) Compares sample wicking speed of various twist tensions of twisted polylactide fiber bundles of the E30 and E70 size. (B) Compares sample wicked into the fiber bundle over the 10-minute wicking study. N=1 sample size.

Nylon Twisting

Each E70 nylon twist tension tested wicked faster and wicked more sample to the top of the fiber bundle system than the most promising 2-twist polylactide bundle as shown in Figure 13A. The 3-twist and 4-twist nylon fiber bundle had the best sample dispersion percentage, each at 41% as

shown in Figure 13B. However, the 4-twist nylon bundle visibly wicked more sample into the fiber bundle system and had the fastest wicking times of each nylon twist tension tested. The nylon fiber bundle is expected to have more favorable wicking properties because it is more hydrophilic than the polylactide fiber material. Both the selected twist tensions for the twisted polylactide and twisted nylon fiber bundles will be tested again with control groups in the following experiment. Variability in wicking time and sample dispersion is likely due to inconsistencies in the cross section when extruding the fibers, inconsistencies introduced when bundling the fibers, as well as inconsistencies introduced when twisting the fiber bundle. Each of these factors have the potential to affect the surface area of contact between fibers within the fiber bundle that allow fluid sample to wick.

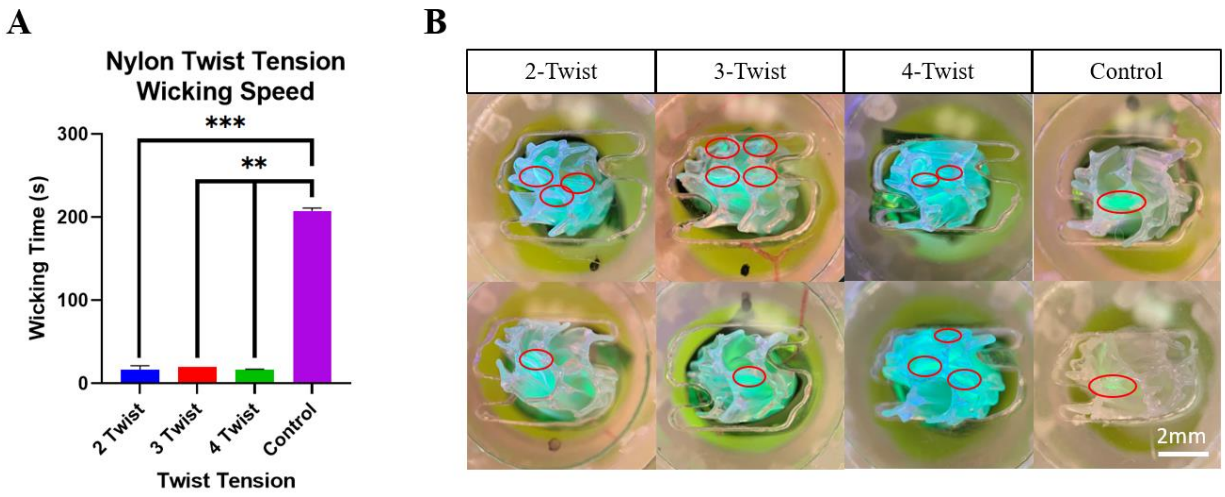

*Figure 13. Measured metrics from 10-minute wicking study comparing twist tension in twisted nylon fiber bundles to a control 2-twist polylactide fiber bundle. (A) Compares sample wicking speed of twisted nylon fiber bundles with various twist tensions and a control polylactide fiber bundle. N=2 sample size. (B) Stereoscope images of the top fiber bundle cross sections showing sample dispersion after 10-minute wicking. Red circles indicate a sample dispersion area filled with sample. N=2 sample size. ** indicates p<0.01. *** indicates p<0.001.*

Polyethylene terephthalate glycol Twisting

The polyethylene terephthalate glycol material was too stiff to twist without experiencing resistance and seeing visible damage to the fiber bundle. Further testing with twisting the polyethylene terephthalate glycol material was not performed.

Comparing Twisted to Untwisted Fiber Bundle Configuration Wicking Properties

Materials and Methods

Fiber Bundle Preparation

Polylactide filament was extruded through a Monoprice Maker Ultimate 3D Printer at 210°C. Nylon filament was extruded through a Monoprice Maker Ultimate 3D Printer at 245°C. Fibers had irregular cross-sectional dimensions of 3.33mm x 2.02mm and were defined as E70 sized fibers. Wicking fibers were laser cut into three individual fiber segments 35 mm in length immediately following the printing process. Three 35 mm fiber segments were then bundled together and secured with one prototype ring on one end of the fiber bundle. The other end of the fiber bundle was fastened tightly into the chuck of an electric power drill, then twisted as slow and consistent as possible to the desired twist tension. The E70 polylactide fiber bundle was twisted 2 rotations with the electric power drill. The E70 nylon fiber bundle was twisted 4 rotations with the electric power drill. The twisted fiber bundle was then held in the twisted position for 60 seconds to solidify the twisted configuration.

Wicking Experiment Set-Up

Four types of fiber bundles were tested for wicking speed and sample dispersion: untwisted polylactide as a control, 2-twist polylactide, untwisted nylon as a control, and 4-twist nylon. One fiber bundle was prepared in the modified cryovial prototype per fiber bundle configuration. Highlighter fluid sample was prepared by soaking one Sharpie Highlighter marker stick in 500

mL of deionized water for 24 hours and stored in a 500 mL glass bottle. 1 mL of highlighter fluid sample was loaded in the sample well of the modified cryovial prototype for wicking. Wicking time began when the fiber bundles were placed in the prototype sample well and time was recorded when the first fluid sample visibly reached the top section of the fiber bundle. Wicking was concluded after 10 minutes. A blacklight flashlight was used to fluoresce the highlighter fluid sample at the top of the fiber bundle throughout the experiment.

Analysis

Before testing the twisted fiber bundles for wicking properties, the visible damage done to the fibers through the twisting process was analyzed with the stereoscope. Fiber bundles were examined for each twist tension to ensure minimal damage to the fiber bundles. When considering which fiber bundle has the most efficient wicking properties, two factors are considered: speed of wicking and sample dispersion at the top of the bundle. The fastest wicking bundle was defined as the fiber bundle with the lowest time it took for the fluid sample to reach the top of the fiber bundle once in contact with the fluid sample. The fiber bundle with the most sample dispersion was defined as the fiber bundle with the highest percentage of sample dispersion. Sample dispersion percentage was calculated by counting the number of sample dispersion areas that were filled with highlighter fluid sample out of the 6 dispersion areas at the top of the E70 fiber bundle. The number of sample filled sample dispersion areas were then divided by 6 and multiplied by 100 to obtain the sample dispersion percentage. For this calculation, images were taken under the stereoscope of the top cross section of the fiber bundle while fluorescing the highlighter fluid sample with the blacklight flashlight. Sample dispersion areas were then counted from that image based upon how many dispersion areas had highlighter fluid fluorescing in them. For the twisted fiber bundles, dispersion areas were counted if the

highlighter fluid sample had reached the top section of the fiber bundle the protrudes out from the modified cryovial prototype. Statistical analysis of the quantifiable results was performed using one-way ANOVA tests in the GraphPad Prism software.

Results and Discussion

Damage from Twisting

The polylactide material easily twisted immediately after printing, but began to show visible signs of damage at the higher twist tensions tested as seen in Figure 14. The nylon material was the easiest to twist immediately after printing, showing minimal signs of damage to the fiber bundle even at the highest twist tension tested due to its flexible nature.

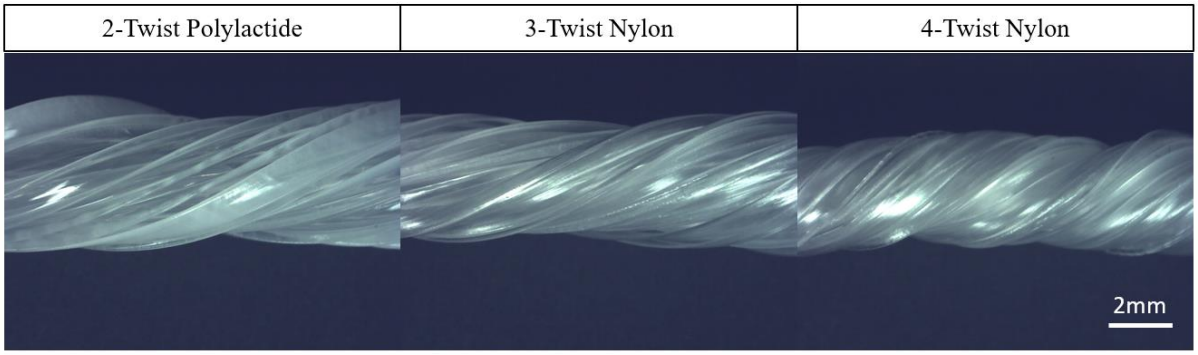

Figure 14. Stereoscope images of twisted polylactide and twisted nylon fiber bundles at various twist tensions for damage analysis. Damage is seen in the 2-twist polylactide fiber bundle as ridges and cracks in the material.

Highlighter Fluid Wicking

There was little to no variation in sample mass wicked into the fiber bundle system for each fiber bundle type tested. The twisted configuration improved wicking speed and sample dispersion for the untreated polylactide fiber bundles as shown in Figure 15. The twisted configuration also improved sample dispersion for the nylon fiber bundles and wicking speed was kept constant. When comparing the twisted polylactide to the twisted nylon fiber bundles, the twisted nylon fiber bundles wicked sample much faster and had a better average sample dispersion percentage

of 41% as compared to twisted polylactide's average sample dispersion percentage of 16%. Overall, the 4-twist nylon fiber bundle was the most promising in wicking time and sample dispersion for an untreated fiber bundle and will be used in further experimentation. Variability in wicking time and sample dispersion is likely due to inconsistencies in the cross section when extruding the fibers, inconsistencies introduced when bundling the fibers, as well as inconsistencies introduced when twisting the fiber bundle. Each of these factors have the potential to affect the surface area of contact between fibers within the fiber bundle that allow fluid sample to wick.

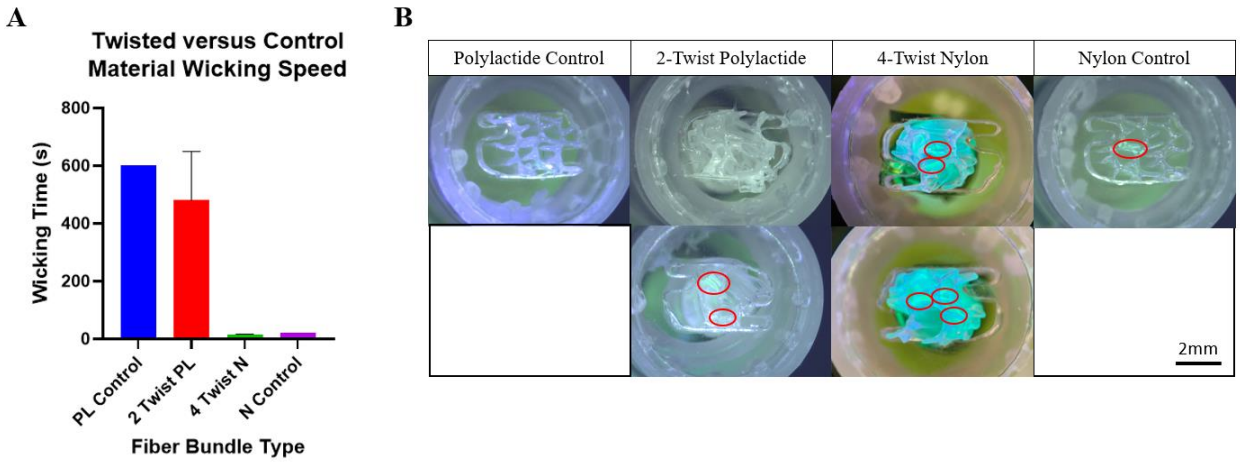

Figure 15. Measured metrics from 10-minute wicking study comparing twisted polylactide and twisted nylon to an untwisted polylactide and untwisted nylon control. (A) Compares sample wicking speed of twisted polylactide and twisted nylon fiber bundles against untwisted control fiber bundles. N=2 sample size for twisted fiber bundles. N=1 sample size for control fiber bundles. (B) Stereoscope images of the top fiber bundle cross sections showing sample dispersion after 10-minute wicking. Red circles indicate a sample dispersion area filled with sample. N=2 sample size for twisted fiber bundles. N=1 sample size for control fiber bundles.

Discussion

The beginning section of the chapter identified a promising fiber bundle prototype configuration to wick a fluid sample in under 10 minutes. This is a major improvement from the previously proposed passive transport system that took anywhere between 30 minutes to 24 hours to process the liquid sample[98,99]. A fiber bundle configuration was selected that maximized contact points

between the fibers within the bundle, while also minimizing the variability involved in creating the fiber bundles. Cross sectional images from previous wicking fiber bundle work showed variable cross-sectional shapes and inconsistent fiber bundle configurations, which is an issue this work successfully addressed[99]. It was shown that the larger E70 fiber size allowed for larger surface area contact points which resulted in an increased amount of fluid sample being wicked into the fiber bundle system, so subsequent experiments focused on the E70 fiber size. Due to the success of wicking fluid sample in under 10 minutes and the consistency of fiber bundle cross section shape and configuration, the E70 fiber bundle size and selected configuration was identified as the fiber bundle preparation for future experiments. It should be noted that there remains to be some inevitable variability in the extruded fiber cross section and bundling of the fiber bundles which leads to variability in wicking time, sample mass wicked, and sample dispersion percentage, however, the proposed solution minimized that variability.

The middle section of the chapter focused on increasing the wicking capabilities of the selected fiber bundle configuration using different fiber materials, chemical surface treatments, or a combination of the two methods. The hypothesis was by increasing the hydrophilicity of the fiber bundle, the fluid sample would wick faster and wick more sample to the top of the fiber bundle. Untreated fiber bundle materials like polylactide, polyethylene terephthalate glycol, and nylon wicked minimal sample to the top of the fiber bundle on their own, which is not ideal for the purposes of this work and did not confirm the initial hypothesis. However, when chemical surface treatments were used on the polylactide, polyethylene terephthalate glycol, and nylon fiber bundles, wicking speed, and amount of sample wicked both improved as hypothesized from the literature[111-124]. The dopamine chemical surface treatment had the most favorable wicking enhancements for each of the fiber materials tested, which did not directly match the initial

hypothesis. The dopamine surface treatment decreased each fiber material's water contact angle and wicking of fluid sample was seen for each fiber material tested in under 10 minutes. There was an observed trend that as the chemical surface treatment decreased the water contact angle, more sample dispersion was seen at the top of the fiber bundle. However, more work would need to be done to prove there was correlation, as the 2M sodium hydroxide surface treatment was the most hydrophilic, yet did not most greatly enhance wicking properties. Overall, dopamine-treated polylactide fiber bundles were shown to be the most promising for wicking speed and sample dispersion in this section of Chapter 2.

The later section of the chapter focused on finding an alternative modification to the fiber bundle system to enhance wicking capabilities while avoiding the time-consuming nature of chemical surface treatments. Here, it was hypothesized that decreasing the size of the capillary channels or increasing the amount of contact points between fibers within the fiber bundle system would increase both the wicking speed and amount of fluid sample wicked into the fiber bundle system. The Laplace equation describes capillary pressure and was used to form the hypothesis that wicking properties would be enhanced as capillary channel radii decreased[125-127]. Twisting the E70 fiber bundles to create smaller capillary channels and more contact points between fibers were tested for this purpose. The twisted fiber bundles proved to be successful in enhancing the wicking properties of the fiber bundle when compared to untreated fiber bundles that were not twisted. The most promising modified bundle was the 4-twist nylon fiber bundle. However, the wicking properties of the twisted fiber bundles did not outperform the wicking properties of the dopamine-treated polylactide fiber when comparing highlighter fluid data from each experiment, so cell separation will be testing in the two fiber bundle types in Chapter 4.

Limitations of using the modified wicking fiber bundles to process a sample include inconsistencies in printing during chemical surface treatment and during twisting. Printing inconsistencies involve variation in cross sectional dimensions that affect the contact points between fibers within the fiber bundle. Difficulties also arise with the Monoprice Maker Ultimate 3D printer experiencing system heating errors and cooling down mid-print. Changing print temperatures in the middle of printing fibers could affect the material properties of the fiber bundles and their wicking capabilities. Twisting the fiber bundles after printing also introduces variability from fiber bundle to fiber bundle. Some materials also experience damage to the fiber bundle when twisting. Further investigation is needed to understand if damage is happening on the inside of the fiber bundle that cannot be seen from the outside. Ideally, a process would be developed that would make the twisting of the fiber bundles more uniform when moving forward with this work. Chemical surface treatments are time consuming and can also be inconsistent if the chemical solution is not prepared following the same Standard Operating Procedure each time. Difficulties were seen with the dopamine treatment due to variable air flow and the chemical reaction not happening at the same speed during each treatment. Each of these factors introduce variability into the experiments and can be represented by the error in the results from this chapter.

Future work would ideally create a fiber bundle system that could process more of the fluid sample from the sample well. The most fluid sample pulled into the fiber bundle was 0.26 g of fluid throughout the fiber bundle experiments. This is approximately 26% of the 1 mL fluid sample mass, which includes the mass of fluid sample that is within the fiber bundle and has not been processed fully by the fiber bundle system. Because cancer cells within a FNA are present at lower concentrations, more of the fluid sample will need to be processed in order to detect

cancer cells within a 1 mL fluid sample. However, using a smaller FNA sample is more promising than the liquid biopsy sample since only 1-10 CTCs are present per mL of blood sample[13]. This means less sample will need to be taken from the patient during an appointment to achieve a diagnosis.

Conclusion

The conclusions of this chapter show that wicking capabilities can be enhanced by increasing the fiber bundle hydrophilicity through chemical surface treatments or by modifying the fiber bundle configuration. The E70 4-twist nylon fiber bundle had the fastest wicking time and most sample dispersion at the top of the fiber bundle for untreated fiber bundles tested. The E70 dopamine-treated polylactide fiber bundle had the fastest wicking time and most sample dispersion at the top of the fiber bundle overall. Future work will need to investigate a twisting procedure that allows for precise twist tension adjustment and introduces less variability to further enhance wicking capabilities of the fiber bundle system.

CHAPTER THREE

CAP BIOMATERIAL CHARACTERIZATION

Introduction

One common method of cancer diagnosis in the veterinary medicine field is by performing a fine needle aspirate on the lump of the animal and then roughly observing the sample on a prepared slide under a basic light microscope. Observation of the sample under the light microscope is not sufficient for a definitive diagnosis, so samples must be sent off for a pathology report[139]. The goal of this work is to design a simple, cheap, rapid diagnostic test that would not require primary care veterinarians to send the fine needle aspirate sample off to a specialty clinic for definitive results. An anonymous survey conducted and published in the Journal of Veterinary Medical Education reported that 99.4% of veterinarians surveyed had at least one light microscope available in their workplace, while 57.5% had access to an onsite diagnostic laboratory[140]. When considering almost half of primary veterinary care clinics have access to minimal diagnostic equipment, we must assume that veterinarians only have access to a basic light microscope when designing a new diagnostic test. For this reason, the ideal cap material for the proposed wicking fiber bundle prototype will collect the separated cell sample off the top of the fiber bundle and will be viewed clearly under a basic light microscope for cancer diagnosis.

In this chapter, we have investigated different types of cap materials for the wicking fiber bundle prototype with two objectives in mind: the first objective is to successfully collect cell sample from the top of the wicking fiber bundle device and the second objective is to clearly be able to view the cells under a microscope on the cap material. To achieve these objectives, the

first part of the chapter focuses on testing different types of materials for the cap application like gels, thin paper-based materials, and thick, absorbent materials. The middle part of the chapter focuses on testing a more solid polymer material for the cap application. Finally, the last part of the chapter focuses on testing an alginate gel material for the cap application and modifying the alginate cap preparation from that used in previous work[98].

In the first part of the chapter, sodium polyacrylate gel, Liqui Block 42K gel, Kim Wipe, sample pad, and western blot materials were tested for sample collection and cell visibility. Sample collection was tested through a series of wicking experiments with a highlighter fluid sample and then a mouse embryonic fibroblast (F3T3) cell sample. Cell visibility on the cap materials was tested by viewing cell samples that had been directly pipetted onto the cap material and by viewing cell samples on the cap materials that had been collected from the top of the wicking fiber bundle prototypes.

Following the assessment of different materials for the cap material application, a solid polymer disc was tested as the cap material for easier loading and unloading of the cap material from the wicking fiber bundle prototypes. Cell sample collection and cell visibility was tested through a mouse embryonic fibroblast (F3T3) cell sample wicking experiment.

Finally, the later part of this chapter tested an alginate gel material used as the cell collection cap material in previous work[98]. Hydrated, air-dried, and freeze-dried alginate gel cap materials were tested for sample collection and cell visibility. The air-dried and freeze-dried alginate gel cap materials were first tested for direct and indirect rehydration abilities with a highlighter fluid sample. Cell collection and cell visibility were then tested on the alginate gel cap materials once rehydration was confirmed by wicking cancerous human female breast, estrogen, and progesterone receptor (MCF-7) cell samples, human female mammary gland, pre-

neoplastic epithelial (MCF-10A) cell samples, and mouse embryonic fibroblast (F3T3) cell samples.

A summary of the cap material types tested, sample type used, and analysis methods are listed in Table 2.

Table 2. Summary of the cap material types tested, the sample type used to test the stated objectives, and the analysis methods used during testing.

Cap material type	Sample type	Analysis
Hydrated sodium polyacrylate	Highlighter fluid and mouse embryonic fibroblast (F3T3) cell sample.	Observation under blacklight and cell count under EVOS fluorescent light microscope.
Dehydrated sodium polyacrylate beads	Highlighter fluid	Observation under blacklight.
Liqui Block 42K gel	Highlighter fluid and mouse embryonic fibroblast (F3T3) cell sample.	Observation under blacklight and EVOS fluorescent light microscope.
Kim Wipe (filter paper)	Highlighter fluid and mouse embryonic fibroblast (F3T3) cell sample.	Observation under blacklight and cell count under EVOS fluorescent light microscope.
Sample pad	Highlighter fluid and mouse embryonic fibroblast (F3T3) cell sample.	Observation under blacklight and EVOS fluorescent light microscope.
Western blot	Highlighter fluid and mouse embryonic fibroblast (F3T3) cell sample.	Observation under blacklight and EVOS fluorescent light microscope.
Dopamine-treated polylactide mesh disc	Mouse embryonic fibroblast (F3T3) cell sample.	Observation and cell count under EVOS fluorescent light microscope.
Air-dried alginate gel	Highlighter fluid, cancerous human female breast, estrogen, and progesterone receptor (MCF-7) and mouse embryonic fibroblast (F3T3) cell sample.	Observation under blacklight and cell count under EVOS fluorescent light microscope.
Freeze-dried alginate gel	Highlighter fluid, cancerous human female breast, estrogen, and progesterone receptor (MCF-7) and mouse embryonic fibroblast (F3T3) cell sample.	Observation under blacklight and cell count under EVOS fluorescent light microscope.

Cell Visibility on Different Cap Material Types

Materials and Methods

Cap Material Preparation

Five different cap materials were prepared to assess cell visibility on the cap material. Hydrated sodium polyacrylate gel was prepared by soaking dehydrated sodium polyacrylate beads in DI water. Liqui Block 42K hydrated gel was also prepared by soaking the dehydrated beads in DI water. The sample pad material was taken from a Clearblue pregnancy test and cut into a square. The filter paper material was taken from a Kim Wipe and cut into a square of similar size to the sample pad material. Lastly, western blot paper was cut into a square, similar to that of the sample pad and filter paper materials for cap material use.

Cell Sample Preparation

Mouse embryonic fibroblast (F3T3) cells were used for the purposes of this experiment. One flask of mouse embryonic fibroblast (F3T3) cells was stained with Cell Tracker red stain and one flask was stained with Cell Tracker green stain to assess cell visibility with different stains on each cap material type.

Experiment Set-Up

Each cap material type was placed on a microscope slide for this experiment, along with a microscope slide with no cap material as the positive control. 20 uL of red stained cell sample and 20 uL of green stained cell sample was pipetted directly onto each cap material type as shown in Figure 16. The cap material was left to sit for 5 minutes, then flipped over on the microscope slide to be analyzed for cell visibility.

Figure 16. Cap materials with red and green stained mouse embryonic fibroblast (F3T3) cell sample. Cap materials appear as follows from left to right: positive control microscope slide, hydrated sodium polyacrylate gel, Liqui Block 42K gel, sample pad, filter paper, western blot material, and positive control fiber material.

Analysis

For cell visibility analysis, cap materials were viewed under the EVOS fluorescent light microscope using the green fluorescent protein 4X objective lens to view the green stained cells and the Texas Red 4X objective lens to view the red stained cells. Cell visibility was then assessed by observing how clearly cells could be seen on the cap material, and how hard it was to focus the microscope on the cells to do a potential cell count.

Results and Discussion

It was observed that the hydrated sodium polyacrylate gel material had the clearest view of cells, both red and green stained as shown in Figure 17. The Liqui Block 42K gel material more difficult to view cells on because the gel sample was more solidified and bulkier than the hydrated sodium polyacrylate. However, a general glow of stained cells could still be seen on the hydrated Liqui Block 42K gel. The sample pad was a dense, absorbent material that did not allow for the sample to disperse. Thus, the cell sample was very concentrated, and the stained cells were seen as a general glow as compared to individual cells that could be counted. The

filter paper is a thinner material, but it is very fibrous. Some individual clusters of cells could be seen, but other cell clusters were hidden by fibers of the filter paper, making the possible cell counts inconsistent. Lastly, the western blot material was like the sample pad material. The western blot material was dense and absorptive, limiting sample dispersion and leaving large clusters of fluorescing cells that made it difficult to differentiate individual cells for cell count. Overall, the hydrated sodium polyacrylate had the most promising cell visibility, followed by the filter paper material. Next, sample collection in each of the cap materials must be tested for efficacy at the top of the fiber bundle system.

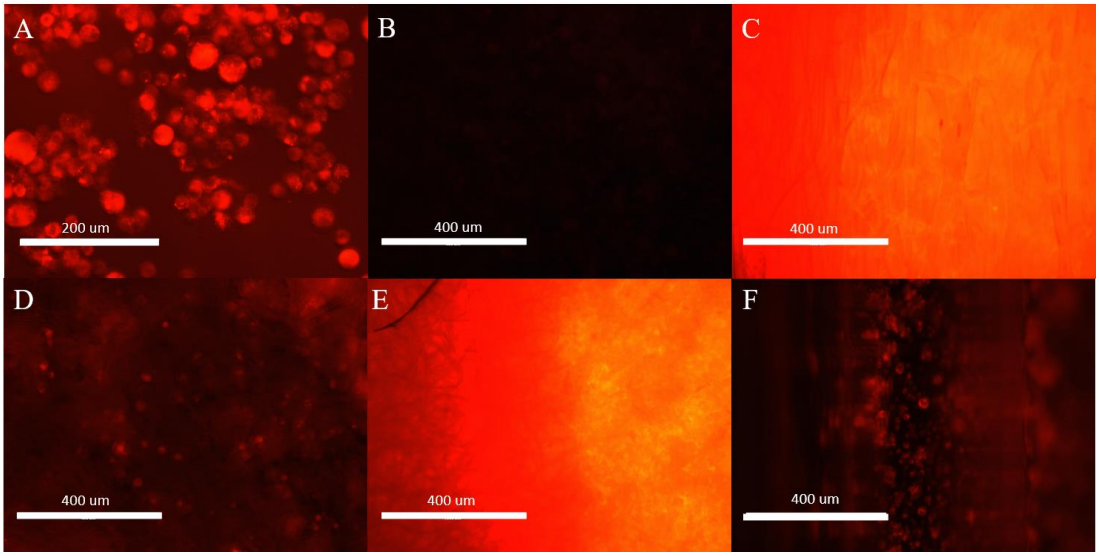

Figure 17. EVOS fluorescent light microscope images of Cell Tracker red mouse embryonic fibroblast (F3T3) cells fluorescing under the Texas Red lens on different material types. (A) Hydrated sodium polyacrylate gel under 20X objective lens. (B) Liqui Block 42K gel under 10X objective lens. (C) Sample pad material under a 10X objective lens. (D) Filter paper under a 10X objective lens. (E) Western blot material under a 10X objective lens. (F) Positive control polylactide fiber under 10X objective lens.

Highlighter Fluid Sample Collection with Different Cap Material Types

Materials and Methods

Fiber Preparation

Polylactide filament was extruded through a Monoprice Maker Ultimate 3D Printer at 210°C. Fibers had irregular cross-sectional dimensions of 3.33mm x 2.02mm and were defined as E70 sized fibers. Wicking fibers were laser cut into three individual fiber segments 35 mm in length. To enhance wicking properties, fiber segments were soaked in 10% Lysol for 15 minutes and left to air-dry for 15 minutes. Then, fiber segments were soaked in 70% ethanol for 15 minutes and left to air-dry for 15 more minutes.

Cap Material Preparation

Four different cap materials were prepared to assess sample collection and absorption on the cap material when wicked in the wicking fiber bundle prototype. Hydrated sodium polyacrylate gel was prepared by soaking dehydrated sodium polyacrylate beads in DI water. Sodium polyacrylate beads were crushed up with a mortar and pestle before hydrating with DI water, which resulted in a more consistent textured gel material. Small samples of the hydrated sodium polyacrylate gel were then transferred to the area surrounding the top of the fiber bundle on the top of the wicking fiber bundle prototype as pictured in Figure 18. Dehydrated sodium polyacrylate beads were also tested in this experiment. The polyacrylate beads were loaded directly into the top portion of the wicking fiber bundle prototype around the top section of the fiber bundle. The sample pad material was cut in a circular shape to fit on top of the wicking fiber bundle prototype from a Clearblue pregnancy test. Lastly, a circle was cut from a Kim Wipe for the filter paper material that fit onto the top of the wicking fiber bundle prototype to be tested.

Figure 18. Dehydrated sodium polyacrylate (left) and hydrated sodium polyacrylate (right) loaded into the top of the wicking fiber bundle prototype.

Wicking Experiment Set-Up

One wicking fiber bundle prototype for each cap material type was prepared in the modified cryovial prototype for the wicking experiment. Cap materials were loaded directly on top of the top section of the fiber bundle at the top of the prototype device. Highlighter fluid sample was prepared by soaking one Sharpie Highlighter marker stick in 500 mL of deionized water for 24 hours and stored in a 500 mL glass bottle. 1 mL of highlighter fluid sample was loaded in the sample well of the modified cryovial prototype for wicking. Wicking time began when the fiber bundles were placed in the prototype sample well and were allowed to wick for 10 minutes. After 10 minutes of wicking was complete, the cap materials were removed from the top of the wicking fiber bundle prototype and placed onto a microscope slide for absorption analysis.

Analysis

Sample collection and absorption was analyzed using a blacklight flashlight to fluoresce the highlighter fluid sample on the cap material post-wicking. Images of the fluorescing sample on each cap material were captured with an iPhone 8 camera.

Results and Discussion

The Kim Wipe and sample pad materials had loose contact with the top of the fiber bundle and were not secured onto the prototype, so no sample was absorbed into the Kim Wipe or sample pad materials as shown in Figure 19A. When light pressure was applied with tweezers to increase the contact between the Kim Wipe and sample pad materials and the top of the fiber bundles, highlighter fluid sample was immediately absorbed off the top of the fibers and into the cap material. The dehydrated sodium polyacrylate beads proved difficult to load and unload from the wicking fiber bundle prototype, however, they did absorb highlighter fluid sample if they were in direct contact with the top section of the fiber bundle. The hydrated sodium polyacrylate was also difficult to load and unload from the wicking fiber bundle prototype, however, this material absorbed the highlighter fluid very well and was easier to handle than the dehydrated sodium polyacrylate beads. Overall, the hydrated sodium polyacrylate and the Kim Wipe materials had the best highlighter fluid absorption at the top of the wicking fiber bundle prototype as shown in Figure 19B. For the gel materials to be functional as the wicking fiber bundle prototype cap material, a new design is needed to aid in the loading and unloading of the material. A new design will also be needed to secure the paper-based materials onto the top of the fiber bundle system. Next, cell sample collection off the top of the wicking fiber bundle will need to be tested.

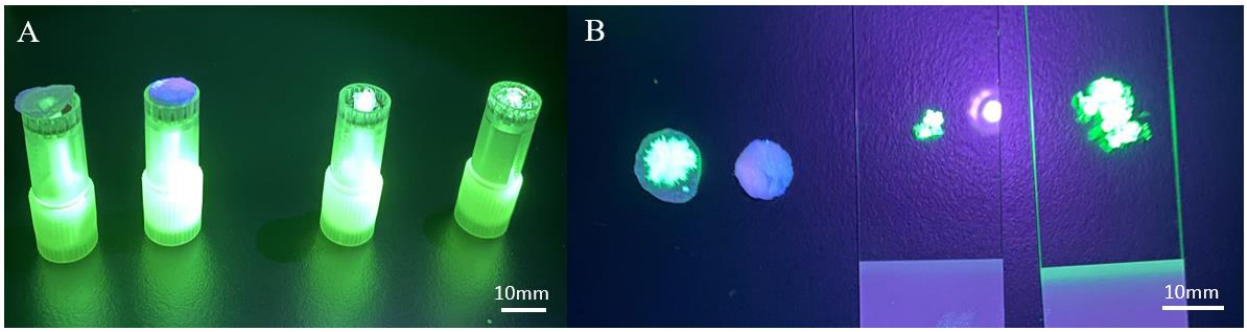

Figure 19. Highlighter fluid sample wicking. (A) Wicking fiber bundle prototypes during the 10-minute wicking period. (B) Cap materials after being removed from the wicking fiber bundle prototype post-wicking from left to right: Kim Wipe, sample pad, dehydrated sodium polyacrylate, and hydrated sodium polyacrylate material.

Cell Sample Collection with Different Cap Material Types

Materials and Methods

Fiber Preparation

Polylactide filament was extruded through a Monoprice Maker Ultimate 3D Printer at 210°C. Fibers had irregular cross-sectional dimensions of 3.33mm x 2.02mm and were defined as E70 sized fibers. Wicking fibers were laser cut into three individual fiber segments 35 mm in length. To enhance wicking properties, fiber segments were soaked in 10% Lysol for 15 minutes and left to air-dry for 15 minutes. Then, fiber segments were soaked in 70% ethanol for 15 minutes and left to air-dry for 15 more minutes.

Cap Material Preparation

Two different cap materials were prepared to assess sample collection and cell visibility on the cap material when wicked in the wicking fiber bundle prototype. Hydrated sodium polyacrylate gel was prepared by soaking dehydrated sodium polyacrylate beads in DI water. Sodium polyacrylate beads were crushed up with a mortar and pestle before hydrating with DI water, which resulted in a more consistent textured gel material. Small samples of the hydrated sodium polyacrylate gel were then transferred to the area surrounding the top of the fiber bundle on the

top of the wicking fiber bundle prototype. For the Kim Wipe filter paper material, a circle was cut from a Kim Wipe that fit onto the top of the wicking fiber bundle prototype to be tested.

Cell Sample Preparation

Mouse embryonic fibroblast (F3T3) cells were used for the purposes of this experiment. One T-150 flask of mouse embryonic fibroblast (F3T3) cells was stained with Cell Tracker red stain to assess sample collection and cell visibility with different cap material types. Mouse embryonic fibroblast (F3T3) cells were resuspended in 7 mL of PBS following centrifugation for wicking. The cell count was 1.96×10^6 cells/mL.

Wicking Experiment Set-Up

Three wicking fiber bundle prototypes for each cap material type was prepared in the modified cryovial prototype for the wicking experiment. A new cap was used that encased the cap material between two clear acrylic rings as shown in Figure 20. Cap materials were loaded directly into the new cap, secured with a clear acrylic ring, and placed on top of the fiber bundle at the top of the prototype device. 1 mL of mouse embryonic fibroblast (F3T3) cell sample was placed in the sample well of each wicking fiber bundle prototype for wicking. Wicking time began when the fiber bundles were placed in the prototype sample well. Wicking fiber bundle prototypes were allowed to wick for 5 minutes. After wicking was complete, the caps were removed from the top of the wicking fiber bundle prototype for cell count. Cap materials were soaked in 1 mL of PBS to rinse the cells from the cap, and 10 uL of the resulting solution was used for the cell count. Positive control cap materials were also analyzed by soaking the cap material in 0.25 mL of cell sample, then removing from the solution for analysis. Fiber bundles were frozen in the -20°C freezer post-wicking to assess cell wicking throughout the fiber bundle that will be further discussed in Chapter 4.

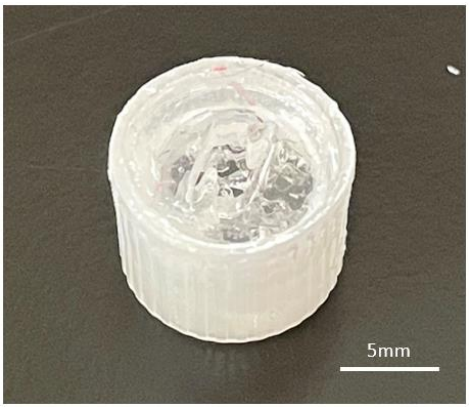

Figure 20. New cap design that encapsulates gel material into the cap for easier loading and unloading from the wicking fiber bundle prototype.

Analysis

Sample collection was analyzed using the hemocytometer for cell count under the EVOS fluorescent light microscope. Cell visibility was analyzed using the EVOS fluorescent light microscope Texas Red 4X and 10X objective lens. Statistical analysis of the quantifiable results was performed using a t-test in the GraphPad Prism software.

Results and Discussion

The Kim Wipe cap material had more cells on average in the rinse solution that was used for the cell count than the hydrated sodium polyacrylate solution, however, was not significant as seen in Figure 21A. The hydrated sodium polyacrylate material had much better cell visibility on the cap material itself as seen in the cap material images in Figure 21B. With the goal being to view and analyze the cell sample on the cap material itself, paper-based materials were ruled out as a contender for the cap material. The new cap design for the gel cap materials had better contact with the top of the fiber bundle system as well as loading and unloading capabilities. However, the gel material still had to be removed from the cap in order to view the cells under the microscope. This was not an effective method for cell sample collection and analysis, so a more solid cap material that has good contact with the top of the fiber bundle and can be easily loaded

and unloaded from the wicking fiber bundle prototype is needed. Variability in the cell counts from the cap material rinse solution could be attributed to fluorescing debris within the PBS rinse, gel material fluorescence in the sodium polyacrylate, or fragmented cells from unloading the sodium polyacrylate gel with tweezers off the top of the prototype.

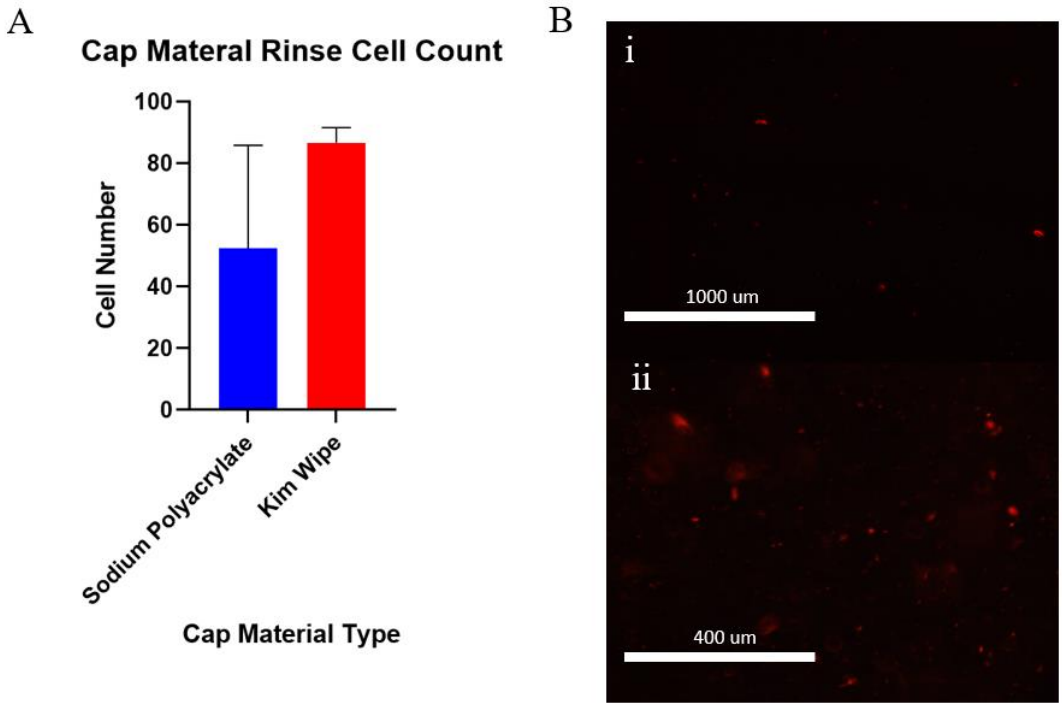

Figure 21. Results of the mouse embryonic fibroblast (F3T3) cell sample wicking after 5 minutes. (A) Cell counts from the cap material rinse solution for the sodium polyacrylate and Kim Wipe materials. N=3 sample size. (B) EVOS fluorescent light microscope images of the cap material for the (i) Kim Wipe cap material under a Texas Red 4X objective lens and (ii) hydrated sodium polyacrylate cap material under a Texas Red 10X objective lens.

Cell Sample Collection with Dopamine-Treated Mesh Cap Material

Materials and Methods

Fiber Preparation

Polylactide filament was extruded through a Monoprice Maker Ultimate 3D Printer at 210°C. Fibers had irregular cross-sectional dimensions of 3.33mm x 2.02mm and were defined as E70

sized fibers. Wicking fibers were laser cut into three individual fiber segments 35 mm in length. To enhance wicking properties, fiber segments were treated in a dopamine solution.

Cap Material Preparation

Dopamine-treated mesh polylactide discs were used as the cap for the purposes of this experiment. Polylactide mesh discs were printed using the Monoprice Maker Ultimate 3D Printer at 210°C. The discs were then placed in a dopamine solution for treatment.

Chemical Surface Treatment

The dopamine surface treatment solution was made by combining a 10mM Tris-HCl buffer solution with dopamine powder. To prepare the Tris-HCl buffer solution, 7.84g of tris powder was added to 450 mL of DI water in a beaker. Four NaOH pellets were then dissolved in 30 mL of DI water and added dropwise into the 450 mL tris solution. The tris-HCl buffer was then diluted with DI water to a total volume of 500 mL. To make the dopamine solution, 0.4g of dopamine was added to 100 mL of tris-HCl buffer solution and dissolved. Direct airflow, 45°C heat, and a stir bar at 400 rpm were then added into the 100 mL dopamine solution to enhance the reaction. Fibers and discs were treated in the dopamine solution for 40 minutes. After treatment, fibers and discs were rinsed with DI water and patted dry with gauze.

Cell Sample Preparation

Mouse embryonic fibroblast (F3T3) cells were used for the purposes of this experiment. One T-150 flask of mouse embryonic fibroblast (F3T3) cells was stained with DAPI stain to assess sample collection and cell visibility with different cap material types. Mouse embryonic fibroblast (F3T3) cells were resuspended in 7 mL of PBS following centrifugation for wicking. The initial cell count using the Cell Scepter was 1.7×10^6 cells/mL.

Wicking Experiment Set-Up

Six wicking fiber bundle prototypes for with the dopamine-treated mesh disc cap were prepared in the modified cryovial prototype for the wicking experiment. The dopamine-treated mesh disc was placed on top of the fiber bundle at the top of the wicking fiber bundle prototype device as shown in Figure 22. 1 mL of mouse embryonic fibroblast (F3T3) cell sample was placed in the sample well of each wicking fiber bundle prototype for wicking. Wicking time began when the fiber bundles were placed in the prototype sample well. Three wicking fiber bundle prototypes were allowed to wick for 10 minutes, while the other three wicking fiber bundle prototypes were allowed to wick for 20 minutes. After wicking was complete, the dopamine-treated mesh discs were removed from the top of the wicking fiber bundle prototype and placed on a microscope slide for cell count. Positive and negative control dopamine-treated mesh discs were also analyzed.

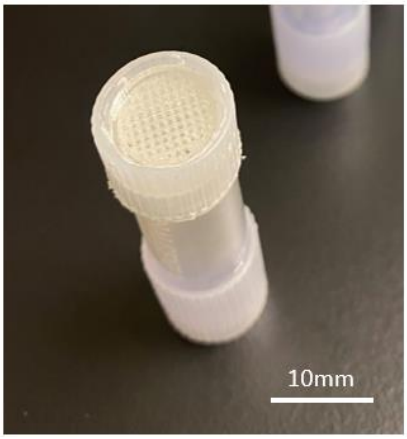

Figure 22. Dopamine-treated polylactide mesh cap loaded into the top of the wicking fiber bundle prototype.

Analysis

Sample collection was analyzed using a manual cell count of cells within the grid-like structure of the dopamine-treated mesh disc under the EVOS fluorescent light microscope. Cell particles were only counted if they were within the mesh disc structure, not if they had moved outside of

the mesh disc once placed on the microscope slide. Cell particles were also not counted in the cell count if they were found on the mesh disc material. Cell visibility was also analyzed using the EVOS fluorescent light microscope 4X and 10X objective lenses with the transmitted and DAPI filters. Statistical analysis of the quantifiable results was performed using a t-test in the GraphPad Prism software.

Results and Discussion

The cell visibility on the dopamine-treated mesh discs was better in comparison to previously tested cap materials, since the gaps in the mesh disc provided for clear viewing of the cells. However, the mesh disc material also blocked some cells from being seen because the material is solid. The dopamine-treated mesh disc material also fluoresced the DAPI blue light, making it more difficult to see cells that were located on the mesh disc material. Few fluorescing particles were seen on the negative control mesh disc as seen in Figure 23. However, they were all on the mesh disc material itself, so fluorescing particles on the mesh disc were not included in the cell counts. While the dopamine-treated polylactide mesh disc was easier to load and unload from the wicking fiber bundle prototype, the cap material did not contain wicked cells within the cap material well and did not make consistent contact with the top of the fiber bundle. For this reason, gel cap materials will be revisited with an effort to create a more solidified gel material that has consistent contact with the top of the wicking fiber bundle.

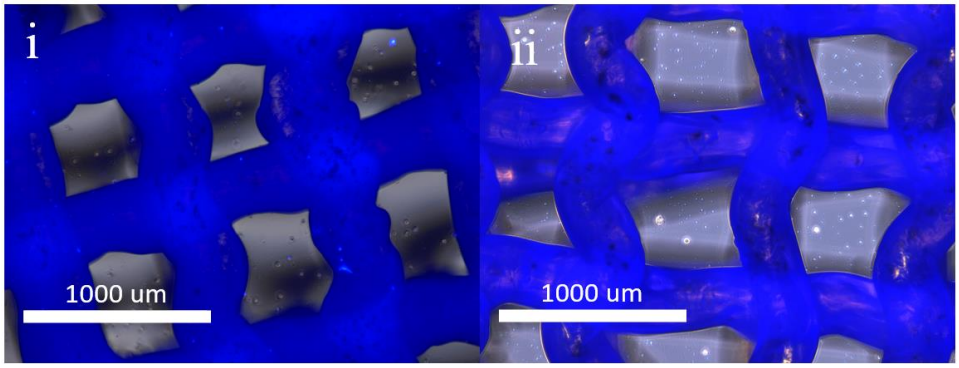

Figure 23. EVOS fluorescent light microscope images of the dopamine-treated polylactide mesh cap material (i) negative control and (ii) after 10 minutes of wicking mouse embryonic fibroblast (F3T3) cells under an overlay of DAPI blue and transmitted 4X objective lenses.

Air-Dried Alginate Cap Material Sample Rehydration Proof of Concept

Materials and Methods

Fiber Preparation

Nylon filament was extruded through a Monoprice Maker Ultimate 3D Printer at 245°C. Fibers had irregular cross-sectional dimensions of 3.33mm x 2.02mm and were defined as E70 sized fibers. Wicking fibers were laser cut into three individual fiber segments 35 mm in length. Immediately after the laser cutting process, nylon fiber bundles were twisted. Three 35 mm nylon fiber segments were configured into a bundle and secured on one end of the bundle with a clear acrylic prototype ring. The other end of the fiber bundle was then secured in the chuck of an electric drill. The nylon fiber bundle was twisted four rotations with the electric drill, then held in that position for 60 seconds to solidify the twisted configuration.

Cap Material Preparation

The alginate gel cap material was prepared by dip coating one end of the fiber bundles in two solutions: a calcium chloride solution and a sodium alginate solution. A 10 mL calcium chloride solution was made by dissolving 5.55 g of calcium chloride granules to 10 mL of DI water. The sodium alginate solution was made by dissolving 0.09 g of reagent grade sodium chloride in 10

mL of DI water. After the sodium chloride was dissolved, 0.14 g of alginic acid sodium salt from brown algae was dissolved in the sodium chloride solution to make to sodium alginate solution. The top 2 mm of the fiber bundles were then carefully dipped in the calcium chloride solution and immediately removed. The same 2 mm end of the fiber bundles were then dipped into the sodium alginate solution and immediately removed, forming the alginate gel cap. The fiber bundles were then left out on the benchtop to air-dry the cap materials for 60 minutes.

Cell Sample Preparation

Cancerous human female breast, estrogen, and progesterone receptor (MCF-7) cells and mouse embryonic fibroblast (F3T3) cells were used for the purposes of this experiment. One T-25 flask of cancerous human female breast, estrogen, and progesterone receptor (MCF-7) cells was stained with Cell Tracker red stain and one T-25 flask of mouse embryonic fibroblast (F3T3) cells was stained with Cell Tracker green stain to visually see the cells on the alginate cap material. Both cell types were resuspended in 3 mL of PBS following centrifugation for wicking. The initial cell count using the hemocytometer was 1.2×10^6 cells/mL for the cancerous human female breast, estrogen, and progesterone receptor (MCF-7) cells and 3.0×10^5 cells/mL for the mouse embryonic fibroblast (F3T3) cells. To have equal concentrations of cancerous human female breast, estrogen, and progesterone receptor (MCF-7) cells to mouse embryonic fibroblast (F3T3) cells, 200 uL of cancerous human female breast, estrogen and progesterone receptor (MCF-7) cell sample and 800 uL of mouse embryonic fibroblast (F3T3) sample was added into the sample well for mixed cell wicking. For cancerous human female breast, estrogen, and progesterone receptor (MCF-7) only wicking, 200 uL of cell sample was added to the sample well and 800 uL of PBS was added to bring the total volume to 1 mL. For mouse embryonic fibroblast (F3T3) only wicking, 800 uL of cell sample was added to the sample well and 200 uL

of PBS was added to bring the total volume up to 1 mL. The estimated total cell number in 800 uL of mouse embryonic fibroblast (F3T3) cells and of 200 uL of cancerous human female breast, estrogen, and progesterone receptor (MCF-7) cells was 2.4×10^5 cells.

Wicking Experiment Set-Up

Five wicking fiber bundle prototypes were prepared in the modified cryovial prototype for the highlighter fluid and cell sample wicking experiments. Highlighter fluid sample was prepared by soaking one Sharpie Highlighter marker stick in 500 mL of deionized water for 24 hours and stored in a 500 mL glass bottle. 1 mL of highlighter fluid sample was loaded into two of the sample wells of the modified cryovial prototype for wicking. One fiber bundle had an air-dried alginate cap and one fiber bundle had no cap for comparison. For cell sample wicking, three fiber bundles were prepared with an air-dried alginate cap: one fiber bundle for cancerous human female breast, estrogen, and progesterone receptor (MCF-7) wicking, one fiber bundle for mouse embryonic fibroblast (F3T3) wicking, and one fiber bundle for mixed cell wicking. Cell sample was prepared in the sample well for each fiber bundle as outlined under Cell Sample Preparation. Highlighter fluid sample was allowed to wick for 10 minutes and cell sample was allowed to wick for 20 minutes. After wicking was complete, the air-dried alginate caps were removed from the top of the wicking fiber bundle prototype and placed on a microscope slide for analysis as shown in Figure 24.

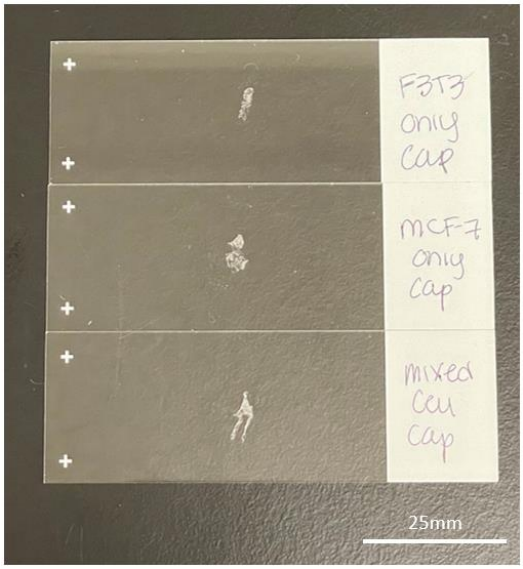

Figure 24. Air-dried alginate cap materials after being removed from the top of the wicking fiber bundle prototypes at the 20-minute wicking time point.

Analysis

Highlighter Fluid Wicking

Sample absorption was analyzed using a blacklight flashlight to fluoresce the highlighter fluid sample on the cap material post-wicking. Images of the fluorescing sample at the top of the wicking fiber bundle prototype were captured under the stereoscope with an iPhone 12 Pro camera.

Cell Sample Wicking

Cell wicking and collection was analyzed by viewing the alginate cap material on the microscope slide under the EVOS fluorescent light microscope. The transmitted, Texas Red, and GFP 10X objective lenses were used for cell viewing.

Results and Discussion

Highlighter Fluid Wicking

The fiber bundle with the air-dried alginate cap wicked the highlighter fluid sample 30 seconds slower than the fiber bundle without a cap. The fiber bundle with no cap also wicked 0.5 g of

highlighter fluid sample more than the fiber bundle with the air-dried alginate cap. However, both fiber bundles successfully wicked highlighter fluid sample to the top of the fiber bundle as shown in Figure 25. The fiber bundle with the air-dried alginate cap successfully rehydrated the cap material with highlighter fluid sample, which was the goal of this proof-of-concept experiment. The rehydration of the cap material proves there is consistent contact between the wicking fiber bundle and air-dried alginate cap material because highlighter fluid sample was successfully absorbed. This is likely because the alginate cap material is formed directly onto the end of the wicking fiber bundle. It was also shown that the dried alginate cap material can be easily removed from the top of the fiber bundle as a thin, flat, singular piece in Figure 24, which is promising for cell viewing and analysis under a microscope.

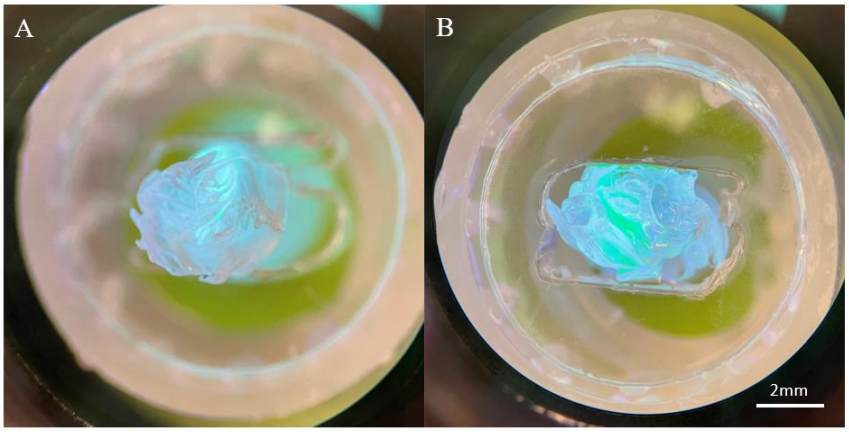

Figure 25. Stereoscope images of wicking fiber bundle cross sections after 10 minutes of highlighter fluid wicking. (A) Wicking fiber bundle without a cap material. (B) Wicking fiber bundle with the air-dried alginate cap material after the air-dried alginate material had been removed.

Cell Sample Wicking

There were no quantifiable results for this proof-of-concept experiment, however, the air-dried alginate cap material successfully rehydrated with the amount of cell sample wicked over the 20-minute time period in each fiber bundle tested. The rehydrated alginate cap material was able to be removed from the top of the fiber bundle in one piece and cells could be easily viewed on the

cap material. The cancerous human female breast, estrogen, and progesterone receptor (MCF-7) only fiber bundle alginate cap material was populated with red fluorescing cells, while the mouse embryonic fibroblast (F3T3) only fiber bundle alginate cap material had minimal green fluorescing cells as seen in Figure 26. The mixed cell sample fiber bundle alginate cap material revealed similar results. This observation is promising for the purposes of cell type separation that will be further discussed in Chapter 4. Next, a freeze-dried alginate cap material will be tested to see if the further dehydration of the gel increases the amount of cell sample wicked into the cap material.

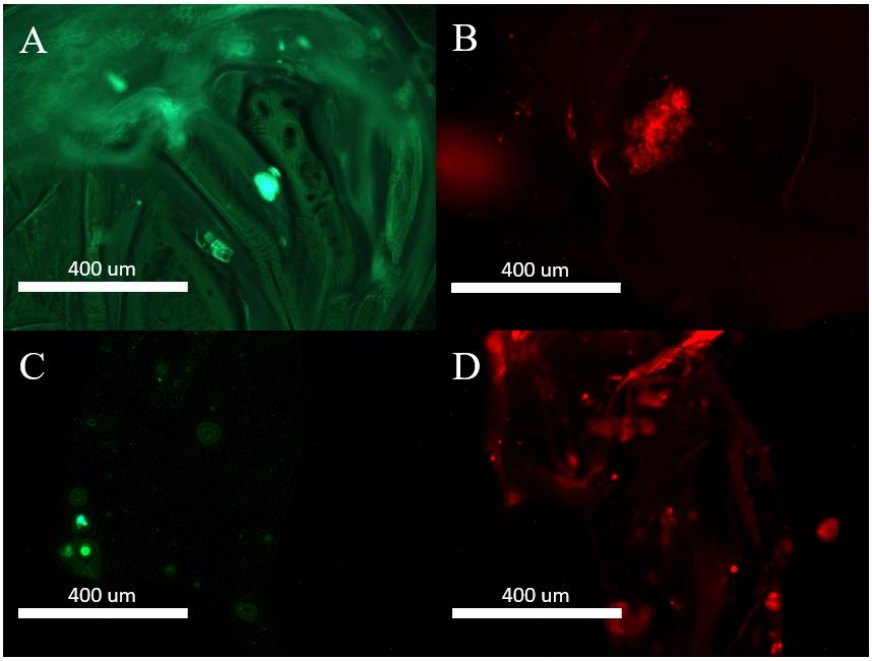

Figure 26. EVOS fluorescent light microscope images of air-dried alginate cap materials after 20 minutes of cell wicking. (A) Mouse embryonic fibroblast (F3T3) cells under GFP 10X objective lens on the F3T3 only wicking fiber bundle cap material. (B) Cancerous human female breast, estrogen, and progesterone receptor (MCF-7) cells under Texas Red 10X objective lens on the MCF-7 only wicking fiber bundle cap material. (C) Mouse embryonic fibroblast (F3T3) cells under GFP 10X objective lens on the mixed cell sample wicking fiber bundle cap material. (D) Cancerous human female breast, estrogen, and progesterone receptor (MCF-7) cells under Texas Red 10X objective lens on the mixed cell sample wicking fiber bundle cap material.

Freeze-Dried Alginate Cap Material Sample Collection with Different Fiber Bundle Types

Materials and Methods

Fiber Preparation

Polylactide filament was extruded through a Monoprice Maker Ultimate 3D Printer at 210°C. Nylon filament was extruded through a Monoprice Maker Ultimate 3D Printer at 245°C. Fibers had irregular cross-sectional dimensions of 3.33mm x 2.02mm and were defined as E70 sized fibers. Wicking fibers were laser cut into three individual fiber segments 35 mm in length. Nylon fiber bundles were twisted immediately following the laser cutting process. Three 35 mm nylon fiber segments were configured into a bundle and secured on one end of the bundle with a clear acrylic prototype ring. The other end of the fiber bundle was then secured in the chuck of an electric drill. The nylon fiber bundle was twisted four rotations with the electric drill, then held in that position for 60 seconds to solidify the twisted configuration. Half of 4-twist nylon fiber bundles were placed in the -80ºC freezer for 5 minutes, then removed and cut approximately 2 mm from the top of the fiber bundle with a razor blade to expose the most twisted portion of the fiber bundle for cap preparation as shown in Figure 27. The other half of the 4-twist nylon fiber bundles were left as they were originally prepared. The polylactide fiber bundles were treated in a dopamine solution for 40 minutes to increase fiber bundle hydrophilicity.

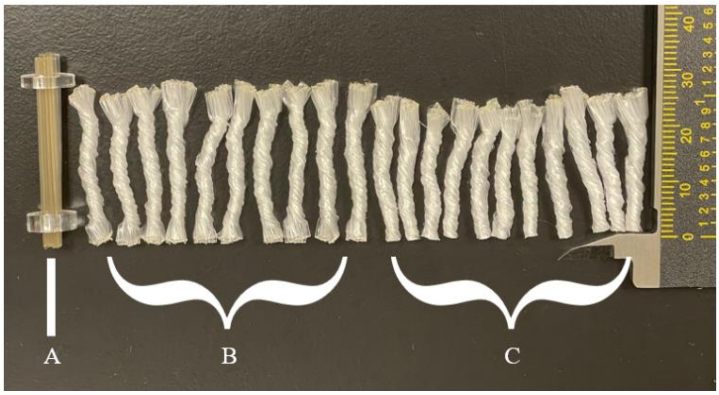

Figure 27. Wicking fiber bundles prepared before the addition of the air-dried or freeze-dried alginate cap material. (A) Dopamine-treated polylactide fiber bundles result in 35mm fiber length. (B) 4-twist nylon fiber bundles result in 30mm fiber length. (C) 4-twist nylon cut approximately 2 mm from the top of the fiber bundle to expose the inner most twisted portion of the fiber bundle result in approximately 27mm fiber length.

Cap Material Preparation

The alginate gel cap material was prepared by dip coating one end of the fiber bundles in two solutions: a calcium chloride solution and a sodium alginate solution. A 10 mL calcium chloride solution was made by dissolving 5.55 g of calcium chloride granules to 10 mL of DI water. The sodium alginate solution was made by dissolving 0.09 g of reagent grade sodium chloride in 10 mL of DI water. After the sodium chloride was dissolved, 0.14 g of alginic acid sodium salt from brown algae was dissolved in the sodium chloride solution to make to sodium alginate solution. The top 2 mm of the fiber bundles were then carefully dipped in the calcium chloride solution and immediately removed. The same 2 mm end of the fiber bundles were then dipped into the sodium alginate solution and immediately removed, forming the alginate gel cap. Half of the fiber bundles were left out on the benchtop to air-dry the cap materials for 60 minutes. The other half of the fiber bundles were placed in the -80ºC freezer to preserve the cap material structure until they could be transferred to a freeze dryer at another location for freeze drying.

Chemical Surface Treatment

The dopamine surface treatment solution was made by combining a 10mM Tris-HCl buffer solution with dopamine powder. To prepare the Tris-HCl buffer solution, 7.84g of tris powder was added to 450 mL of DI water in a beaker. Four NaOH pellets were then dissolved in 30 mL of DI water and added dropwise into the 450 mL tris solution. The tris-HCl buffer was then diluted with DI water to a total volume of 500 mL. To make the dopamine solution, 0.4g of dopamine was added to 100 mL of tris-HCl buffer solution and dissolved. Direct airflow, 45°C heat, and a stir bar at 400 rpm were then added into the 100 mL dopamine solution to enhance the reaction. Fibers were treated in the dopamine solution for 40 minutes. After treatment, fibers were rinsed with DI water and patted dry with gauze.

Cell Sample Preparation

Cancerous human female breast, estrogen, and progesterone receptor (MCF-7) cells were used for the purposes of this experiment. One T-75 flask of cancerous human female breast, estrogen, and progesterone receptor (MCF-7) cells was stained with Cell Tracker red stain to assess cell wicking and collection capabilities with different cap material and fiber bundle types. Cancerous human female breast, estrogen, and progesterone receptor (MCF-7) cells were resuspended in 13 mL of DI water following centrifugation for wicking. The initial cell count using the hemocytometer was 1.2×10^5 cells/mL.

Wicking Experiment Set-Up

Two wicking fiber bundle prototypes were prepared for highlighter fluid wicking and for cancerous human female breast, estrogen, and progesterone receptor (MCF-7) cell wicking per fiber bundle type and cap preparation in the modified cryovial prototype. Highlighter fluid sample was prepared by soaking one Sharpie Highlighter marker stick in 500 mL of deionized

water for 24 hours and stored in a 500 mL glass bottle. 1 mL of highlighter fluid sample was loaded in the sample well of the modified cryovial prototype for wicking. For cell sample wicking, 1 mL of cancerous human female breast, estrogen, and progesterone receptor (MCF-7) cell sample was loaded in the sample well of the modified cryovial prototype. Wicking time began when the fiber bundles were placed in the prototype sample well. Highlighter fluid was allowed to wick for 10 minutes and cell sample was allowed to wick for 60 minutes. After wicking was complete, the cap materials were removed from the top of the wicking fiber bundle prototype with tweezers and placed onto a microscope slide for analysis.

Analysis

Highlighter Fluid Wicking

Sample absorption was analyzed using a blacklight flashlight to fluoresce the highlighter fluid sample on the cap material post-wicking. Images of the fluorescing sample on each cap material were captured with an iPhone 12 Pro camera for comparison.

Cell Sample Wicking

Cell wicking and collection was analyzed by viewing the alginate cap material on the microscope slide under the EVOS fluorescent light microscope. The transmitted and Texas Red 10X objective lenses were used for cell viewing. Three images were taken in the most cell dense areas of the alginate cap material for cell count purposes. Statistical analysis of the quantifiable results was performed using two-way ANOVA tests in the GraphPad Prism software.

Results and Discussion

Highlighter Fluid Wicking

The dopamine-treated polylactide fiber bundles wicked the most highlighter fluid sample into the cap material in both the freeze-dried and air-dried alginate cap material groups as seen in Figure

28. The normal 4-twist and cut 4-twist nylon fiber bundles had minimal sample wicked into the alginate cap material in both the freeze-dried and air-dried alginate cap material groups. While minimal sample was observed in the nylon fiber bundle alginate material caps, the alginate cap material was rehydrated, indicating that some sample had to come into contact with the alginate cap material during the 10-minute wicking process. Overall, the air-dried alginate cap material seemed to collect more sample in the dopamine-treated polylactide fiber bundles than the freeze-dried alginate cap material did. Sample collection will be further tested in the cell sample wicking experiment.

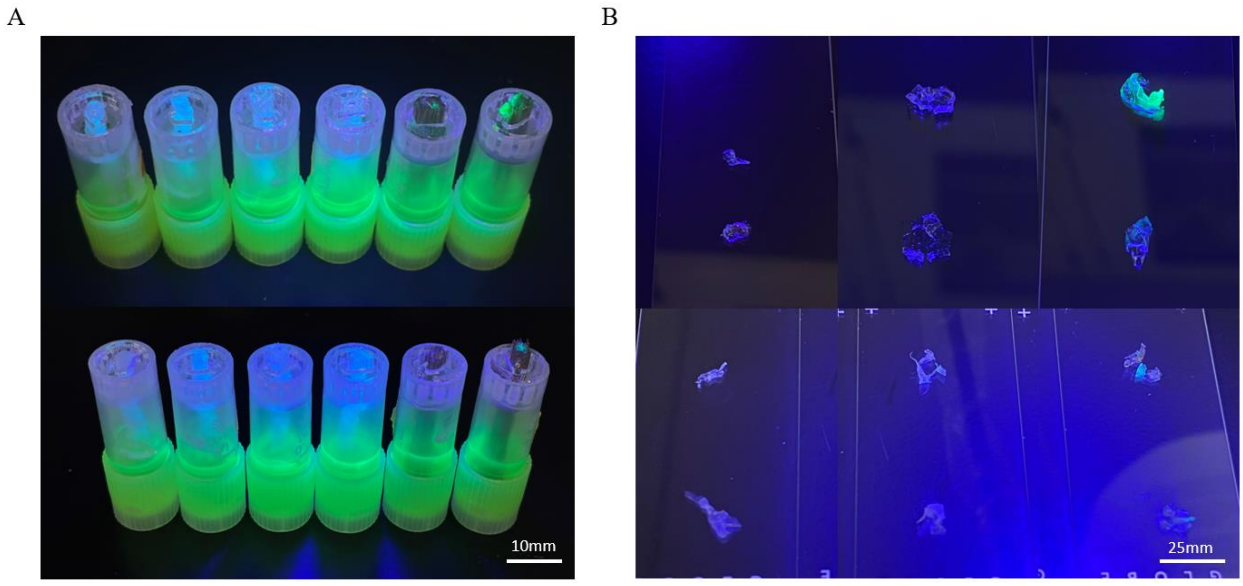

Figure 28. Images of the wicking fiber bundle prototypes and alginate cap materials after 20 minutes of highlighter fluid sample wicking. (A) Wicking fiber bundle prototypes with air-dried alginate cap materials (top) and freeze-dried alginate cap materials (bottom) nearing the end of the 20-minute wicking period. There were two wicking fiber bundle prototypes per fiber bundle type from left to right as follows: cut 4-twist nylon, normal 4-twist nylon, and dopamine-treated polylactide. (B) Air-dried alginate cap materials (top) and freeze-dried alginate cap materials (bottom) after being removed from the wicking fiber bundle prototype after 20 minutes of sample wicking. Two cap materials per fiber bundle type were analyzed from left to right as follows: cut 4-twist nylon, normal 4-twist nylon, and dopamine-treated polylactide.

Cell Sample Wicking

The dopamine-treated polylactide fiber bundles had the highest cell counts in both the air-dried and freeze-dried alginate cap material groups as shown in Figure 29A. Two-way ANOVA statistical analysis showed significant difference in cell count by both cap type ($F(1,12)=12.38$, $p<0.0042$) and by fiber bundle type ($F(2,12)$, $p<0.0094$), though the interaction between the two variables was not significant. Variability could be attributed to fluorescing debris on the cap material and the cap material itself fluorescing or folding which inhibits cells visibility. When considering cell visibility, the air-dried alginate cap material had better cell visibility than the freeze-dried alginate cap material did as shown in Figure 29B. However, as the air-dried alginate cap material sat on the benchtop and fluid began to evaporate from the cap material, sodium chloride crystals and a type of calcium crystal began to form, decreasing the cell visibility on the air-dried alginate cap material as shown in Figure 30. Due to the increased number of cells isolated in the cap material and the inconsistent visibility on the air-dried alginate cap material, the freeze-dried alginate cap material was identified as the most promising cap material and will be tested against the fresh alginate cap as a control from previous work in the cell separation experiments of Chapter 4[98]. Before moving on to cell separation, wicking equilibrium time needs to be established to know how long it takes before the freeze-dried alginate cap material reaches saturation and ceases to wick more cells into the cap material.

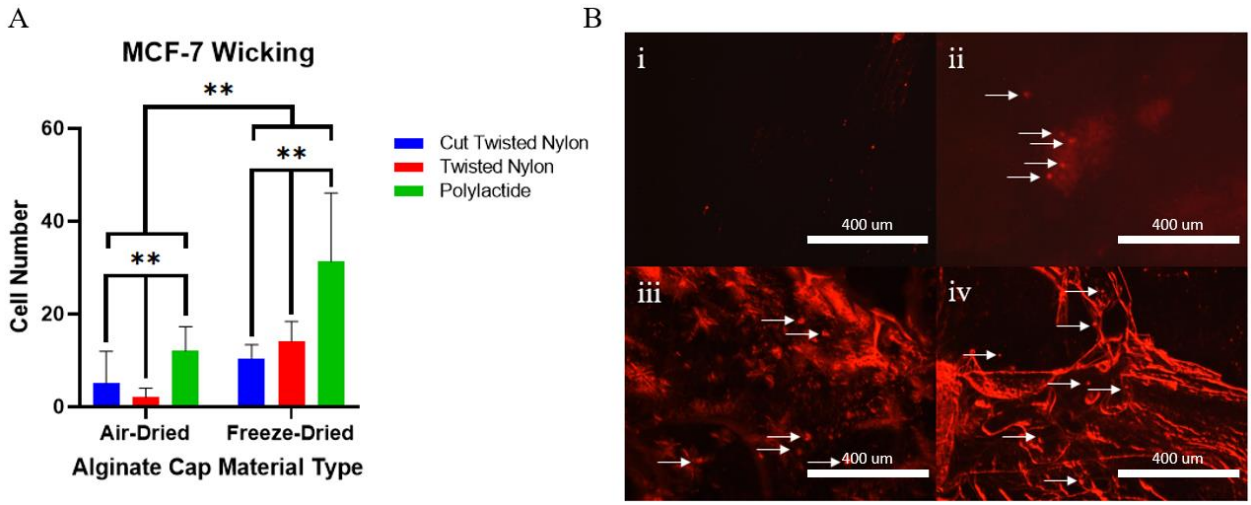

*Figure 29. Results from 60-minute cancerous human female breast, estrogen, and progesterone receptor (MCF-7) cell sample wicking experiment. (A) Cell count on each alginate cap material of the cut 4-twist nylon, normal 4-twist nylon, and dopamine-treated polylactide wicking fiber bundles. Cell counts are grouped by fiber bundle type then by alginate cap material preparation. N=3 sample size. (B) EVOS fluorescent light microscope images using the Texas Red 10X objective lens of the (i) negative control microscope slide, (ii) positive control microscope slide, (iii) air-dried alginate cap material, and (iv) freeze-dried alginate cap material. Cells are indicated by white arrows. ** indicates $p<0.01$.*

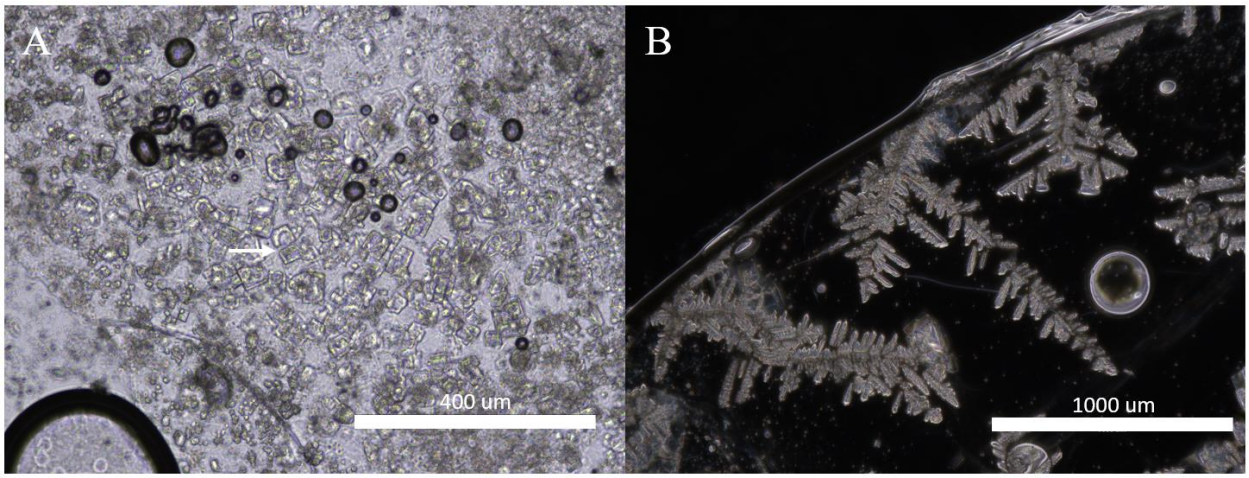

Figure 30. Crystal formation in alginate cap material when left on the benchtop for wicking or air-dried for extended amounts of time. (A) Sodium chloride square crystal formation observed under the EVOS fluorescent light microscope transmitted 10X objective lens. An example of a sodium chloride crystal is indicated by the white arrow. (B) A type of calcium crystal formation observed under the EVOS fluorescent light microscope transmitted 4X objective lens.

Identifying Cell Sample Wicking Equilibrium Time

Materials and Methods

Fiber Preparation

Nylon filament was extruded through a Monoprice Maker Ultimate 3D Printer at 245°C. Fibers had irregular cross-sectional dimensions of 3.33mm x 2.02mm and were defined as E70 sized fibers. Wicking fibers were laser cut into three individual fiber segments 35 mm in length. Immediately following the laser cutting process, three 35 mm nylon fiber segments were configured into a bundle and secured on one end of the bundle with a clear acrylic prototype ring. The other end of the fiber bundle was then secured in the chuck of an electric drill. The nylon fiber bundle was twisted four rotations with the electric drill, then held in that position for 60 seconds to solidify the twisted configuration.

Cap Material Preparation

The alginate gel cap material was prepared by dip coating one end of the fiber bundles in two solutions: a calcium chloride solution and a sodium alginate solution. A 10 mL calcium chloride solution was made by dissolving 5.55 g of calcium chloride granules to 10 mL of DI water. The sodium alginate solution was made by dissolving 0.09 g of reagent grade sodium chloride in 10 mL of DI water. After the sodium chloride was dissolved, 0.14 g of alginic acid sodium salt from brown algae was dissolved in the sodium chloride solution to make to sodium alginate solution. The top 2 mm of the fiber bundles were then carefully dipped in the calcium chloride solution and immediately removed. The same 2 mm end of the fiber bundles were then dipped into the sodium alginate solution and immediately removed, forming the alginate gel cap. The fiber bundles were then placed in the -80ºC freezer to preserve the cap material structure until they could be transferred to a freeze dryer at another location for freeze drying.

Cell Sample Preparation

Cancerous human female breast, estrogen, and progesterone receptor (MCF-7) cells were used for the purposes of this experiment. One T-25 flask of cancerous human female breast, estrogen, and progesterone receptor (MCF-7) cells was stained with Cell Tracker red stain to assess cell wicking capabilities over time. Cancerous human female breast, estrogen, and progesterone receptor (MCF-7) cells were resuspended in 13 mL of DI water following centrifugation for wicking. The initial cell count using the hemocytometer was 5.1×10^5 cells/mL.

Wicking Experiment Set-Up

Three wicking fiber bundle prototypes were prepared for cancerous human female breast, estrogen, and progesterone receptor (MCF-7) cell sample wicking per wicking time point in the modified cryovial prototype. 1 mL of cancerous human female breast, estrogen, and progesterone receptor (MCF-7) cell sample was loaded in the sample well of the modified cryovial prototype for wicking. Wicking time began when the fiber bundles were placed in the prototype sample well and one group was allowed to wick for 15, 30, and 60 minutes. After the specified wicking time point was met, the cap materials were removed from the top of the wicking fiber bundle prototype with tweezers and placed onto a microscope slide for absorption analysis. It was important to place the side of the cap material that met the fiber bundle down on the microscope slide for optimal cell viewing.

Analysis

Cell wicking and collection was analyzed by viewing the alginate cap material on the microscope slide under the EVOS fluorescent light microscope. The transmitted and Texas Red 10X objective lenses were used for cell viewing. The entirety of the alginate cap material was analyzed for manually counting the cells present on the alginate cap material. Statistical analysis

of the quantifiable results was performed using one-way ANOVA tests in the GraphPad Prism software.

Results and Discussion

Cell counts were performed on the freeze-dried alginate cap materials at 15 minutes, 30 minutes, and 60 minutes. When comparing the cell counts of the alginate cap materials in each of these groups, no significant difference was found between wicking time points as shown in Figure 31. The 15-minute time point had slightly higher cell count numbers than that of the 30-minute or 60-minute wicking time points. Variability of the cell counts could be attributed to fluorescent debris on the cap material or the cap material itself fluorescing or folding which inhibits cell visibility. For the cell separation experiments in Chapter 4, a wicking time of 15 minutes will be used since there is not a continual increase in cells wicked into the cap material after 15 minutes.

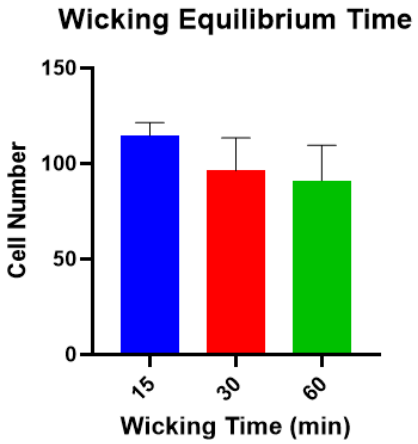

Figure 31. Cell counts on freeze-dried alginate cap materials that wicked cancerous human female breast, estrogen, and progesterone receptor (MCF-7) cell sample over 15-, 30-, and 60-minute time intervals. N=3 sample size.

Discussion

The beginning section of this chapter focused on sample absorption and cell visibility on different types of cap materials. Our work showed that hydrated sodium polyacrylate gel and thin paper materials like a Kim Wipe or filter paper worked best when trying to view a cell sample on

the cap material itself. Thicker, more fibrous materials like a sample pad or western blot material proved inadequate for this work because they are too dense to clearly observe under a microscope. However, one promising aspect of these materials are they are very absorptive. When translating the sodium polyacrylate gel and the Kim Wipe material from a microscope slide to part of the wicking fiber bundle prototype, each material had distinct difficulties. The sodium polyacrylate gel absorbed highlighter fluid sample off the top of the fiber bundle, but was hard to load and unload from the wicking fiber bundle prototype. The Kim Wipe material absorbed the highlighter fluid sample off the top of the wicking fiber bundle prototype, however, did not do so until pressure was applied with tweezers to the cap material because there was insufficient contact between the top of the fiber bundle and the cap material. Future work with the sodium polyacrylate gel and Kim Wipe cap materials would need to focus on a better prototype design to secure the cap material to the top of the fiber bundle more consistently.

The middle section of this chapter focused on a more solid cap material that aimed to solve the problem of being difficult to load and unload from the wicking fiber bundle prototype and to further improve cell visibility and cell count processes when compared to the previously explored gel and paper-based cap materials. The mesh polylactide cap was created to have gaps in the disc that would serve as windows for clear cell visibility. A procedure like that of a hemocytometer cell count could then be followed to consistently count all the cells within the cap material. The mesh polylactide cap was then treated in a dopamine solution to make the cap material more hydrophilic and become more attractive to the cells, causing them to wick to the mesh cap material and remain on the cap material when being unloaded onto a microscope slide[119-124]. The dopamine-treated mesh caps successfully collected cells; however, some cells were seen outside of the dopamine-treated mesh cap once placed on the microscope slide. Future

work with the dopamine-treated mesh cap material could include the addition of a stickier material that may retain the cells in the cap once wicked. The consistency of contact between the top of the fiber bundle and the cap material was still an issue with the wicking fiber bundle prototype used.

The later section of this chapter focused on a cap material that would solve the problem of inconsistent contact between the top of the fiber bundle and the cap material, while still addressing the difficulties in loading and unloading the cap material from the wicking fiber bundle prototype. Instead of creating a cap material and then loading that cap material onto the wicking fiber bundle prototype, the cap material was synthesized on the wicking fiber bundle prototype. The alginate gel cap material was previously used and proved to successfully capture cells at the top of a wicking fiber bundle prototype[98]. Our work focused on dehydrating the alginate gel onto the top of the wicking fiber bundle prototype to give the cap material a more solid shape for ease of removal when partially rehydrated. The freeze-dried alginate cap material showed to roughly retain its original shape when rehydrated, exhibiting promising abilities to increase shelf life of the product by freeze-drying the alginate cap material until use[136]. The air-dried alginate cap material slowed the wicking time and decreased the amount of sample wicked into the wicking fiber bundle prototype, however, the wicking fiber bundle prototype with the air-dried alginate cap still wicked in under 10 minutes and did not unreasonable decrease the amount of sample wicked into the wicking fiber bundle prototype. It was then proven that freeze-dried alginate cap materials wick more sample into the cap material through highlighter fluid and cancerous human female breast, estrogen, and progesterone receptor (MCF-7) cell trials, which helped to support the hypothesis that freeze-drying the alginate cap material will shift wicking equilibrium to allow more sample to wick before reaching a saturation point[132-135]. Further work

would need to be conducted to confirm this hypothesis. The air-dried alginate cap material had the clearest cell visibility of any material used up to this point for the wicking fiber bundle prototype cap, with the freeze-dried alginate cap material being the next best material for cell visibility due to the thin nature of the dehydrated materials. It should be noted that crystal formation in the air-dried alginate cap material was an issue if left on the benchtop for too long due to the slow evaporation of fluid from the alginate cap material. Crystal formation within the cap material is not ideal for cell visibility, therefore, the freeze-dried alginate cap material was identified as the most viable option for the wicking fiber bundle prototype cap material.

Finally, this chapter explored the ideal wicking time for the alginate cap material before the cap material becomes saturated and stops wicking cell sample. It was found that 15 minutes was a sufficient time period for wicking a cell sample, which aligns with our goal of creating a wicking fiber bundle prototype that can process a cell sample within a 15-minute appointment time. Future work could be performed to see if wicking equilibrium is reached before 15 minutes, as 15 minutes was the shortest time period that was tested.

The major limitations of this work revolve around the accuracy of the cell counts performed on the cap materials under the EVOS fluorescent light microscope. The biggest obstacle faced during the cap material experiments was the fluorescing of debris particles that should have indicated the particles were cells. When running positive and negative control microscope slides particles on the negative control microscope slides would fluoresce as if they were cells. This raised concern as to how accurate the cell counts were on the cap materials tested and analyzed on microscope slides. The 4X objective lens on the EVOS fluorescent light microscope was also used in the earlier stage cap material experiments. Cells are best seen and distinguished under the 10X objective lens, raising further question as to the accuracy of the

earlier cap material experiments. There was also an issue of cells bursting during the process of being prepared, wicking, and then being removed from the cap materials for cell count. In this case, cell particles would fluoresce and each particle would be counted as one full cell, elevating the cell counts in the cap for the earlier cap material experiments. Finally, a major limitation throughout all the cap material experiments was the cap material fluorescing under the EVOS fluorescent light microscope. Cells could still be seen in most cases, but the fluorescing cells were not as distinct as they normally are on just a microscope slide. This could have hindered cell counts in some cases if cells were masked by the fluorescence of the cap material. However, it is important to note that these limitations will only be encountered while attempting to validate and precisely tune the wicking fiber bundle device. If the wicking fiber bundle prototype goes to market, the end user will not be using fluorescence to view the cell sample and will avoid many of these issues.

Conclusion

The freeze-dried alginate cap material was the most promising due to its increased, consistent contact with the top of the wicking fiber bundle prototype and its cell visibility on the material. Freeze-drying the material will also be valuable for shelf-life considerations if the product is put on the market. The freeze-dried alginate cap material will be compared to the fresh alginate cap material used in previous work for cell separation in Chapter 4[98]. Future work will focus on continuing to improve cell visibility and decreasing the amount the cap material itself fluoresces under the EVOS fluorescent light microscope. It also may be worth looking into how to make an alginate cap material more solid with a definite shape like the dopamine-treated polylactide mesh disc.

CHAPTER FOUR

CHARACTERIZING CELL SEPARATION WITHIN THE FIBER BUNDLE

Introduction

Non-affinity-based cancer cell detection has been shown to be more promising than affinity-based cancer cell detection due to the ability to identify and isolate both epithelial and mesenchymal cancer cell phenotypes, which is more representative of tumor heterogenicity[66]. Previous research on physical separation of cancer cells from a liquid biopsy through microchips for human medicine applications has proven to be promising, but is still relatively expensive to be integrated into veterinary medicine applications[83,84]. For this reason, a cheaper rapid diagnostic test is being developed that employs the same cell separating characteristics: cell size and cell deformability. The wicking fiber bundle cancer diagnostic device should be able to effectively separate cancer cells from non-cancerous cells in a fine needle aspirate sample over the length of the fiber bundle system and isolate those cancer cells within the proposed freeze-dried alginate cap material for cell analysis under a light microscope. The success of the device prototype will be assessed by the degree of cell separation within the fiber bundle system and the cancer cell purity isolated in the freeze-dried alginate cap material.

In this chapter, we have investigated the ability of a wicking fiber bundle prototype to separate cell types based on cancerous cell characteristics. To test the ability of a wicking fiber bundle prototype, first, a method for fixing the cell sample to the final wicking location must be identified for analysis. Next, individual cell lines will be tested to see how and where the cells wick to within the wicking fiber bundle prototype. Then, a heterogenous cell sample will be

tested to determine whether the wicking fiber bundle prototype can separate cell types based upon cancer cell characteristics.

In the first part of the chapter, three methods are tested for cell sample fixation: methanol liquid fixative, UV resin liquid fixative, and a freezing method for fixation. These methods were tested with a highlighter fluid and cancerous human female breast, estrogen, and progesterone receptor (MCF-7) cell sample. The method identified as the most promising fixation method from these tests is used in the chapter's following cell type separation experiments.

In the last part of the chapter, the wicking of cancerous human female breast, estrogen, and progesterone receptor (MCF-7) cells and human female mammary gland, pre-neoplastic epithelial (MCF-10A) cells were tested individually and together in a heterogenous cell sample for cell type separation within a wicking fiber bundle prototype. Varying initial cell concentrations within the cell sample were also tested for their effect on the final number of cells wicked into the cap material. These tests were performed with the 4-twist nylon fiber bundle and the dopamine-treated polylactide fiber bundle to identify which fiber bundle from Chapter 2 would be the best for cell type separation. These tests were also performed with a fresh alginate cap used in previous work and a freeze-dried alginate cap to determine which cap material from Chapter 3 will be the best for cell capture and analysis[98].

A summary of the fiber bundle tested, cap material type tested, sample type used, and analysis methods are listed in Table 3.

Table 3. Summary of the fiber bundle types tested, the sample types used to test the stated objective, and the analysis methods used during testing.

Fiber bundle type	Sample type	Analysis
4-twist nylon	Cancerous human female breast, estrogen, and progesterone receptor (MCF-7) cells	EVOS fluorescent light microscope alginate cap material cell count.
	Human female mammary gland, pre-neoplastic epithelial (MCF-10A) cells	EVOS fluorescent light microscope alginate cap material cell count.
	Cancerous human female breast, estrogen, and progesterone receptor (MCF-7) cells and human female mammary gland, pre-neoplastic epithelial (MCF-10A) cells	EVOS fluorescent light microscope alginate cap material cell count.
Dopamine-treated polylactide	Cancerous human female breast, estrogen, and progesterone receptor (MCF-7) cells	EVOS fluorescent light microscope alginate cap material cell count.
	Human female mammary gland, pre-neoplastic epithelial (MCF-10A) cells	EVOS fluorescent light microscope alginate cap material cell count.
	Cancerous human female breast, estrogen, and progesterone receptor (MCF-7) cells and human female mammary gland, pre-neoplastic epithelial (MCF-10A) cells	EVOS fluorescent light microscope alginate cap material cell count.

Cell Sample Fixation Methods

Methanol

Materials and Methods

Fiber Bundle Preparation

Polylactide filament was extruded through a Monoprice Maker Ultimate 3D Printer at 210°C. Fibers had irregular cross-sectional dimensions of 3.33mm x 2.02mm and were defined as E70 sized fibers. Wicking fibers were laser cut into three individual fiber segments 35 mm in length and arranged with three fiber segments per fiber bundle as previously described in Chapter 1.

Cell Sample Preparation

Cancerous human female breast, estrogen, and progesterone receptor (MCF-7) cells were used for the purposes of this experiment. One T-25 flask of cancerous human female breast, estrogen, and progesterone receptor (MCF-7) cells was stained with Cell Tracker red stain to help identify cells on the microscope slide for fixation. Cancerous human female breast, estrogen, and progesterone receptor (MCF-7) cells were resuspended in 5 mL of serum-free DMEM media following centrifugation. The initial cell count using the hemocytometer was 6.4×10^5 cells/mL.

Experiment Set-Up

Methanol fixation was tested on a microscope slide and on a wicking fiber bundle. For the microscope slide experiment, 250 uL of cancerous female breast, estrogen, and progesterone receptor (MCF-7) cell sample was pipetted directly onto the microscope slide. The cell sample was left to dry for 5 minutes, then the microscope slide was dipped into a beaker of pesticide grade methanol five times for one second each. The slide was then gently rinsed with DI water. For the fiber bundle experiment, 250 uL of cancerous female breast, estrogen, and progesterone receptor (MCF-7) cell sample was pipetted directly into the top of the fiber bundle and allowed to sit for 5 minutes before fixing the cell sample. The fiber bundle was then dipped into the pesticide grade methanol five times for one second each. The fiber bundle was then gently rinsed with DI water.

Analysis

Cell sample fixation was analyzed by viewing the microscope slide under the EVOS fluorescent light microscope using the Texas Red and transmitted 4X and 10X objective lenses. Microscope slides and fiber bundles were analyzed with the cell sample before fixation and after fixation to visually assess the differences in the amount of cell sample left on the microscope slide and fiber

bundle after the methanol fixation process. Images were taken under the EVOS fluorescent light microscope to show the differences in cell number before and after the methanol fixation process.

Results and Discussion

For the microscope slide experiment, a portion of the cell sample was successfully fixed to the microscope slide. However, much of the sample was lost when dipped initially dipped into the beaker of methanol for fixation since the sample was not completely dried on the microscope slide prior to dipping. For the fiber bundle experiment, there was a noticeable difference between the amount of cell sample that was present on the fiber bundle before methanol fixation and the minimal amount of cell sample that was still present on the fiber bundle after methanol fixation as shown in Figure 32. Overall, the methanol fixation method worked much better on the flat microscope slide than the three-dimensional fiber bundle, however, will not be a sufficient fixation method for the cell separation testing of the wicking fiber bundle prototype. Next, we will test a resin fixation method that uses ultraviolet (UV) light to fix the sample instead of evaporation like the methanol fixative.

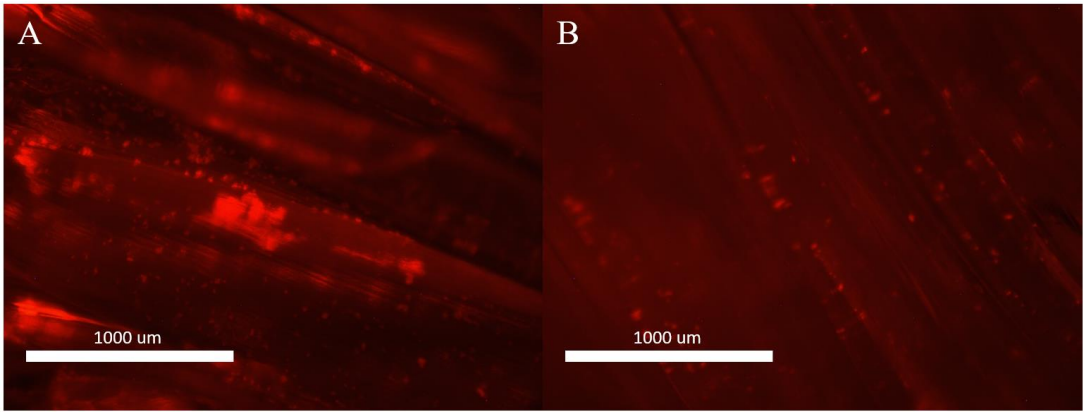

Figure 32. EVOS fluorescent light microscope images under a Texas Red 4X objective lens of a wicking fiber bundle (A) before and (B) after methanol fixation.

UV Resin

Materials and Methods

Fiber Bundle Preparation

Nylon filament was extruded through a Monoprice Maker Ultimate 3D Printer at 245°C. Fibers had irregular cross-sectional dimensions of 3.33mm x 2.02mm and were defined as E70 sized fibers. Wicking fibers were laser cut into three individual fiber segments 35 mm in length. Nylon fiber bundles were twisted immediately following the laser cutting process. Three 35 mm nylon fiber segments were configured into a bundle and secured on one end of the bundle with a clear acrylic prototype ring. The other end of the fiber bundle was then secured in the chuck of an electric drill. The nylon fiber bundle was twisted four rotations with the electric drill, then held in that position for 60 seconds to solidify the twisted configuration. Some nylon fiber bundles were left not twisted and configured as previously described in Chapter 1.

Experiment Set-Up

JDiction UV resin hard type 100g was used for UV resin experimentation along with a JDiction UV lamp for curing the resin. The viscosity of the UV resin was first tested by dipping a non-twisted and twisted nylon fiber bundles into the UV resin and observing how far the UV resin would penetrate the fiber bundle. Isopropyl alcohol was added to UV resin mixtures in 0%, 25%, and 50% volume ratios and tested for differences in viscosity in both the non-twisted and twisted nylon fiber bundles. For experimentation, a cryovial was filled with the UV resin mixture and the nylon fiber bundle was inserted into the UV resin mixture. The cryovial was then placed under the UV lamp and cured for 60 seconds. Next, the cryovial was laid on its either side and cured for an additional 60 seconds each. The cured UV resin encasing the fiber bundle was carefully removed with tweezers and the excess UV resin removed from the outside of the fiber bundle. A

1 mL highlighter fluid sample was tested to assess the ability of UV resin to fix a fluid sample within the fiber bundle. Highlighter fluid sample was prepared by soaking one Sharpie Highlighter marker stick in 500 mL of deionized water for 24 hours and stored in a 500 mL glass bottle. 1 mL of highlighter fluid sample was loaded in the sample well of the modified cryovial prototype for wicking and allowed to wick for 10 minutes. The fiber bundle was then removed and placed in the -80°C freezer for 5 minutes. The frozen fiber bundle was then removed and inserted into the UV resin mixture for fixing. The change in highlighter fluid level was then assessed to decide whether sample fixation using UV resin would be adequate for the purposes of this project.

Analysis

UV resin viscosity was analyzed by observing the level of penetration into the fiber bundle's inner channels where the wicking occurs. This was done by visually observing the UV resin level from the outside of the fiber bundle and by sectioning the fiber bundle with a razor blade to expose the inner channels of the fiber bundle under the stereoscope. The ability of the UV resin to fix a fluid sample within the fiber bundle was assessed by visually observing the highlighter fluid sample levels within the fiber bundle before and after UV resin fixation. Images were taken with an iPhone 12 Pro camera for documentation. The fiber bundles were also sectioned to see if the UV resin just fixed the highlighter fluid level or if it fixed all the sample within the fiber bundle.

Results and Discussion

From UV resin viscosity observations, it was observed that the UV resin mixture with 0% isopropyl alcohol was too viscous to penetrate the inner channels of the fiber bundle as seen in Figure 33A. The UV resin mixture with 25% isopropyl alcohol could wick to the top of the non-

twisted nylon fiber bundle within 60 seconds, however, could not reach the top of the twisted fiber bundle because of the smaller inner capillary channels. The UV resin mixture with 50% isopropyl alcohol had a water-like viscosity and could wick to the top of the non-twisted and twisted nylon fiber bundle within a minute. This means both the UV resin mixtures with 25% and 50% isopropyl alcohol could penetrate the inner channels of the non-twisted fiber bundles, but only the UV resin mixture with 50% isopropyl alcohol could penetrate the inner channels of the twisted nylon fiber bundle as seen in Figure 33A. When highlighter fluid sample fixation was assessed, the highlighter fluid level remained the same in the twisted nylon fiber bundle, but had moved slightly in the non-twisted nylon fiber bundle. However, when the twisted nylon fiber bundle was sectioned to expose the inner channels of the fiber bundle, the highlighter fluid sample was still in liquid form and had not been fixed all the way through the fiber as seen in Figure 33B. Because the UV resin was not able to be cured in a timely manner in the inner most channels of the fiber bundle, the UV resin will also not be sufficient for the cell separation tests of the wicking fiber bundle prototype.

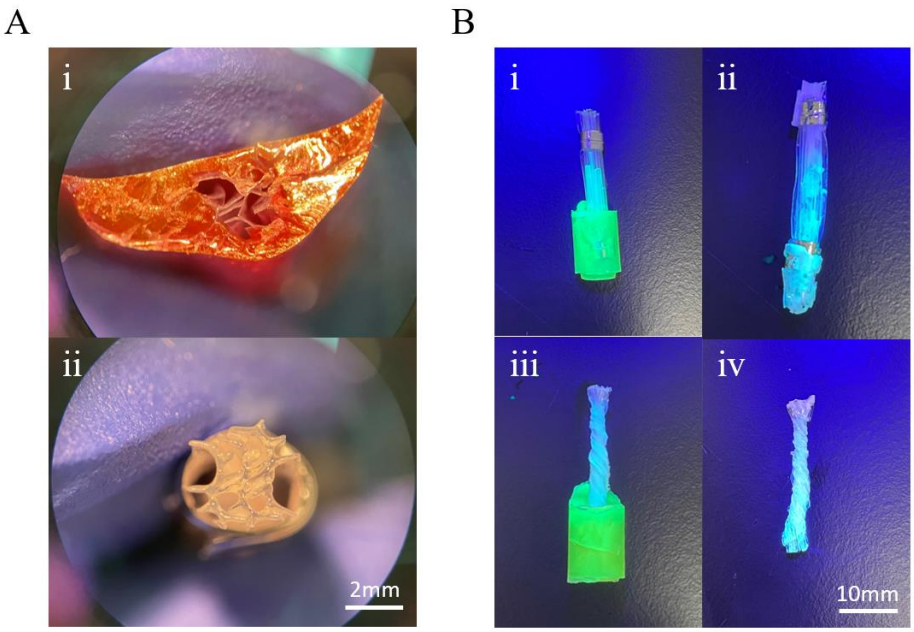

Figure 33. Images of fiber bundles cured with varying concentrations of UV resin and isopropyl alcohol. (A) Stereoscope images of nylon fiber bundle cross sections fixed with UV resin mixtures with (i) 0% isopropyl alcohol and (ii) 50% isopropyl alcohol. (B) iPhone 12 Pro images of non-twisted nylon fiber bundles (i) before and (ii) after UV resin fixation of a highlighter fluid sample. Twisted nylon fiber bundles (iii) before and (iv) after UV resin fixation for a highlighter fluid sample is also pictured.

Freezing

Materials and Methods

Fiber Preparation

Nylon filament was extruded through a Monoprice Maker Ultimate 3D Printer at 245°C. Fibers had irregular cross-sectional dimensions of 3.33mm x 2.02mm and were defined as E70 sized fibers. Wicking fibers were laser cut into three individual fiber segments 35 mm in length. Nylon fiber bundles were twisted immediately following the laser cutting process. Three 35 mm nylon fiber segments were configured into a bundle and secured on one end of the bundle with a clear acrylic prototype ring. The other end of the fiber bundle was then secured in the chuck of an electric drill. The nylon fiber bundle was twisted four rotations with the electric drill, then held in that position for 60 seconds to solidify the twisted configuration.

Wicking Experiment Set-Up

Three wicking fiber bundle prototypes were prepared for highlighter fluid wicking and freezing in the modified cryovial prototype. Highlighter fluid sample was prepared by soaking one Sharpie Highlighter marker stick in 500 mL of deionized water for 24 hours and stored in a 500 mL glass bottle. 1 mL of highlighter fluid sample was loaded in the sample well of the modified cryovial prototype for wicking and allowed to wick for 10 minutes. Wicking time began when the fiber bundles were placed in the prototype sample well. After wicking was complete, wicking fiber bundle prototypes were placed in the -80°C freezer for 5 minutes to thoroughly freeze the wicked sample. After 5 minutes, the fiber bundles were removed from the wicking fiber bundle prototype and melting time of the sample was observed and recorded.

Analysis

Sample melting time was determined by observing the condensation and movement of highlighter fluid sample levels under the stereoscope. A blacklight flashlight was used to fluoresce the highlighter fluid sample and identify and movement of sample within the fiber bundle.

Results and Discussion

At the 60 second mark, the sample frozen in the sample well had melted enough to be chiseled off and removed from the bottom of the fiber bundle, but no other fluid sample movement had been detected. At the 180 second mark, the frozen sample was beginning to condensate within the bundle and a small puddle formed at the bottom end of the fiber bundle. At the 300 second mark, the sample had melted and began to disperse the length of the fiber bundle. Overall, the sample seemed to stay frozen in place within the 4-twist nylon fiber bundle for up to 60 seconds before beginning to show signs of melting at 180 seconds. This fixation method proved to be the

most promising at fixing the cell sample in place within the fiber bundle so the final wicking location of cell types could be most accurately analyzed. There still may be some concern of cell movement within the fiber bundle during sectioning due to the pressure applied onto the fiber bundle as the sample is melting. The freezing method will be used to fix cell samples in the experiments moving forward.

Assessing Differences in Initial Cell Concentration for Separation

Materials and Methods

Fiber Preparation

Nylon filament was extruded through a Monoprice Maker Ultimate 3D Printer at 245°C. Fibers had irregular cross-sectional dimensions of 3.33mm x 2.02mm and were defined as E70 sized fibers. Wicking fibers were laser cut into three individual fiber segments 35 mm in length. Immediately following the laser cutting process, three 35 mm nylon fiber segments were configured into a bundle and secured on one end of the bundle with a clear acrylic prototype ring. The other end of the fiber bundle was then secured in the chuck of an electric drill. The nylon fiber bundle was twisted four rotations with the electric drill, then held in that position for 60 seconds to solidify the twisted configuration.

Cap Material Preparation

The alginate gel cap material was prepared by dip coating one end of the fiber bundles in two solutions: a calcium chloride solution and a sodium alginate solution. A 10 mL calcium chloride solution was made by dissolving 5.55 g of calcium chloride granules to 10 mL of DI water. The sodium alginate solution was made by dissolving 0.09 g of reagent grade sodium chloride in 10 mL of DI water. After the sodium chloride was dissolved, 0.14 g of alginic acid sodium salt from brown algae was dissolved in the sodium chloride solution to make to sodium alginate solution.

The top 2 mm of the fiber bundles were then carefully dipped in the calcium chloride solution and immediately removed. The same 2 mm end of the fiber bundles were then dipped into the sodium alginate solution and immediately removed, forming the alginate gel cap. The fiber bundles were then placed in the -80ºC freezer to preserve the cap material structure until they could be transferred to a freeze dryer at another location for freeze drying.

Cell Sample Preparation

Cancerous human female breast, estrogen, and progesterone receptor (MCF-7) cells were used for the purposes of this experiment. Two T-25 flasks of cancerous human female breast, estrogen, and progesterone receptor (MCF-7) cells were stained with Cell Tracker red stain to assess cell wicking capabilities over time. The first flask had an initial cell concentration of 2.9 x 10^5 cells/mL, which was determined by a hemocytometer cell count under the EVOS fluorescent light microscope. The first flask of cancerous human female breast, estrogen, and progesterone receptor (MCF-7) cells was resuspended in 9 mL of DI water. A cell count was performed on the cell sample after resuspension and had a resulting cell concentration of 1.3 x 10^5 cells/mL. The second flask had an initial cell concentration of 1.4 x 10^5 cells/mL. The second flask of cancerous human female breast, estrogen, and progesterone receptor (MCF-7) cells was resuspended in 42 mL of DI water. A cell count was performed on the cell sample after resuspension and had a resulting cell concentration of 2.0 x 10^4 cells/mL.

Wicking Experiment Set-Up

Three wicking fiber bundle prototypes were prepared for cancerous human female breast, estrogen, and progesterone receptor (MCF-7) cell sample wicking for each of the cell concentrations to be tested. 1 mL of 1.3 x 10^5 cells/mL cancerous human female breast, estrogen, and progesterone receptor (MCF-7) cell sample was loaded into three of the sample wells of the

modified cryovial prototype for wicking. 1 mL of 2.0 x 10^4 cells/mL cancerous human female breast, estrogen, and progesterone receptor (MCF-7) cell sample was loaded into the other three sample wells of the modified cryovial prototype for wicking. Wicking time began when the fiber bundles were placed in the prototype sample well and each bundle was allowed to wick for 15 minutes. After wicking was complete, the cap materials were removed from the top of the wicking fiber bundle prototype with tweezers and placed onto a microscope slide for analysis. It was important to place the side of the cap material that met the fiber bundle down on the microscope slide for optimal cell viewing.

Analysis

Cell wicking and collection was analyzed by viewing the alginate cap material on the microscope slide under the EVOS fluorescent light microscope. The transmitted and Texas Red 10X objective lenses were used for cell viewing. The entirety of the alginate cap material was analyzed for manually counting the cells present on the alginate cap material. Statistical analysis of the quantifiable results was performed using a t-test in the GraphPad Prism software.

Results and Discussion

From the EVOS fluorescent light microscope cell counts on each of the alginate cap materials, it was determined that a higher initial cell concentration in the cell sample resulted in slightly higher cell counts in the alginate cap material as shown in Figure 34. However, the difference in cell count in the alginate cap material is not significantly different. For an approximately 500% increase in initial cell concentration, there was only a 37.7% increase in the average cell number seen in the alginate cap material. This confirmed that a cell sample with a cell concentration of approximately 1 x 10^5 cells/mL was not too many cells to overwhelm the fiber bundle system and hinder further cell wicking. It seems that by decreasing the number of cells in the initial cell

sample, the number of cells that are wicked into the alginate cap material will also decrease. This poses a concern that when the wicking fiber bundle prototype processes a fine needle aspirate or other type of cell sample that is smaller in volume, enough cells may not be processed by the wicking fiber bundle prototype to make a definitive diagnosis. Future work with the wicking fiber bundle prototype will need to address this issue by increasing the amount of sample processed by the wicking fiber bundle prototype. For the purposes of these experiments, a cell sample varying by a degree of magnitude should yield similar results. Variability with cell counts on the freeze-dried alginate cap material could be attributed to the cap material fluorescing and folding, inhibiting cell visibility in some areas of the cap material.

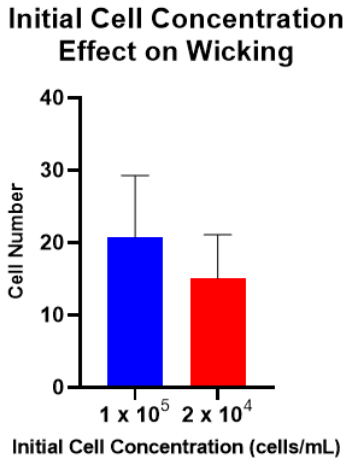

Figure 34. Cell counts from the alginate cap materials of 4-twist nylon fiber bundles with either an initial cell concentration of 1 x 10^5 or 2 x 10^4 cells/mL. N=3 sample size.

MCF-7 Only Wicking Experiment

Materials and Methods

Fiber Preparation

Polylactide filament was extruded through a Monoprice Maker Ultimate 3D Printer at 210°C. Nylon filament was extruded through a Monoprice Maker Ultimate 3D Printer at 245°C. Fibers had irregular cross-sectional dimensions of 3.33mm x 2.02mm and were defined as E70 sized

fibers. Wicking fibers were laser cut into three individual fiber segments 35 mm in length. Nylon fiber bundles were twisted immediately following the laser cutting process. Three 35 mm nylon fiber segments were configured into a bundle and secured on one end of the bundle with a clear acrylic prototype ring. The other end of the fiber bundle was then secured in the chuck of an electric drill. The nylon fiber bundle was twisted four rotations with the electric drill, then held in that position for 60 seconds to solidify the twisted configuration. The polylactide fiber bundles were treated in a dopamine solution for 40 minutes to increase fiber bundle hydrophilicity.

Cap Material Preparation

The alginate gel cap material was prepared by dip coating one end of the fiber bundles in two solutions: a calcium chloride solution and a sodium alginate solution. A 10 mL calcium chloride solution was made by dissolving 5.55 g of calcium chloride granules to 10 mL of DI water. The sodium alginate solution was made by dissolving 0.09 g of reagent grade sodium chloride in 10 mL of DI water. After the sodium chloride was dissolved, 0.14 g of alginic acid sodium salt from brown algae was dissolved in the sodium chloride solution to make to sodium alginate solution. The top 2 mm of the fiber bundles were then carefully dipped in the calcium chloride solution and immediately removed. The same 2 mm end of the fiber bundles were then dipped into the sodium alginate solution and immediately removed, forming the alginate gel cap. Half of the fiber bundles were placed in the -80ºC freezer to preserve the cap material structure until they could be transferred to a freeze dryer at another location for freeze drying. The other half of the fiber bundles were prepared with a fresh alginate cap just before the wicking experiment to test a fresh alginate cap material versus a freeze-dried alginate cap material.

Chemical Surface Treatment

The dopamine surface treatment solution was made by combining a 10mM Tris-HCl buffer solution with dopamine powder. To prepare the Tris-HCl buffer solution, 7.84g of tris powder was added to 450 mL of DI water in a beaker. Four NaOH pellets were then dissolved in 30 mL of DI water and added dropwise into the 450 mL tris solution. The tris-HCl buffer was then diluted with DI water to a total volume of 500 mL. To make the dopamine solution, 0.4g of dopamine was added to 100 mL of tris-HCl buffer solution and dissolved. Direct airflow, 45°C heat, and a stir bar at 400 rpm were then added into the 100 mL dopamine solution to enhance the reaction. Fibers were treated in the dopamine solution for 40 minutes. After treatment, fibers were rinsed with DI water and patted dry with gauze.

Cell Sample Preparation

Cancerous human female breast, estrogen, and progesterone receptor (MCF-7) cells were used for the purposes of this experiment. One T-25 flask of cancerous human female breast, estrogen, and progesterone receptor (MCF-7) cells was stained with Cell Tracker red stain to assess cell wicking and collection capabilities with different cap material and fiber bundle types. Cancerous human female breast, estrogen, and progesterone receptor (MCF-7) cells were resuspended in 13 mL of DI water following centrifugation for wicking. The initial cell count using the hemocytometer was 8.2×10^5 cells/mL.

Wicking Experiment Set-Up

Three wicking fiber bundle prototypes were prepared for cancerous human female breast, estrogen, and progesterone receptor (MCF-7) cell wicking per fiber bundle type and cap preparation in the modified cryovial prototype. 1 mL of cancerous human female breast, estrogen, and progesterone receptor (MCF-7) cell sample was loaded into the sample well of the

modified cryovial prototype. Wicking time began when the fiber bundles were placed in the prototype sample well. Cell sample was allowed to wick for 15 minutes. After wicking was complete, the cap materials were removed from the top of the wicking fiber bundle prototype with tweezers and placed onto a microscope slide for analysis.

Analysis

Cell wicking and collection was analyzed by viewing the alginate cap material on the microscope slide under the EVOS fluorescent light microscope. The transmitted and Texas Red 10X objective lenses were used for cell viewing. The entire alginate cap material was analyzed for cell count. Statistical analysis of the quantifiable results was performed using two-way ANOVA tests in the GraphPad Prism software.

Results and Discussion

There was no significant difference between cancerous human female breast, estrogen, and progesterone receptor (MCF-7) cells wicked in the 4-twist nylon fiber bundle versus the dopamine-treated polylactide fiber bundle. There was also no significant difference in cancerous human female breast, estrogen, and progesterone receptor (MCF-7) cells wicked in the fresh alginate cap material versus the freeze-dried alginate cap material as shown in Figure 35. Variability with cell counts on the fresh and freeze-dried alginate cap material could be attributed to the cap material fluorescing and folding, inhibiting cell visibility in some areas of the cap material. Variability could also be due to fluorescent debris particles on the alginate cap materials. Next, we will test the wicking of human female mammary gland, pre-neoplastic epithelial (MCF-10A) cells in the 4-twist nylon fiber bundle and the dopamine-treated polylactide fiber bundle with both the fresh and freeze-dried alginate cap to determine if there is possibility for separation of the cell types when wicked together in a heterogenous cell sample.

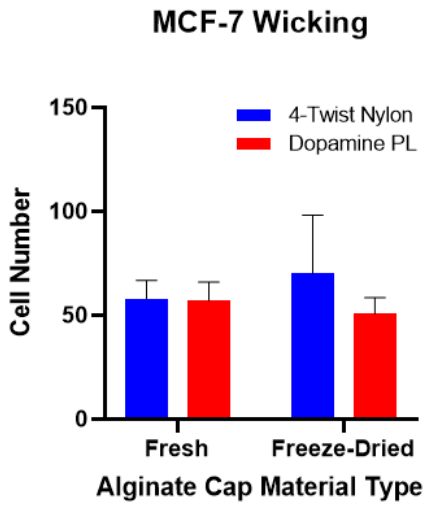

Figure 35. Cell counts on fresh and freeze-dried alginate cap materials that wicked a cancerous human female breast, estrogen, and progesterone receptor (MCF-7) cell sample in both 4-twist nylon and dopamine-treated polylactide (PL) fiber bundles. N=3 sample size.

MCF-10A Only Wicking Experiment

Materials and Methods

Fiber Preparation

Polylactide filament was extruded through a Monoprice Maker Ultimate 3D Printer at 210°C. Nylon filament was extruded through a Monoprice Maker Ultimate 3D Printer at 245°C. Fibers had irregular cross-sectional dimensions of 3.33mm x 2.02mm and were defined as E70 sized fibers. Wicking fibers were laser cut into three individual fiber segments 35 mm in length. Nylon fiber bundles were twisted immediately following the laser cutting process. Three 35 mm nylon fiber segments were configured into a bundle and secured on one end of the bundle with a clear acrylic prototype ring. The other end of the fiber bundle was then secured in the chuck of an electric drill. The nylon fiber bundle was twisted four rotations with the electric drill, then held in that position for 60 seconds to solidify the twisted configuration. The polylactide fiber bundles were treated in a dopamine solution for 40 minutes to increase fiber bundle hydrophilicity.

Cap Material Preparation

The alginate gel cap material was prepared by dip coating one end of the fiber bundles in two solutions: a calcium chloride solution and a sodium alginate solution. A 10 mL calcium chloride solution was made by dissolving 5.55 g of calcium chloride granules to 10 mL of DI water. The sodium alginate solution was made by dissolving 0.09 g of reagent grade sodium chloride in 10 mL of DI water. After the sodium chloride was dissolved, 0.14 g of alginic acid sodium salt from brown algae was dissolved in the sodium chloride solution to make to sodium alginate solution. The top 2 mm of the fiber bundles were then carefully dipped in the calcium chloride solution and immediately removed. The same 2 mm end of the fiber bundles were then dipped into the sodium alginate solution and immediately removed, forming the alginate gel cap. Half of the fiber bundles were placed in the -80ºC freezer to preserve the cap material structure until they could be transferred to a freeze dryer at another location for freeze drying. The other half of the fiber bundles were prepared with a fresh alginate cap just before the wicking experiment to test a fresh alginate cap material versus a freeze-dried alginate cap material.

Chemical Surface Treatment

The dopamine surface treatment solution was made by combining a 10mM Tris-HCl buffer solution with dopamine powder. To prepare the Tris-HCl buffer solution, 7.84g of tris powder was added to 450 mL of DI water in a beaker. Four NaOH pellets were then dissolved in 30 mL of DI water and added dropwise into the 450 mL tris solution. The tris-HCl buffer was then diluted with DI water to a total volume of 500 mL. To make the dopamine solution, 0.4g of dopamine was added to 100 mL of tris-HCl buffer solution and dissolved. Direct airflow, 45°C heat, and a stir bar at 400 rpm were then added into the 100 mL dopamine solution to enhance

the reaction. Fibers were treated in the dopamine solution for 40 minutes. After treatment, fibers were rinsed with DI water and patted dry with gauze.

Cell Sample Preparation

Human female mammary gland, pre-neoplastic epithelial (MCF-10A) cells were used for the purposes of this experiment. One T-25 flask of human female mammary gland, pre-neoplastic epithelial (MCF-10A) cells was stained with Cell Tracker green stain to assess cell wicking and collection capabilities with different cap material and fiber bundle types. Human female mammary gland, pre-neoplastic epithelial (MCF-10A) cells were resuspended in 13 mL of DI water following centrifugation for wicking. The initial cell count using the hemocytometer was 1.4×10^5 cells/mL.

Wicking Experiment Set-Up

Three wicking fiber bundle prototypes were prepared for human female mammary gland, pre-neoplastic epithelial (MCF-10A) cell wicking per fiber bundle type and cap preparation in the modified cryovial prototype. 1 mL of human female mammary gland, pre-neoplastic epithelial (MCF-10A) cell sample was loaded into the sample well of the modified cryovial prototype. Wicking time began when the fiber bundles were placed in the prototype sample well. Cell sample was allowed to wick for 15 minutes. After wicking was complete, the cap materials were removed from the top of the wicking fiber bundle prototype with tweezers and placed onto a microscope slide for analysis.

Analysis

Cell wicking and collection was analyzed by viewing the alginate cap material on the microscope slide under the EVOS fluorescent light microscope. The transmitted and GFP 10X objective lenses were used for cell viewing. The entire alginate cap material was analyzed for cell count.

Statistical analysis of the quantifiable results was performed using two-way ANOVA tests in the GraphPad Prism software.

Results and Discussion

There was no significant difference in human female mammary gland, pre-neoplastic epithelial (MCF-10A) cell wicking between cap types. There was also no significant difference between cell wicking in fiber bundle types, however, there did seem to be a difference in human female mammary gland, pre-neoplastic epithelial (MCF-10A) cell wicking between the 4-twist nylon fiber bundle and the dopamine-treated polylactide fiber bundle, where the 4-twist nylon fiber bundle had higher human female mammary gland, pre-neoplastic epithelial (MCF-10A) cell counts as shown in Figure 36. This could indicate that there will not be as much cell type separation observed in the 4-twist nylon fiber bundle. Variability with cell counts on the alginate cap materials could be attributed to fluorescent debris on the cap material or from the cap material fluorescing and folding in the case of the freeze-dried alginate cap, inhibiting cell visibility in some areas of the cap material. Because cell sample collection was consistent with both cap material types, the final cap material types will be selected due to cell visibility and other factors. The fresh alginate cap experienced similar difficulties to the air-dried alginate cap previously discussed in Chapter 3, where crystals would begin to form and inhibit cell visibility when left on the counter for too long. Freeze-drying the alginate hydrogel cap will also improve shelf-life capabilities for the prototype long term, so the freeze-dried alginate cap material was selected as the most promising and will be used in the final cell separation experiment.

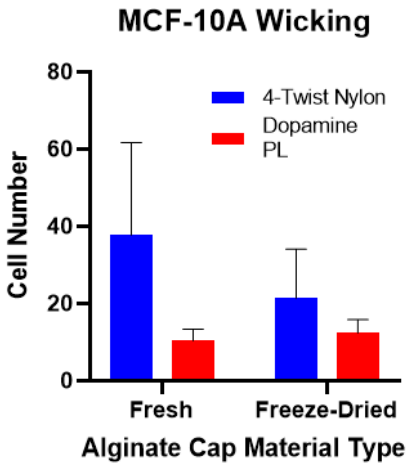

Figure 36. Cell counts on fresh and freeze-dried alginate cap materials that wicked a human female mammary gland, pre-neoplastic epithelial (MCF-10A) cell sample in both 4-twist nylon and dopamine-treated polylactide (PL) fiber bundles. N=3 sample size.

MCF-7/MCF-10A Cell Separation

Materials and Methods

Fiber Preparation

Polylactide filament was extruded through a Monoprice Maker Ultimate 3D Printer at 210°C. Nylon filament was extruded through a Monoprice Maker Ultimate 3D Printer at 245°C. Fibers had irregular cross-sectional dimensions of 3.33mm x 2.02mm and were defined as E70 sized fibers. Wicking fibers were laser cut into three individual fiber segments 35 mm in length. Nylon fiber bundles were twisted immediately following the laser cutting process. Three 35 mm nylon fiber segments were configured into a bundle and secured on one end of the bundle with a clear acrylic prototype ring. The other end of the fiber bundle was then secured in the chuck of an electric drill. The nylon fiber bundle was twisted four rotations with the electric drill, then held in that position for 60 seconds to solidify the twisted configuration. The polylactide fiber bundles were treated in a dopamine solution for 40 minutes to increase fiber bundle hydrophilicity.

Chemical Surface Treatment

The dopamine surface treatment solution was made by combining a 10mM Tris-HCl buffer solution with dopamine powder. To prepare the Tris-HCl buffer solution, 7.84g of tris powder was added to 450 mL of DI water in a beaker. Four NaOH pellets were then dissolved in 30 mL of DI water and added dropwise into the 450 mL tris solution. The tris-HCl buffer was then diluted with DI water to a total volume of 500 mL. To make the dopamine solution, 0.4g of dopamine was added to 100 mL of tris-HCl buffer solution and dissolved. Direct airflow, 45°C heat, and a stir bar at 400 rpm were then added into the 100 mL dopamine solution to enhance the reaction. Fibers were treated in the dopamine solution for 40 minutes. After treatment, fibers were rinsed with DI water and patted dry with gauze.

Cap Material Preparation

The alginate gel cap material was prepared by dip coating one end of the fiber bundles in two solutions: a calcium chloride solution and a sodium alginate solution. A 10 mL calcium chloride solution was made by dissolving 5.55 g of calcium chloride granules to 10 mL of DI water. The sodium alginate solution was made by dissolving 0.09 g of reagent grade sodium chloride in 10 mL of DI water. After the sodium chloride was dissolved, 0.14 g of alginic acid sodium salt from brown algae was dissolved in the sodium chloride solution to make to sodium alginate solution. The top 2 mm of the fiber bundles were then carefully dipped in the calcium chloride solution and immediately removed. The same 2 mm end of the fiber bundles were then dipped into the sodium alginate solution and immediately removed, forming the alginate gel cap. Fiber bundles were placed in the -80ºC freezer to preserve the cap material structure until they could be transferred to a freeze dryer at another location for freeze drying.

Cell Sample Preparation

Cancerous human female breast, estrogen, and progesterone receptor (MCF-7) cells and human female mammary gland, pre-neoplastic epithelial (MCF-10A) cells were used for the purposes of this experiment. One T-25 flask of cancerous human female breast, estrogen, and progesterone receptor (MCF-7) cells was stained with Cell Tracker red stain to assess cell wicking and collection capabilities. One T-25 flask of human female mammary gland, pre-neoplastic epithelial (MCF-10A) cells was also stained with Cell Tracker green stain. Both cell types were resuspended in deionized water following centrifugation. The initial concentrations of both cell types in the heterogenous cell sample were $3x10^4$ cells/mL.

Wicking Experiment Set-Up

Three wicking fiber bundle prototypes were prepared with the dopamine-treated polylactide fiber bundles and with the 4-twist nylon fiber bundles. All six prototypes were prepared with the freeze-dried alginate cap material in the modified cryovial prototype. 1 mL of heterogenous cell sample containing equal concentrations of cancerous human female breast, estrogen, and progesterone receptor (MCF-7) cells and human female mammary gland, pre-neoplastic epithelial (MCF-10A) cells was added to each sample well for wicking. Wicking time began when the fiber bundles were placed in the prototype sample well. Cell sample was allowed to wick for 15 minutes. After wicking was complete, the cap materials were removed from the top of the wicking fiber bundle prototype with tweezers and placed onto a microscope slide for analysis. Cap materials were flattened with a coverslip for more clear viewing under the EVOS fluorescent light microscope. A 100 uL sample was taken from the sample well after wicking was completed to record the cell concentration not wicked after 15 minutes. Fiber bundle prototypes were then placed in the -80°C freezer for 10 minutes to fix the wicked cell sample in

place. Following 10 minutes of freezing, fiber bundle prototypes were removed from the freezer, sectioned into three even fiber bundle segments, and placed in a microcentrifuge tube one at a time. Fiber bundle segments were left on the benchtop for 5 minutes to allow for the sample to melt. Fiber bundle segments were then rinsed with 150 uL of deionized water and placed in the centrifuge for 5 minutes at 1600 rpm. Once centrifuged, fiber bundle segments were removed from the microcentrifuge tube, and the cell pellets were resuspended within the microcentrifuge tube with a micropipette. A 10 uL sample from each fiber segment sample was then used for a hemocytometer cell count of the wicked cells.

Analysis

Cell wicking and collection was analyzed by viewing the alginate cap material on the microscope slide under the EVOS fluorescent light microscope. The transmitted, Texas Red, and GFP 10X objective lenses were used for cell viewing. The entire alginate cap material was analyzed for cell count. Initial and post-wicking cell counts in the sample well and cell counts of the wicked cells within each fiber bundle segment were performed with the hemocytometer under the EVOS fluorescent light microscope with the transmitted, Texas Red, and GFP 10X objective lenses. Statistical analysis of the quantifiable results was performed using two-way ANOVA tests in the GraphPad Prism software.

Results and Discussion

Cell type separation between cancerous human female breast, estrogen, and progesterone receptor (MCF-7) cells and human female mammary gland, pre-neoplastic epithelial (MCF-10A) cells was confirmed to be significant ($F(1,8)=132.7$, $p<0.0001$) in both the 4-twist nylon fiber bundle and the dopamine-treated polylactide fiber bundle as shown in Figure 37A, however, statistical analysis showed that there was no significant difference between cell number in the

different fiber bundle types ($F(1,8)=2.391$, $p=0.1607$) as well as no interaction between the two variables tested ($F(1,8)=3.405$, $p=0.1022$). The 4-twist nylon fiber bundle showed a higher degree of cell type separation within the freeze-dried alginate cap material as shown in Figure 37A, with 95% of cells in the cap being cancerous human female breast, estrogen, and progesterone receptor (MCF-7) cells compared to the approximately 91% cell separation in the dopamine-treated polylactide fiber bundle. These separation percentages in the freeze-dried alginate cap material are higher than those previously reported for the passive transport system and in non-affinity-based CTC detection microchips[83,84,98]. Variability in the freeze-dried alginate cap cell counts could be attributed to fluorescent debris particles, the fluorescence of the cap material itself, or the folding of the freeze-dried alginate cap, all contributing to a decreased cell visibility.

From the cell concentrations remaining in the sample well shown in Figure 37B, there is a significant difference in the cell concentrations wicked into the fiber bundles between fiber bundle types ($F(1,8)=8.067$, $p=0.0218$), however, no significance was found in cell concentration uptake between cell types ($F(1,8)=1.667$, $p=0.2328$). Figure 37C shows significant difference in cell concentration between cell types in each fiber bundle segment ($F(1,12)=26.28$, $p=0.0003$) as well as significant differences between cell concentrations within each fiber bundle segment ($F(2,12)=7.689$, $p=0.0071$) in the 4-twist nylon fiber bundle. Interaction between the two tested variables was also shown to be significant ($F(2,12)=6.219$, $p=0.0140$). Lastly, Figure 37D shows the cell concentrations between cell types within the fiber bundle segments to be significantly different ($F(1,12)=60.50$, $p<0.0001$) as well as the cell concentrations wicked between fiber bundle segments to be significantly different ($F(2,12)=8.000$, $p=0.0062$) in the dopamine-treated polylactide fiber bundle. Interaction between the two tested variables was also shown to be

significant ($F(2,12)=14.00$, $p=0.0007$). These results indicate that the 4-twist nylon fiber bundle show increased cell sample uptake and separation of cancerous human female breast, estrogen, and progesterone receptor (MCF-7) cells and human female mammary gland, pre-neoplastic epithelial (MCF-10A) cells compared to that of the dopamine-treated polylactide fiber bundle.

Cancerous human female breast, estrogen, and progesterone receptor (MCF-7) cells have been found to be 19.9-33.9 um in size and human female mammary gland, pre-neoplastic epithelial (MCF-10A) cells have been found to be 14.5-26.2 um is size when in suspension, indicating that this cell separation was likely due to differences in cell deformability more so than cell size[142]. The concept of physical separation being due to cell deformability more so than cell size was also supported in the literature[85,94,95]. It should also be noted that adding the cell concentrations remaining in the sample well with the cell concentrations left in the fiber bundle segments after wicking gives higher cell concentrations than initially recorded before wicking began. Cell fragmentation from the freezing and centrifugation process as well as debris from the freeze-dried alginate cap material fluorescing during the cell counts could contribute to the variability and error seen in cell concentrations.

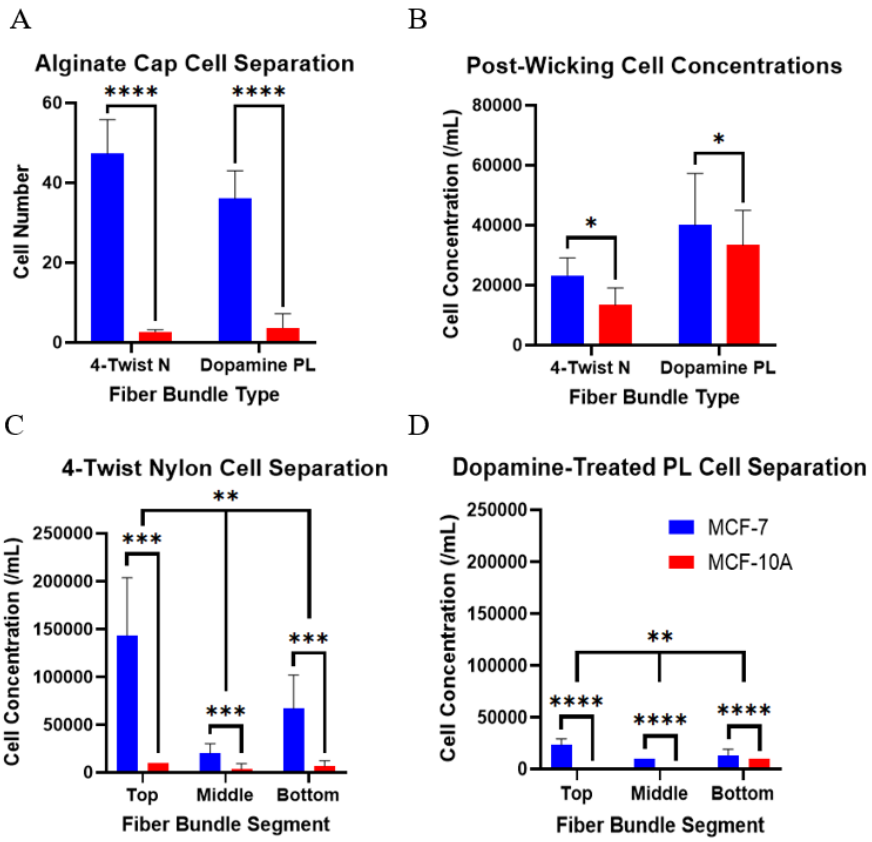

*Figure 37. Characterizing heterogenous cell sample separation of cancerous human female breast, estrogen, and progesterone receptor (MCF-7) and human female mammary gland, pre-neoplastic epithelial (MCF-10A) cells in both 4-twist nylon (N) and dopamine-treated polylactide (PL) fiber bundles. (A) Cell counts on freeze-dried alginate cap material. N=3 sample size. (B) Cell concentrations in the sample well of both cell types post-wicking. N=3 sample size. (C) Cell concentrations of both cell types in each fiber segment post-wicking in the 4-twist nylon fiber bundle. N=3 sample size. (D) Cell concentrations of both cell types in each fiber segment post-wicking in the dopamine-treated polylactide fiber bundle. N=3 sample size. * indicates $p<0.05$. ** indicates $p<0.01$. *** indicates $p<0.001$. **** indicates $p<0.0001$.*

Discussion

The beginning section of this chapter focused on identifying a method to fix a fluid sample to the location it wicked for analysis. It was determined that freezing the fluid sample within the fiber bundle, sectioning the fiber bundle, and then removing the fluid sample from the fiber bundle using centrifugation was the best method for the purposes of our experiments because the -80°C freezer can rapidly freeze such a small volume of sample to the location it wicked to. Previous work used a 4% paraformaldehyde solution to fix the cell sample to the fiber bundles, but using a

liquid fixative for the purposes of fixing a liquid sample to the inner channels of the fiber bundles did not seem to work[98]. While this work did not explore using 4% paraformaldehyde as a fixative, methanol and UV resin was tested as a liquid fixative. When either liquid fixative was pipetted into the top of the fiber bundle or wicked through the bottom of the fiber bundle, the liquid fixative would displace the fluid sample as the fixative penetrated the inner channels of the fiber bundle. This will affect the final location of the cells for separation analysis and was deemed an inaccurate method for fixing cells to the fiber bundle system for separation analysis.

More specifically, the methanol fixative must be able to evaporate in order to dehydrate the cells and fix them to a surface. Because the inner channels of the fiber bundle are not readily exposed to the air, it is very difficult for the methanol fixative to evaporate and successfully fix the cells to the fiber bundle for analysis. The UV resin also had issues with fixing the fluid sample within the inner channels of the fiber bundle because the UV resin solution would not mix with the fluid sample and thus only cured on either end of the fluid sample. For this reason, the fluid sample level remained the same when fixed with the UV resin, but the fluid sample on the inside of the fiber bundle was still able to move freely within the fixed level of sample.

The later section of this chapter focused on separating a cancerous human female breast, estrogen, and progesterone receptor (MCF-7) cell sample from a human female mammary gland, pre-neoplastic epithelial (MCF-10A) cell sample by using an alginate cap material. The human female mammary gland, pre-neoplastic epithelial (MCF-10A) cells used had a cell size of 14.5-26.2 um, which is comparable to that of the cancerous human female breast, estrogen, and progesterone receptor (MCF-7) cells used[142]. Because of the similarity in cell size when in suspension, it is believed the physical separation of these two cell lines may be due to cell deformability more so than cell size as supported in the literature[85,94,95]. Fiber bundle type and

cap type did not seem to make a difference in cancerous human female breast, estrogen, and progesterone receptor (MCF-7) cell wicking. However, the human female mammary gland, pre-neoplastic epithelial (MCF-10A) cell sample seemed to wick better in the 4-twist nylon fiber bundle than the dopamine-treated polylactide fiber bundle, which could indicate that the dopamine-treated polylactide fiber bundle will have better separation of the two cell types than the 4-twist nylon fiber bundle will. However, the cancerous human female breast, estrogen, and progesterone receptor (MCF-7) cells were seen in greater number in the alginate cap material than the human female mammary gland, pre-neoplastic epithelial (MCF-10A) cells when each individual cell type was wicked.

The separation between the two cell types was then confirmed by wicking a heterogenous cell sample into the freeze-dried alginate cap material over a 4-twist nylon fiber bundle and a dopamine-treated polylactide fiber bundle. Varying initial cell concentration in the cell sample by one degree of magnitude was found to not greatly affect the number of cells wicked into the cap material, however, as the initial cell concentration decreased, so did the number of cells wicked into the cap material. This could be an issue when processing a smaller volume cell sample, not allowing enough cells to be processed by the wicking fiber bundle prototype to make a definitive diagnosis. Future work will need to address this issue by increasing the percentage of the sample processed by the wicking fiber bundle prototype. Heterogenous cell separation results indicated that the 4-twist nylon fiber bundle had a greater degree of separation between the two cell types than did the dopamine-treated polylactide fiber bundle. The separation percentages in the freeze-dried alginate cap were also higher than the previously reported separation percentages of the alginate cap from the passive transport system and microchip devices[83,84,98]. The 4-twist nylon fiber bundle had greater sample uptake and cell wicking overall, which is

likely due to the increase in contact points between fibers in the fiber bundle and decreased capillary channel radii.

Some major limitations of this work stem from the fixation and analysis process throughout the separation experiments. It was shown that freezing the fluid sample in the -80°C freezer was sufficient for keeping the fluid sample in place after wicking, but could have damaging effects on the cells prior to analysis. The untwisting of the fiber bundles within the microcentrifuge tube after melting and centrifuging also introduces further damaging effects on the cell sample. When analyzing the final cell sample under the EVOS fluorescent light microscope on the hemocytometer, some cells were fragmented, affecting the final cell count in each fiber segment. Additionally, there were still cells observed on the fiber bundle segments after rinsing and centrifugation, meaning that cells were excluded from the cell count in each of the fiber segments. Previous work has used a custom vertical microscope to observe the cell sample location directly on the fiber bundle, but this technology was unavailable to use for this work. Future work should be done to identify a more promising method for analyzing the cell sample in each fiber segment in order to characterize cell type separation more accurately within the fiber bundle system. The lack of cell recovery in the wicking fiber bundle cancer diagnostic prototype is also of concern. Compared to the microchip devices that have reported an approximate 90% cell recovery, the 4-twist nylon bundle recovered an average of approximately 0.15% of the cancerous human female breast, estrogen, and progesterone receptor (MCF-7) cells. This would pose a problem when processing a 1 mL cell sample with extremely low concentrations of cancer cells present and may not successfully separate the few cancer cells present within the sample. This is another reason that future work should continue to modify the

fiber bundle to where the whole fluid sample is processed through the fiber bundle system to ensure cancer cells can be separated even if in low concentrations.

Conclusion

The proposed wicking fiber bundle cancer diagnostic prototype has the potential to be a promising solution to more expensive microchips that separate CTCs from a whole blood sample by physical characteristics. The wicking fiber bundle prototype has successfully shown the ability to separate cell types (MCF-7/MCF-10A) through the means of physical separation based on cancer cell characteristics and separated cancer cells from non-cancer cells with higher purity than the previously proposed passive transport system and microchips devices[83,84,98]. Microchips are limited by clogging due to forced fluid flow through the microchip, while the wicking fiber bundle prototype uses a passive wicking mechanism to separate cell types[83]. However, the wicking fiber bundle prototype application is limited by the small volume of sample processed, so future work should explore increasing the volume of sample the device can process for better cell recovery.

CHAPTER FIVE

CONCLUSIONS AND FUTURE WORK

Throughout this work, conclusions have been drawn from the initial hypotheses stated in Chapter 1. The initial hypothesis of Chapter 2 was that increasing the hydrophilicity of the fiber bundle materials and decreasing the capillary channel radii would increase the capillary action within the wicking fiber bundle prototype, therefore increasing the amount of sample processed. It was concluded in this work that increased fiber bundle hydrophilicity and decreased capillary channel radii did in fact enhance wicking properties through a series of experiments. The dopamine-treated polylactide and the 4-twist nylon fiber bundle were identified as the fiber bundles with the most promising wicking properties. These experiments, however, were limited by variability cross sectional variability introduced during extrusion and twisting variability introduced through the twisting process. The twisting process also introduced damage to some materials which could have a negative impact on wicking properties. Future work with the fiber bundle modifications would include the development of a consistent twisting process for the 4-twist nylon fiber bundle that could precisely adjust the twist tension and twisting speed to avoid internal and external damage to the fiber bundle. The fiber bundle should also be modified to process more of the fluid sample to ensure adequate cell separation for a definitive diagnosis to be made.

The initial hypothesis in Chapter 3 was that the freeze-dried alginate cap material would increase cell sample uptake through transpiration-like mechanisms. This hypothesis was confirmed that the freeze-dried alginate cap material wicked more cell sample into the cap

material than that of the air-dried alginate cap material. Cell visibility was also shown to be the most promising for the freeze-dried alginate cap material when compared to other cap materials that had consistent contact with the top of the wicking fiber bundle prototype. It was also confirmed that the freeze-dried alginate cap material reached saturation and collected the maximum amount of cells within 15 minutes of wicking. These experiments, however, were limited by the fluorescing of the cap material itself, limiting cell visibility in certain areas of the cap. Cap material fluorescence was most often observed when the cap material had been folded or not fully rehydrated by the fluid sample. It should be noted that this will not be an end user problem, as they will not be using a fluorescent light microscope to analyze the isolated cell sample. However, the cap material fluorescence is currently an issue when attempting to fine-tune the wicking fiber bundle prototype. Future work on the cap material modifications will include improving cell visibility and reducing the freeze-dried alginate cap material fluorescence under the EVOS fluorescent light microscope. Experimenting with other forms of alginate for the freeze-dried alginate cap material could also allow for better gelling time, mechanical properties, and sample absorption rates.

Lastly, the initial hypothesis for Chapter 4 was that the enhancements made in Chapter 2 and Chapter 3 would enhance cell separation and that the presence of cancerous human female breast, estrogen, and progesterone receptor (MCF-7) cell population would be more abundant at the top of the fiber bundle than the human female mammary gland, pre-neoplastic epithelial (MCF-10A) cell population. It was also hypothesized that a higher initial cell concentration would result in a higher number of cancerous human female breast, estrogen, and progesterone receptor (MCF-7) cells isolated in the freeze-dried alginate cap material. From Chapter 4 experiments, it was shown that the initial cell concentration had no significant effect on the

number of cancerous human female breast, estrogen, and progesterone receptor (MCF-7) cells isolated in the freeze-dried alginate cap material when looking at 10^5 and 10^4 cell/mL magnitudes. However, Chapter 4 experiments did prove a significant degree of separation between cancerous human female breast, estrogen, and progesterone receptor (MCF-7) and human female mammary gland, pre-neoplastic epithelial (MCF-10A) cell populations within the 4-twist nylon and dopamine-treated polylactide fiber bundles, where the 4-twist nylon fiber bundle separated the cell populations with 95% purity and the dopamine-treated polylactide fiber bundle separated the cell populations with a 91% purity. Each of these results had higher cell purity than the previously proposed passive transport system and the microchip devices in the literature[83,84,98]. These experiments, however, were limited by the inadequate fixation of the cell sample post-wicking, cell fragmentation throughout the process of obtaining cell counts within the fiber bundle segments, and the lack of cell recovery. For this reason, future work for characterizing cell separation within the wicking fiber bundle prototype includes determining whether increased cell recovery is important for rapid diagnostic purposes, then increasing the cell recovery by either modifying the fiber bundle to process more of the fluid sample, or redesigning the prototype to allow the wicking fiber bundle prototype to work with a smaller volume of initial sample.

REFERENCES

1. Flory, A., McLennan, L., Peet, B., Kroll, M., Stuart, D., Brown, D., Stuebner, K., Phillips, B., Coomber, B. L., Woods, J. P., Miller, M., Tripp, C. D., Wolf-Ringwall, A., Kruglyak, K. M., McCleary-Wheeler, A. L., Phelps-Dunn, A., Wong, L. K., Warren, C. D., Brandstetter, G., … Rafalko, J. M. (2023). Cancer detection in clinical practice and using blood-based liquid biopsy: A retrospective audit of over 350 dogs. *Journal of Veterinary Internal Medicine*, *37*(1), 258–267. https://doi.org/10.1111/jvim.16616

2. *Diagnosis & staging*. Cornell University College of Veterinary Medicine. (2017, June 12). Retrieved from https://www.vet.cornell.edu/research-departments/institutes/sprecher-institute-comparative-cancer-research/treatment-strategies/diagnosis-staging

3. Kruglyak, K. M., Chibuk, J., McLennan, L., Nakashe, P., Hernandez, G. E., Motalli-Pepio, R., Fath, D. M., Tynan, J. A., Holtvoigt, L. E., Chorny, I., Grosu, D. S., Tsui, D. W. Y., & Flory, A. (2021). Blood-based liquid biopsy for comprehensive cancer genomic profiling using next-generation sequencing: An emerging paradigm for non-invasive cancer detection and management in dogs. *Frontiers in Veterinary Science*, *8*. https://doi.org/10.3389/fvets.2021.704835

4. *Liquid biopsy: Revolutionizing cancer detection with a simple blood draw*. Veterinary Practice News. (2022, March 1). Retrieved from https://www.veterinarypracticenews.com/liquid-biopsy-revolutionizing-cancer-detection-with-a-simple-blood-draw/

5. Chibuk, J., Flory, A., Kruglyak, K. M., Leibman, N., Nahama, A., Dharajiya, N., van den Boom, D., Jensen, T. J., Friedman, J. S., Shen, M. R., Clemente-Vicario, F., Chorny, I., Tynan, J. A., Lytle, K. M., Holtvoigt, L. E., Murtaza, M., Diaz, L. A., Tsui, D. W., & Grosu, D. S. (2021). Horizons in veterinary precision oncology: Fundamentals of cancer genomics and applications of liquid biopsy for the detection, characterization, and management of cancer in dogs. *Frontiers in Veterinary Science, 8*. https://doi.org/10.3389/fvets.2021.664718

6. Taylor, W. C. (2020). Comment on 'sensitive and specific multi-cancer detection and localization using methylation signatures in cell-free DNA' by M. C. Liu et al.. *Annals of Oncology, 31*(9), 1266–1267. https://doi.org/10.1016/j.annonc.2020.04.013

7. Cohen, J. D., Li, L., Wang, Y., Thoburn, C., Afsari, B., Danilova, L., Douville, C., Javed, A. A., Wong, F., Mattox, A., Hruban, R. H., Wolfgang, C. L., Goggins, M. G., Dal Molin, M., Wang, T.-L., Roden, R., Klein, A. P., Ptak, J., Dobbyn, L., … Papadopoulos, N. (2018). Detection and localization of surgically resectable cancers with a multi-analyte blood test. *Science*, *359*(6378), 926–930. https://doi.org/10.1126/science.aar3247

8. Hubbell, E., Clarke, C. A., Aravanis, A. M., & Berg, C. D. (2021). Modeled reductions in late-stage cancer with a multi-cancer early detection test. *Cancer Epidemiology, Biomarkers & Prevention*, *30*(3), 460–468. https://doi.org/10.1158/1055-9965.epi-20-1134

9. Ofman, J. J. (2020, November 1). *Taking early cancer detection to the next level*. Scientific American. Retrieved from https://www.scientificamerican.com/article/taking-early-cancer-detection-to-the-next-level/

10. Ciriello, G., Miller, M. L., Aksoy, B. A., Senbabaoglu, Y., Schultz, N., & Sander, C. (2013). Emerging landscape of oncogenic signatures across human cancers. *Nature Genetics*, *45*(10), 1127–1133. https://doi.org/10.1038/ng.2762
11. Alix-Panabières, C., & Pantel, K. (2013). Circulating tumor cells: Liquid biopsy of cancer. *Clinical Chemistry*, *59*(1), 110–118. https://doi.org/10.1373/clinchem.2012.194258
12. Pecot, C. V., Bischoff, F. Z., Mayer, J. A., Wong, K. L., Pham, T., Bottsford-Miller, J., Stone, R. L., Lin, Y. G., Jaladurgam, P., Roh, J. W., Goodman, B. W., Merritt, W. M., Pircher, T. J., Mikolajczyk, S. D., Nick, A. M., Celestino, J., Eng, C., Ellis, L. M., Deavers, M. T., & Sood, A. K. (2011). A novel platform for detection of CK+ and CK− ctcs. *Cancer Discovery*, *1*(7), 580–586. https://doi.org/10.1158/2159-8290.cd-11-0215
13. Balmer, C. (2015, July 1). *Circulating tumor cell analysis*. AACC. Retrieved from https://www.aacc.org/cln/articles/2015/july/circulating-tumor-cell-analysis-on-the-frontlines-of-cancer-diagnosis-and-management
14. Du, H. X., Wang, Z. G., Yang, Z. L., Chen, D., Chen, J. D., & Hu, R. J. (2011). Separation of circulating cancer cells by unique microfluidic chip in colorectal cancer. *Oncology Research Featuring Preclinical and Clinical Cancer Therapeutics*, *19*(10), 487–500. https://doi.org/10.3727/096504012x13286534482476
15. Spiliotaki, M., Markomanolaki, H., Kallergi, G., Papadaki, M. A., Georgoulias, V., Mavroudis, D., & Agelaki, S. (2013). Evaluation of proliferation and apoptosis markers in circulating tumor cells (ctcs) of women with early breast cancer who are candidates for tumor dormancy. *Journal of Clinical Oncology*, *31*(15_suppl). https://doi.org/10.1200/jco.2013.31.15_suppl.e22101

16. Tsai, W.-S., Chen, J.-S., Shao, H.-J., Wu, J.-C., Lai, J.-M., Lu, S.-H., Hung, T.-F., Chiu, Y.-C., You, J.-F., Hsieh, P.-S., Yeh, C.-Y., Hung, H.-Y., Chiang, S.-F., Lin, G.-P., Tang, R., & Chang, Y.-C. (2016). Circulating tumor cell count correlates with colorectal neoplasm progression and is a prognostic marker for distant metastasis in non-metastatic patients. *Scientific Reports*, *6*(1). https://doi.org/10.1038/srep24517

17. Bluemke, K., Bilkenroth, U., Meye, A., Fuessel, S., Lautenschlaeger, C., Goebel, S., Melchior, A., Heynemann, H., Fornara, P., & Taubert, H. (2009). Detection of circulating tumor cells in peripheral blood of patients with renal cell carcinoma correlates with prognosis. *Cancer Epidemiology, Biomarkers & Prevention*, *18*(8), 2190–2194. https://doi.org/10.1158/1055-9965.epi-08-1178

18. de Bono, J. S., Scher, H. I., Montgomery, R. B., Parker, C., Miller, M. C., Tissing, H., Doyle, G. V., Terstappen, L. W. W. M., Pienta, K. J., & Raghavan, D. (2008). Circulating tumor cells predict survival benefit from treatment in metastatic castration-resistant prostate cancer. *Clinical Cancer Research*, *14*(19), 6302–6309. https://doi.org/10.1158/1078-0432.ccr-08-0872

19. CRISTOFANILLI, M. (2006). Circulating tumor cells, disease progression, and survival in metastatic breast cancer. *Seminars in Oncology*, *33*, 9–14. https://doi.org/10.1053/j.seminoncol.2006.03.016

20. Farace, F., Massard, C., Vimond, N., Drusch, F., Jacques, N., Billiot, F., Laplanche, A., Chauchereau, A., Lacroix, L., Planchard, D., Le Moulec, S., André, F., Fizazi, K., Soria, J. C., & Vielh, P. (2011). A direct comparison of CellSearch and Iset for circulating tumour-cell detection in patients with metastatic carcinomas. *British Journal of Cancer*, *105*(6), 847–853. https://doi.org/10.1038/bjc.2011.294

21. Myung, J. H., Gajjar, K. A., Saric, J., Eddington, D. T., & Hong, S. (2011). Dendrimer-mediated multivalent binding for the enhanced capture of tumor cells. *Angewandte Chemie*, *123*(49), 11973–11976. https://doi.org/10.1002/ange.201105508

22. Hoshino, K., Huang, Y.-Y., Lane, N., Huebschman, M., Uhr, J. W., Frenkel, E. P., & Zhang, X. (2011). Microchip-based immunomagnetic detection of circulating tumor cells. *Lab on a Chip*, *11*(20), 3449. https://doi.org/10.1039/c1lc20270g

23. Liu, Y.-J., Guo, S.-S., Zhang, Z.-L., Huang, W.-H., Baigl, D., Xie, M., Chen, Y., & Pang, D.-W. (2007). A micropillar-integrated smart microfluidic device for specific capture and sorting of cells. *ELECTROPHORESIS*, *28*(24), 4713–4722. https://doi.org/10.1002/elps.200700212

24. Saliba, A.-E., Saias, L., Psychari, E., Minc, N., Simon, D., Bidard, F.-C., Mathiot, C., Pierga, J.-Y., Fraisier, V., Salamero, J., Saada, V., Farace, F., Vielh, P., Malaquin, L., & Viovy, J.-L. (2010). Microfluidic sorting and multimodal typing of cancer cells in self-assembled magnetic arrays. *Proceedings of the National Academy of Sciences*, *107*(33), 14524–14529. https://doi.org/10.1073/pnas.1001515107

25. Danila, D. C., Samoila, A., Patel, C., Schreiber, N., Herkal, A., Anand, A., Bastos, D., Heller, G., Fleisher, M., & Scher, H. I. (2016). Clinical validity of detecting circulating tumor cells by adnatest assay compared with direct detection of tumor mrna in stabilized whole blood, as a biomarker predicting overall survival for metastatic castration-resistant prostate cancer patients. *The Cancer Journal*, *22*(5), 315–320. https://doi.org/10.1097/ppo.0000000000000220

26. *Cancer invasion and metastasis: Molecular and cellular perspective*. Retrieved from https://www.ncbi.nlm.nih.gov/books/NBK164700/

27. Agerbæk, M. Ø., Bang-Christensen, S. R., Yang, M.-H., Clausen, T. M., Pereira, M. A., Sharma, S., Ditlev, S. B., Nielsen, M. A., Choudhary, S., Gustavsson, T., Sorensen, P. H., Meyer, T., Propper, D., Shamash, J., Theander, T. G., Aicher, A., Daugaard, M., Heeschen, C., & Salanti, A. (2018). The VAR2CSA malaria protein efficiently retrieves circulating tumor cells in an EPCAM-independent manner. *Nature Communications*, *9*(1). https://doi.org/10.1038/s41467-018-05793-2

28. Patriarca, C., Macchi, R. M., Marschner, A. K., & Mellstedt, H. (2012). Epithelial cell adhesion molecule expression (CD326) in cancer: A short review. *Cancer Treatment Reviews*, *38*(1), 68–75. https://doi.org/10.1016/j.ctrv.2011.04.002

29. Belthier, G., Homayed, Z., Grillet, F., Duperray, C., Vendrell, J., Krol, I., Bravo, S., Boyer, J.-C., Villeronce, O., Vitre-Boubaker, J., Heaug-Wane, D., Macari-Fine, F., Smith, J., Merlot, M., Lossaint, G., Mazard, T., Portales, F., Solassol, J., Ychou, M., … Pannequin, J. (2021). CD44V6 defines a new population of circulating tumor cells not expressing epcam. *Cancers*, *13*(19), 4966. https://doi.org/10.3390/cancers13194966

30. Wu, L., Wang, Y., Xu, X., Liu, Y., Lin, B., Zhang, M., Zhang, J., Wan, S., Yang, C., & Tan, W. (2021). Aptamer-based detection of circulating targets for precision medicine. *Chemical Reviews*, *121*(19), 12035–12105. https://doi.org/10.1021/acs.chemrev.0c01140

31. Peng, J., Zhao, Q., Zheng, W., Li, W., Li, P., Zhu, L., Liu, X., Shao, B., Li, H., Wang, C., & Yang, Y. (2017). Peptide-functionalized nanomaterials for the efficient isolation of HER2-positive circulating tumor cells. *ACS Applied Materials & Interfaces*, *9*(22), 18423–18428. https://doi.org/10.1021/acsami.7b03905

32. Gorges, T. M., Tinhofer, I., Drosch, M., Röse, L., Zollner, T. M., Krahn, T., & von Ahsen, O. (2012). Circulating tumour cells escape from epcam-based detection due to epithelial-to-mesenchymal transition. *BMC Cancer*, *12*(1). https://doi.org/10.1186/1471-2407-12-178

33. Deng, G., Herrler, M., Burgess, D., Manna, E., Krag, D., & Burke, J. F. (2008). Enrichment with anti-cytokeratin alone or combined with anti-epcam antibodies significantly increases the sensitivity for circulating tumor cell detection in metastatic breast cancer patients. *Breast Cancer Research*, *10*(4). https://doi.org/10.1186/bcr2131

34. Patriarca, C., Macchi, R. M., Marschner, A. K., & Mellstedt, H. (2012). Epithelial cell adhesion molecule expression (CD326) in cancer: A short review. *Cancer Treatment Reviews*, *38*(1), 68–75. https://doi.org/10.1016/j.ctrv.2011.04.002

35. Grover, P. K., Cummins, A. G., Price, T. J., Roberts-Thomson, I. C., & Hardingham, J. E. (2014). Circulating tumour cells: The evolving concept and the inadequacy of their enrichment by EPCAM-based methodology for basic and clinical cancer research. *Annals of Oncology*, *25*(8), 1506–1516. https://doi.org/10.1093/annonc/mdu018

36. Gabriel, M. T., Calleja, L. R., Chalopin, A., Ory, B., & Heymann, D. (2016). Circulating tumor cells: A review of non–EPCAM-based approaches for cell enrichment and isolation. *Clinical Chemistry*, *62*(4), 571–581. https://doi.org/10.1373/clinchem.2015.249706

37. Deng, Z., Wu, S., Wang, Y., & Shi, D. (2022). Circulating tumor cell isolation for cancer diagnosis and prognosis. *EBioMedicine*, *83*, 104237. https://doi.org/10.1016/j.ebiom.2022.104237

38. Miller, M. C., Doyle, G. V., & Terstappen, L. W. (2010). Significance of circulating tumor cells detected by the CellSearch system in patients with metastatic breast colorectal and prostate cancer. *Journal of Oncology*, *2010*, 1–8. https://doi.org/10.1155/2010/617421

39. Wang, L., Balasubramanian, P., Chen, A. P., Kummar, S., Evrard, Y. A., & Kinders, R. J. (2016). Promise and limits of the CellSearch platform for evaluating pharmacodynamics in circulating tumor cells. *Seminars in Oncology*, *43*(4), 464–475. https://doi.org/10.1053/j.seminoncol.2016.06.004

40. Schiffman, J. D., Fisher, P. G., & Gibbs, P. (2015). Early detection of cancer: Past, present, and future. *American Society of Clinical Oncology Educational Book*, (35), 57–65. https://doi.org/10.14694/edbook_am.2015.35.57

41. Bettegowda, C., Sausen, M., Leary, R., Kinde, I., Agrawal, N., Bartlett, B., Wang, H., Luber, B., Kinzler, K., Vogelstein, B., & Papadopoulos, N. (2014). Detection of circulating tumor DNA in early and late stage human malignancies. *Neuro-Oncology*, *16*(suppl 3), iii7–iii7. https://doi.org/10.1093/neuonc/nou206.24

42. Feng, Z., Feng, Y., & Wang, N. (2022). Circulating tumor cells in the early detection of human cancers. *Handbook of Cancer and Immunology*, 1–20. https://doi.org/10.1007/978-3-030-80962-1_323-1

43. Campos-Carrillo, A., Weitzel, J. N., Sahoo, P., Rockne, R., Mokhnatkin, J. V., Murtaza, M., Gray, S. W., Goetz, L., Goel, A., Schork, N., & Slavin, T. P. (2020). Circulating tumor DNA as an early cancer detection tool. *Pharmacology & Therapeutics*, *207*, 107458. https://doi.org/10.1016/j.pharmthera.2019.107458

44. Chen, B., Le, W., Wang, Y., Li, Z., Wang, D., Lin, L., Cui, S., Hu, J. J., Hu, Y., Yang, P., Ewing, R. C., Shi, D., & Cui, Z. (2016). Targeting negative surface charges of cancer cells by multifunctional nanoprobes. *Theranostics*, *6*(11), 1887–1898. https://doi.org/10.7150/thno.16358

45. Wu, S., Gu, L., Qin, J., Zhang, L., Sun, F., Liu, Z., Wang, Y., & Shi, D. (2020). Rapid label-free isolation of circulating tumor cells from patients' peripheral blood using electrically charged Fe3O4 nanoparticles. *ACS Applied Materials & Interfaces*, *12*(4), 4193–4203. https://doi.org/10.1021/acsami.9b16385

46. Wu, S., Wang, Y., & Shi, D. (2020). Positively charged magnetic nanoparticles for capture of circulating tumor cells from clinical blood samples. *Nano LIFE*, *10*(03), 1971001. https://doi.org/10.1142/s1793984419710016

47. Wang, P., Xue, J., Wu, S., Pei, Y., Xu, L., & Wang, Y. (2021). Cell-friendly isolation and Ph-sensitive controllable release of circulating tumor cells by Fe 3 O 4 @caco 3 nanoplatform. *Advanced Materials Interfaces*, *8*(21), 2101191. https://doi.org/10.1002/admi.202101191

48. Zhao, J., Wu, S., Qin, J., Shi, D., & Wang, Y. (2018). Electrical-charge-mediated cancer cell targeting via protein corona-decorated superparamagnetic nanoparticles in a simulated physiological environment. *ACS Applied Materials & Interfaces*, *10*(49), 41986–41998. https://doi.org/10.1021/acsami.8b15098

49. Han, X., Deng, Z., Yang, Z., Wang, Y., Zhu, H., Chen, B., Cui, Z., Ewing, R. C., & Shi, D. (2017). Biomarkerless targeting and photothermal cancer cell killing by surface-electrically-charged superparamagnetic Fe3o4composite nanoparticles. *Nanoscale*, *9*(4), 1457–1465. https://doi.org/10.1039/c6nr07161a

50. Deng, Z., Kalin, G. T., Shi, D., & Kalinichenko, V. V. (2021). Nanoparticle Delivery Systems with cell-specific targeting for pulmonary diseases. *American Journal of Respiratory Cell and Molecular Biology*, *64*(3), 292–307. https://doi.org/10.1165/rcmb.2020-0306tr

51. Deng, Z., Lin, J., Bud'ko, S. L., Webster, B., Kalin, T. V., Kalinichenko, V. V., & Shi, D. (2021). Dual targeting with cell surface electrical charge and folic acid via superparamagnetic fe3o4@cu2–XS for photothermal cancer cell killing. *Cancers*, *13*(21), 5275. https://doi.org/10.3390/cancers13215275

52. Dunn, A. W., Kalinichenko, V. V., & Shi, D. (2018). Highly efficient in vivo targeting of the pulmonary endothelium using novel modifications of polyethylenimine: An importance of charge. *Advanced Healthcare Materials*, *7*(23), 1800876. https://doi.org/10.1002/adhm.201800876

53. Lv, P., Tang, Z., Liang, X., Guo, M., & Han, R. P. (2013). Spatially gradated segregation and recovery of circulating tumor cells from peripheral blood of cancer patients. *Biomicrofluidics*, *7*(3), 034109. https://doi.org/10.1063/1.4808456

54. Hou, H. W., Warkiani, M. E., Khoo, B. L., Li, Z. R., Soo, R. A., Tan, D. S.-W., Lim, W.-T., Han, J., Bhagat, A. A., & Lim, C. T. (2013). Isolation and retrieval of circulating tumor cells using centrifugal forces. *Scientific Reports*, *3*(1). https://doi.org/10.1038/srep01259

55. Sun, J., Li, M., Liu, C., Zhang, Y., Liu, D., Liu, W., Hu, G., & Jiang, X. (2012). Double spiral microchannel for label-free tumor cell separation and enrichment. *Lab on a Chip*, *12*(20), 3952. https://doi.org/10.1039/c2lc40679a

56. Sun, J., Liu, C., Li, M., Wang, J., Xianyu, Y., Hu, G., & Jiang, X. (2013). Size-based hydrodynamic rare tumor cell separation in curved microfluidic channels. *Biomicrofluidics*, *7*(1), 011802. https://doi.org/10.1063/1.4774311

57. Karabacak, N. M., Spuhler, P. S., Fachin, F., Lim, E. J., Pai, V., Ozkumur, E., Martel, J. M., Kojic, N., Smith, K., Chen, P.-i, Yang, J., Hwang, H., Morgan, B., Trautwein, J., Barber, T. A., Stott, S. L., Maheswaran, S., Kapur, R., Haber, D. A., & Toner, M. (2014). Microfluidic, marker-free isolation of circulating tumor cells from blood samples. *Nature Protocols*, *9*(3), 694–710. https://doi.org/10.1038/nprot.2014.044

58. Gupta, V., Jafferji, I., Garza, M., Melnikova, V. O., Hasegawa, D. K., Pethig, R., & Davis, D. W. (2012). Apostream™, a new dielectrophoretic device for antibody independent isolation and recovery of viable cancer cells from blood. *Biomicrofluidics*, *6*(2), 024133. https://doi.org/10.1063/1.4731647

59. Gascoyne, P., & Shim, S. (2014). Isolation of circulating tumor cells by dielectrophoresis. *Cancers*, *6*(1), 545–579. https://doi.org/10.3390/cancers6010545

60. Shim, S., Stemke-Hale, K., Noshari, J., Becker, F. F., & Gascoyne, P. R. (2013). Dielectrophoresis has broad applicability to marker-free isolation of tumor cells from blood by microfluidic systems. *Biomicrofluidics*, *7*(1), 011808. https://doi.org/10.1063/1.4774307

61. Holdich, R., Kosvintsev, S., Cumming, I., & Zhdanov, S. (2005). Pore design and engineering for filters and membranes. *Philosophical Transactions of the Royal Society A: Mathematical, Physical and Engineering Sciences*, *364*(1838), 161–174. https://doi.org/10.1098/rsta.2005.1690

62. Desitter, I., Guerrouahen, B. S., Benali-Furet, N., Wechsler, J., Janne, P. A., Kuang, Y., Yanagita, M., Wang, L., Berkowitz, J. A., Distel, R. J., & Cayre, Y. E. (2011). A New Device for Rapid Isolation by Size and Characterization of Rare Circulating Tumor Cells. *Anticancer Research*, *31*.

63. Zheng, S., Lin, H. K., Lu, B., Williams, A., Datar, R., Cote, R. J., & Tai, Y.-C. (2010). 3D microfilter device for viable circulating tumor cell (CTC) enrichment from blood. *Biomedical Microdevices*, *13*(1), 203–213. https://doi.org/10.1007/s10544-010-9485-3

64. Lim, L. S., Hu, M., Huang, M. C., Cheong, W. C., Gan, A. T., Looi, X. L., Leong, S. M., Koay, E. S.-C., & Li, M.-H. (2012). Microsieve lab-chip device for rapid enumeration and fluorescence in situ hybridization of circulating tumor cells. *Lab on a Chip*, *12*(21), 4388. https://doi.org/10.1039/c2lc20750h

65. Coumans, F. A., van Dalum, G., Beck, M., & Terstappen, L. W. (2013). Filter characteristics influencing circulating tumor cell enrichment from whole blood. *PLoS ONE*, *8*(4). https://doi.org/10.1371/journal.pone.0061770

66. Tang, Y., Shi, J., Li, S., Wang, L., Cayre, Y. E., & Chen, Y. (2014). Microfluidic device with integrated microfilter of conical-shaped holes for high efficiency and high purity capture of circulating tumor cells. *Scientific Reports*, *4*(1). https://doi.org/10.1038/srep06052

67. Lagoudianakis, E. E., Kataki, A., Manouras, A., Memos, N., Papadima, A., Derventzi, A., Zografos, G., Papadopoulos, S., Katergiannakis, V., & Konstadoulakis, M. M. (2009). Detection of epithelial cells by RT-PCR targeting CEA, CK20, and TEM-8 in colorectal carcinoma patients using OncoQuick density gradient centrifugation system. *Journal of Surgical Research*, *155*(2), 183–190. https://doi.org/10.1016/j.jss.2007.10.013

68. Di Trapani, M., Manaresi, N., & Medoro, G. (2018). DEPArray™ system: An Automatic image-based sorter for isolation of pure circulating tumor cells. *Cytometry Part A*, *93*(12), 1260–1266. https://doi.org/10.1002/cyto.a.23687

69. Rossi, T., Gallerani, G., Angeli, D., Cocchi, C., Bandini, E., Fici, P., Gaudio, M., Martinelli, G., Rocca, A., Maltoni, R., & Fabbri, F. (2020). Single-cell NGS-based analysis of copy number alterations reveals new insights in circulating tumor cells persistence in early-stage breast cancer. *Cancers*, *12*(9), 2490. https://doi.org/10.3390/cancers12092490

70. Habli, Z., AlChamaa, W., Saab, R., Kadara, H., & Khraiche, M. L. (2020). Circulating tumor cell detection technologies and clinical utility: Challenges and opportunities. *Cancers*, *12*(7), 1930. https://doi.org/10.3390/cancers12071930

71. Miller, M. C., Robinson, P. S., Wagner, C., & O'Shannessy, D. J. (2018). The parsortix™ cell separation system—a versatile liquid biopsy platform. *Cytometry Part A*, *93*(12), 1234–1239. https://doi.org/10.1002/cyto.a.23571

72. Hvichia, G. E., Parveen, Z., Wagner, C., Janning, M., Quidde, J., Stein, A., Müller, V., Loges, S., Neves, R. P. L., Stoecklein, N. H., Wikman, H., Riethdorf, S., Pantel, K., & Gorges, T. M. (2016). A novel microfluidic platform for size and deformability based separation and the subsequent molecular characterization of viable circulating tumor cells. *International Journal of Cancer*, *138*(12), 2894–2904. https://doi.org/10.1002/ijc.30007

73. Farace, F., Massard, C., Vimond, N., Drusch, F., Jacques, N., Billiot, F., Laplanche, A., Chauchereau, A., Lacroix, L., Planchard, D., Le Moulec, S., André, F., Fizazi, K., Soria, J. C., & Vielh, P. (2011). A direct comparison of CellSearch and Iset for circulating

tumour-cell detection in patients with metastatic carcinomas. *British Journal of Cancer*, *105*(6), 847–853. https://doi.org/10.1038/bjc.2011.294

74. Morris, K. L., Tugwood, J. D., Khoja, L., Lancashire, M., Sloane, R., Burt, D., Shenjere, P., Zhou, C., Hodgson, C., Ohtomo, T., Katoh, A., Ishiguro, T., Valle, J. W., & Dive, C. (2014). Circulating biomarkers in hepatocellular carcinoma. *Cancer Chemotherapy and Pharmacology*, *74*(2), 323–332. https://doi.org/10.1007/s00280-014-2508-7
75. Xu, L., Mao, X., Imrali, A., Syed, F., Mutsvangwa, K., Berney, D., Cathcart, P., Hines, J., Shamash, J., & Lu, Y.-J. (2015). Optimization and evaluation of a novel size based circulating tumor cell isolation system. *PLOS ONE*, *10*(9). https://doi.org/10.1371/journal.pone.0138032
76. Tan, S. J., Yobas, L., Lee, G. Y., Ong, C. N., & Lim, C. T. (2009). Microdevice for the isolation and enumeration of cancer cells from blood. *Biomedical Microdevices*, *11*(4), 883–892. https://doi.org/10.1007/s10544-009-9305-9
77. Zhang, W., Kai, K., Choi, D. S., Iwamoto, T., Nguyen, Y. H., Wong, H., Landis, M. D., Ueno, N. T., Chang, J., & Qin, L. (2012). Microfluidics separation reveals the stem-cell–like deformability of tumor-initiating cells. *Proceedings of the National Academy of Sciences*, *109*(46), 18707–18712. https://doi.org/10.1073/pnas.1209893109
78. Ozkumur, E., Shah, A. M., Ciciliano, J. C., Emmink, B. L., Miyamoto, D. T., Brachtel, E., Yu, M., Chen, P.-i, Morgan, B., Trautwein, J., Kimura, A., Sengupta, S., Stott, S. L., Karabacak, N. M., Barber, T. A., Walsh, J. R., Smith, K., Spuhler, P. S., Sullivan, J. P., … Toner, M. (2013). Inertial focusing for tumor antigen–dependent and –independent sorting of rare circulating tumor cells. *Science Translational Medicine*, *5*(179). https://doi.org/10.1126/scitranslmed.3005616

79. Pei, H., Li, L., Wang, Y., Sheng, R., Wang, Y., Xie, S., Shui, L., Si, H., & Tang, B. (2019). Single-cell phenotypic profiling of ctcs in whole blood using an integrated microfluidic device. *Analytical Chemistry*, *91*(17), 11078–11084. https://doi.org/10.1021/acs.analchem.9b01647

80. Smith, K. J., Jana, J. A., Kaehr, A., Purcell, E., Opdycke, T., Paoletti, C., Cooling, L., Thamm, D. H., Hayes, D. F., & Nagrath, S. (2021). Inertial focusing of circulating tumor cells in whole blood at high flow rates using the microfluidic ctckey™ device for CTC Enrichment. *Lab on a Chip*, *21*(18), 3559–3572. https://doi.org/10.1039/d1lc00546d

81. Shiriny, A., & Bayareh, M. (2021). Inertial focusing of ctcs in a novel spiral microchannel. *Chemical Engineering Science*, *229*, 116102. https://doi.org/10.1016/j.ces.2020.116102

82. Li, Q., Cui, S., Xu, Y., Wang, Y., Jin, F., Si, H., Li, L., & Tang, B. (2019). Consecutive sorting and phenotypic counting of ctcs by an optofluidic flow cytometer. *Analytical Chemistry*, *91*(21), 14133–14140. https://doi.org/10.1021/acs.analchem.9b04035

83. Pang, L., Shen, S., Ma, C., Ma, T., Zhang, R., Tian, C., Zhao, L., Liu, W., & Wang, J. (2015). Deformability and size-based cancer cell separation using an integrated microfluidic device. *The Analyst*, *140*(21), 7335–7346. https://doi.org/10.1039/c5an00799b

84. Bu, J., Kang, Y.-T., Lee, Y.-S., Kim, J., Cho, Y.-H., & Moon, B.-I. (2017). Lab on a fabric: Mass producible and low-cost fabric filters for the high-throughput viable isolation of circulating tumor cells. *Biosensors and Bioelectronics*, *91*, 747–755. https://doi.org/10.1016/j.bios.2017.01.039

85. McFaul, S. M., Lin, B. K., & Ma, H. (2012). Cell separation based on size and deformability using microfluidic funnel ratchets. *Lab on a Chip*, *12*(13), 2369. https://doi.org/10.1039/c2lc21045b

86. Wirtz, D., Konstantopoulos, K., & Searson, P. C. (2011). The physics of cancer: The role of physical interactions and mechanical forces in metastasis. *Nature Reviews Cancer*, *11*(7), 512–522. https://doi.org/10.1038/nrc3080

87. Swaminathan, V., Mythreye, K., O'Brien, E. T., Berchuck, A., Blobe, G. C., & Superfine, R. (2011). Mechanical stiffness grades metastatic potential in patient tumor cells and in cancer cell lines. *Cancer Research*, *71*(15), 5075–5080. https://doi.org/10.1158/0008-5472.can-11-0247

88. Guck, J., Schinkinger, S., Lincoln, B., Wottawah, F., Ebert, S., Romeyke, M., Lenz, D., Erickson, H. M., Ananthakrishnan, R., Mitchell, D., Käs, J., Ulvick, S., & Bilby, C. (2005). Optical deformability as an inherent cell marker for testing malignant transformation and metastatic competence. *Biophysical Journal*, *88*(5), 3689–3698. https://doi.org/10.1529/biophysj.104.045476

89. Beil, M., Micoulet, A., von Wichert, G., Paschke, S., Walther, P., Omary, M. B., Van Veldhoven, P. P., Gern, U., Wolff-Hieber, E., Eggermann, J., Waltenberger, J., Adler, G., Spatz, J., & Seufferlein, T. (2003). Sphingosylphosphorylcholine regulates keratin network architecture and Visco-elastic properties of human cancer cells. *Nature Cell Biology*, *5*(9), 803–811. https://doi.org/10.1038/ncb1037

90. Cross, S. E., Jin, Y.-S., Rao, J., & Gimzewski, J. K. (2007). Nanomechanical analysis of cells from cancer patients. *Nature Nanotechnology*, *2*(12), 780–783. https://doi.org/10.1038/nnano.2007.388

91. Swaminathan, V., Mythreye, K., O'Brien, E. T., Berchuck, A., Blobe, G. C., & Superfine, R. (2011). Mechanical stiffness grades metastatic potential in patient tumor cells and in cancer cell lines. *Cancer Research*, *71*(15), 5075–5080. https://doi.org/10.1158/0008-5472.can-11-0247

92. Remmerbach, T. W., Wottawah, F., Dietrich, J., Lincoln, B., Wittekind, C., & Guck, J. (2009). Oral cancer diagnosis by mechanical phenotyping. *Cancer Research*, *69*(5), 1728–1732. https://doi.org/10.1158/0008-5472.can-08-4073

93. Darling, E. M., Zauscher, S., Block, J. A., & Guilak, F. (2007). A thin-layer model for viscoelastic, stress-relaxation testing of cells using atomic force microscopy: Do cell properties reflect metastatic potential? *Biophysical Journal*, *92*(5), 1784–1791. https://doi.org/10.1529/biophysj.106.083097

94. Lee, W. C., Shi, H., Poon, Z., Nyan, L. M., Kaushik, T., Shivashankar, G. V., Chan, J. K., Lim, C. T., Han, J., & Van Vliet, K. J. (2014). Multivariate biophysical markers predictive of mesenchymal stromal cell multipotency. *Proceedings of the National Academy of Sciences*, *111*(42). https://doi.org/10.1073/pnas.1402306111

95. Zhang, W., Kai, K., Choi, D. S., Iwamoto, T., Nguyen, Y. H., Wong, H., Landis, M. D., Ueno, N. T., Chang, J., & Qin, L. (2012). Microfluidics separation reveals the stem-cell–like deformability of tumor-initiating cells. *Proceedings of the National Academy of Sciences*, *109*(46), 18707–18712. https://doi.org/10.1073/pnas.1209893109

96. Beattie, W., Qin, X., Wang, L., & Ma, H. (2014). Clog-free cell filtration using resettable cell traps. *Lab Chip*, *14*(15), 2657–2665. https://doi.org/10.1039/c4lc00306c

97. Tang, Y., Shi, J., Li, S., Wang, L., Cayre, Y. E., & Chen, Y. (2014). Microfluidic device with integrated microfilter of conical-shaped holes for high efficiency and high purity

capture of circulating tumor cells. *Scientific Reports*, *4*(1). https://doi.org/10.1038/srep06052

98. Tabbaa, S. M. (2016). *Evelopment Of A Transport System For Advancing Tissue Engineering And Cell Identification* (dissertation). ProQuest LLC, Ann Arbor, MI.

99. Tabbaa, S. M., Sharp, J. L., & Burg, K. J. (2017). Characterization and separation of cancer cells with a wicking fiber device. *Annals of Biomedical Engineering*, *45*(12), 2933–2941. https://doi.org/10.1007/s10439-017-1909-2

100. Rattle, S., Hofmann, O., Price, C. P., Kricka, L. J., & Wild, D. (2013). Lab-on-a-chip, micro- and nanoscale immunoassay systems, and Microarrays. *The Immunoassay Handbook*, 175–202. https://doi.org/10.1016/b978-0-08-097037-0.00013-0

101. *Polylactide (PLA): Complete guide to accelerate your 'green' approach*. PLA Plastic (Polylactic Acid) - Uses, Structure & Material Properties. (n.d.). Retrieved March 19, 2023, from https://omnexus.specialchem.com/selection-guide/polylactide-pla-bioplastic

102. Tejada-Oliveros, R., Gomez-Caturla, J., Sanchez-Nacher, L., Montanes, N., & Quiles-Carrillo, L. (2021). Improved toughness of polylactide by binary blends with polycarbonate with glycidyl and maleic anhydride-based compatibilizers. *Macromolecular Materials and Engineering*, *306*(12), 2100480. https://doi.org/10.1002/mame.202100480

103. Vagholkar, P. K. (2016). Nylon (Chemistry, Properties and Uses). *International Journal of Scientific Research*, *5*(9), 349–351.

104. Du, J., Luo, X., Fu, Z., Xu, C., Ren, X., Gao, W., & Li, Y. (2015). Improving the hydrophobicity of nylon fabric by consecutive treatment with poly(acrylic acid), tetraethylorthosilicate, and octadecylamine. *Journal of Applied Polymer Science*, *132*(34). https://doi.org/10.1002/app.42456

105. Ellison, A. H., & Zisman, W. A. (1954). Wettability studies on Nylon, polyethylene terephthalate and polystyrene. *The Journal of Physical Chemistry*, *58*(6), 503–506. https://doi.org/10.1021/j150516a013

106. Takeuti, K. L., de Barcellos, D. E. S. N., & Pieters, M. (2017). Mycoplasma hyopneumoniae detection in nylon-flocked and rayon-Bud Swabs. *Journal of Microbiological Methods*, *141*, 118–120. https://doi.org/10.1016/j.mimet.2017.08.007

107. *Quantiswab microorganism recovery - biomerieux-usa.com*. (2022, April). Retrieved from https://www.biomerieux-usa.com/sites/subsidiary_us/files/quantiswab-microorganism-recovery-1.pdf

108. Jindal, K. (2023, March 19). *What is PETG material?: The definitive guide*. PlasticRanger. Retrieved from https://plasticranger.com/what-is-petg-material/#:~:text=Key%20Properties%20of%20PETG%201%20As%20polyethylene%20terephthalate,resistance%20on%20par%20with%20other%20thermoplastics%20More%20items

109. *Comprehensive guide on polyethylene terephthalate (PET)*. Polyethylene Terephthalate (PET) - Uses, Properties & Structure. (n.d.). Retrieved from https://omnexus.specialchem.com/selection-guide/polyethylene-terephthalate-pet-plastic

110. *What is PETG? (everything you need to know)*. TWI. Retrieved from https://www.twi-global.com/technical-knowledge/faqs/what-is-petg

111. Negm, N. A., Mohamed, A. S., Ahmed, S. M., & El-Raouf, M. A. (2015). Polymer-cationic surfactant interaction: 1. surface and physicochemical properties of Polyvinyl Alcohol (PVA)-S-alkyl isothiouronium bromide surfactant mixed systems. *Journal of Surfactants and Detergents*, *18*(2), 245–250. https://doi.org/10.1007/s11743-014-1665-3

112. Ismail, A. F., Khulbe, K. C., & Matsuura, T. (2019). *Reverse osmosis*. Elsevier.

113. U.S. National Library of Medicine. (n.d.). *Sodium hydroxide*. National Center for Biotechnology Information. PubChem Compound Database. Retrieved from https://pubchem.ncbi.nlm.nih.gov/compound/Sodium-hydroxide

114. Yoo, H. S., Kim, T. G., & Park, T. G. (2009). Surface-functionalized electrospun nanofibers for tissue engineering and drug delivery. *Advanced Drug Delivery Reviews*, *61*(12), 1033–1042. https://doi.org/10.1016/j.addr.2009.07.007

115. Cipitria, A., Skelton, A., Dargaville, T. R., Dalton, P. D., & Hutmacher, D. W. (2011). Design, fabrication and characterization of PCL Electrospun Scaffolds—a review. *Journal of Materials Chemistry*, *21*(26), 9419. https://doi.org/10.1039/c0jm04502k

116. Luo, Y., Jiang, Y., Zhu, J., Tu, J., & Jiao, S. (2020). Surface treatment functionalization of sodium hydroxide onto 3D printed porous ti6al4v for improved biological activities and osteogenic potencies. *Journal of Materials Research and Technology*, *9*(6), 13661–13670. https://doi.org/10.1016/j.jmrt.2020.09.076

117. Zhou, Z.-X., Chen, Y.-R., Zhang, J.-Y., Jiang, D., Yuan, F.-Z., Mao, Z.-M., Yang, F., Jiang, W.-B., Wang, X., & Yu, J.-K. (2020). Facile strategy on hydrophilic modification of poly(ε-CAPROLACTONE) scaffolds for assisting tissue-engineered meniscus constructs in vitro. *Frontiers in Pharmacology*, *11*. https://doi.org/10.3389/fphar.2020.00471

118. Tavanai, H. (2009). A new look at the modification of polyethylene terephthalate by sodium hydroxide. *Journal of the Textile Institute*, *100*(7), 633–639. https://doi.org/10.1080/00405000802128489

119. Mulyati, S., Muchtar, S., Arahman, N., Meirisa, F., Syamsuddin, Y., Zuhra, Z., Rosnelly, C. M., Shamsuddin, N., Mat Nawi, N. I., Wirzal, M. D., Bilad, M. R., Takagi, R., & Matsuyama, H. (2020). One-pot polymerization of dopamine as an additive to enhance permeability and antifouling properties of Polyethersulfone membrane. *Polymers*, *12*(8), 1807. https://doi.org/10.3390/polym12081807

120. Muchtar, S., Wahab, M. Y., Fang, L. F., Jeon, S., Rajabzadeh, S., Takagi, R., Mulyati, S., Arahman, N., Riza, M., & Matsuyama, H. (2018). Polydopamine-coated poly(vinylidene fluoride) membranes with high ultraviolet resistance and antifouling properties for a photocatalytic membrane reactor. *Journal of Applied Polymer Science*, 47312. https://doi.org/10.1002/app.47312

121. Foong, C. Y., Wirzal, M. D., & Bustam, M. A. (2020). A review on nanofibers membrane with amino-based ionic liquid for heavy metal removal. *Journal of Molecular Liquids*, *297*, 111793. https://doi.org/10.1016/j.molliq.2019.111793

122. Sutthiwanjampa, C., Hong, S., Kim, W. J., Kang, S. H., & Park, H. (2023). Hydrophilic modification strategies to enhance the surface biocompatibility of Poly(dimethylsiloxane)-based biomaterials for medical applications. *Advanced Materials Interfaces*, 2202333. https://doi.org/10.1002/admi.202202333

123. Mulyati, S., Muchtar, S., Arahman, N., Syamsuddin, Y., Mat Nawi, N. I., Yub Harun, N., Bilad, M. R., Firdaus, Y., Takagi, R., & Matsuyama, H. (2020). Two-step dopamine-to-polydopamine modification of Polyethersulfone ultrafiltration membrane for enhancing anti-fouling and ultraviolet resistant properties. *Polymers*, *12*(9), 2051. https://doi.org/10.3390/polym12092051

124. Jiang, J., Zhu, L., Zhu, L., Zhu, B., & Xu, Y. (2011). Surface characteristics of a self-polymerized dopamine coating deposited on hydrophobic polymer films. *Langmuir*, *27*(23), 14180–14187. https://doi.org/10.1021/la202877k

125. Masoodi, R., Pillai, K. M., & Varanasi, P. P. (2008). Role of hydraulic and capillary radii in improving the effectiveness of capillary model in wicking. *Volume 1: Symposia, Parts A and B*. https://doi.org/10.1115/fedsm2008-55172

126. Ravi, S., Dharmarajan, R., & Moghaddam, S. (2015). Measurement of capillary radius and contact angle within Porous Media. *Langmuir*, *31*(47), 12954–12959. https://doi.org/10.1021/acs.langmuir.5b03113

127. Fanchi, J. R. (2018). Rock–Fluid Interaction. *Principles of Applied Reservoir Simulation*, 81–99. https://doi.org/10.1016/b978-0-12-815563-9.00005-7

128. MAIER-MAERCKER, U. T. A. (1983). The role of peristomatal transpiration in the mechanism of stomatal movement. *Plant, Cell and Environment*, *6*(5), 369–380. https://doi.org/10.1111/j.1365-3040.1983.tb01269.x

129. Steudle, E. (2001). Water uptake by plant roots: An integration of views. *Recent Advances of Plant Root Structure and Function*, 71–82. https://doi.org/10.1007/978-94-017-2858-4_9

130. Steudle, E. (1995). Trees under tension. *Nature*, *378*(6558), 663–664. https://doi.org/10.1038/378663a0

131. Tyree, M. T. (1997). The cohesion-tension theory of SAP ascent: Current controversies. *Journal of Experimental Botany*, *48*(10), 1753–1765. https://doi.org/10.1093/jxb/48.10.1753

132. Mukhopadhyay, A., & Midha, V. K. (2016). Waterproof breathable fabrics. *Handbook of Technical Textiles*, 27–55. https://doi.org/10.1016/b978-1-78242-465-9.00002-1

133. Wheeler, T. D., & Stroock, A. D. (2008). The transpiration of water at negative pressures in a synthetic tree. *Nature*, *455*(7210), 208–212. https://doi.org/10.1038/nature07226

134. Lee, S. J., Kim, H., & Ahn, S. (2014). Water transport in porous hydrogel structures analogous to leaf mesophyll cells. *Microfluidics and Nanofluidics*, *18*(5-6), 775–784. https://doi.org/10.1007/s10404-014-1418-7

135. Cezan, S. D., Baytekin, H. T., & Baytekin, B. (2020). Self-regulating plant robots: Bioinspired heliotropism and Nyctinasty. *Soft Robotics*, *7*(4), 444–450. https://doi.org/10.1089/soro.2019.0036

136. Thornton, A. J., Alsberg, E., Albertelli, M., & Mooney, D. J. (2004). Shape-defining scaffolds for minimally invasive tissue engineering. *Transplantation*, *77*(12), 1798–1803. https://doi.org/10.1097/01.tp.0000131152.71117.0e

137. *What is comparative oncology?* COP - Pet Owners - What is Comparative Oncology | Center for Cancer Research. Retrieved from https://ccr.cancer.gov/Comparative-Oncology-Program/pet-owners/what-is-comp-onc

138. *Is my dog at risk for cancer?* AAHA. Retrieved from https://www.aaha.org/your-pet/pet-owner-education/ask-aaha/canine-cancer

139. Cytopathology: Fine needle aspiration (FNA) " pathology laboratories " college of medicine " university of Florida. University of Florida Pathology Laboratories. Retrieved from https://pathlabs.ufl.edu/tests/test-directory-c/cytopathology-fine-needle-aspiration-fna/

140. Stewart, S. M., Dowers, K. L., Cerda, J. R., Schoenfeld-Tacher, R. M., & Kogan, L. R. (2014). Microscope use in clinical veterinary practice and potential implications for veterinary school curricula. Journal of Veterinary Medical Education, 41(4), 331–336. https://doi.org/10.3138/jvme.0614-063r

141. Gibon, E., Batke, B., Jawad, M. U., Fritton, K., Rao, A., Yao, Z., Biswal, S., Gambhir, S. S., & Goodman, S. B. (2012). MC3T3-E1 osteoprogenitor cells systemically migrate to a bone defect and enhance bone healing. Tissue Engineering Part A, 18(9-10), 968–973. https://doi.org/10.1089/ten.tea.2011.0545

142. Geltmeier, A., Rinner, B., Bade, D., Meditz, K., Witt, R., Bicker, U., Bludszuweit-Philipp, C., & Maier, P. (2015). Characterization of dynamic behaviour of MCF7 and MCF10A cells in ultrasonic field using modal and harmonic analyses. PLOS ONE, 10(8). https://doi.org/10.1371/journal.pone.0134999

143. Long, C., Kim, H.J., Collins, K., Chen, W., Burg, T., Burg, K.J.L., "Design of a Wicking Fiber Technology for Cancer Prognosis", poster presentation at the 2022 UGA CURO Symposium, University of Georgia, Athens, GA, (April, 2022). * denotes collaborating student first authors

144. Hussain, A., Long, C., Farooq, A., Chen, W., Burg, T., Burg, K., “Development of a Cancer Detection Wicking Fiber Device”, poster presentation at the 2023 UGA CURO Symposium, University of Georgia, Athens, GA, (April, 2023).

145. Long, C., Collins, K., Chen, W., Burg, T., Burg, K.J.L, “Biomaterial Optimization for Cell Separation in Wicking Fiber Bundles”, Transactions of the 2023 Annual Meeting and Exposition of the Society For Biomaterials, San Diego, CA (April, 2023).

146. Burg, T., Collins, K., Long, C., Kim, H.J., Chen, W., Burg, K.J.L, “Promoting and Assessing Cell Capture in a Wicking Fiber Cancer Predictive Tool”, Transactions of the 2022 Annual Meeting and Exposition of the Society For Biomaterials, Baltimore, MD (April, 2022). Poster presentation #560.